AGE-ASSOCIATED LAMIN-B1 REDUCTION IN THE THYMIC EPITHELIAL CELLS AND ITS ROLE IN THYMIC INVOLUTION

by
Sibiao Yue

A dissertation submitted to Johns Hopkins University in conformity with the requirements for the degree of Doctor of Philosophy

Baltimore, Maryland
January 2018

ABSTRACT

As a major component of the nuclear lamina, the type V intermediate filament proteins called lamins are important for the structure and function of the nucleus. Lamins are subdivided into A- and B-types. B-type lamins are implicated in the regulation of many aspects of nuclear function. However, the role of lamins in the context of adult organ maintenance and tissue aging remains largely unknown. Thymic involution, which is an age-related regression of the thymus, causes a decline in naive T cell production and is mainly responsible for immune senescence. The underlying mechanism for this process is still poorly understood. I developed a novel flow cytometry based method to quantify the protein level of nuclear lamins in vivo. By applying this new tool to the thymus, the primary immune organ for T-cell development, I identified an age-associated reduction of lamin-B1 in thymic epithelial cells (TECs). I further demonstrated that macrophage- and dendritic cell-derived proinflammatory cytokines led to lamin-B1 reduction in TECs *via* cellular senescence. I found that TEC-specific deletion of *Lmnb1,* but not *Lmnb2 or Lmna,* leads to thymic atrophy and a number of changes in the TEC compartment that are remarkably similar to reported age-related defects. I also demonstrated that lamin-B1 is required for proper antigen presentation in TECs and that lamin-B1 deficiency in TECs leads to inefficient positive and negative selection of T cells. My RNA-seq data strongly suggest that *Lmnb1*-loss-mediated transcriptome change contributes, at least in part, to the age-associated change in the transcriptional program in TECs and that this in turn leads to the observed degenerative phenotypes.

Advisor: Yixian Zheng

ACKNOWLEDGMENTS

My journey through five-year graduate study has been a truly challenging experience, and I feel very fortunate to have tremendous amount of help and support from many people throughout this period of my life. First, I would like to especially thank my advisor, Yixian Zheng, for her ideas, enthusiasm and constructive advice, all of which provided significant guidance to my research and life. Her knowledge and devotion to science have set up the highest standard in my research, which always makes me to think how to become a real scientist. I also admire her perseverance to achieve research goals, which is the key to overcome the difficulties in current research environment. Yixian has been a role model of a successful scientist for the new generation of young scientists. Her influence on me will continue to boost my research in the future.

My thesis committee members Dr. Powell Jonathan and Dr. Chen-Ming Fan have been amazing throughout my time here. They have provided me with great advice and invaluable insights into my project at every committee meeting, making me view things from different perspectives. They also help me keep correct directions and timely progression in my research and develop as an independent scientist.

I must also thank all lab members in Zheng lab, who have shared their ideas and technique skills with me, provided me invaluable suggestions, helpful critiques for my study. I am also grateful to other research fellows at the Embryology department of Carnegie Science who offer me very helpful advice and critiques from diverse angles. I am extremely grateful to be a graduate student at the Embryology department as it

provides me the opportunity and freedom to pursuit my science, which would not been possible in many other places.

Finally I would like to thank my friends and my family, without their support and encouragement my time as a graduate student would become boring. I especially want to thank my wife Xiaoshu Peng. She has done her best to take care of our family so I can focus on my work. I must also thank all my parents and parents in law for their constant and selfless support and love.

TABLE OF CONTENTS

INDEX OF FIGURES

Chapter 1: Introduction

Overview

My thesis research is divided into two parts. Part 1 involves the study of lamin-B1 in tissue homeostasis. Part 2 is devoted to develop method to enable chromatin immunoprecipitation-seq (ChIP-seq). Below I introduce each of the two subjects of my thesis separately.

I. Thymic involution, inflammation and nuclear lamins

Aging is characterized by a progressive loss of tissue homeostasis and function, and is believed to underly many age-associated diseases. The age-associated deterioration of the immune system, often referred to as immunosenescence, leads to decreased immune function and is considered to be a major cause of increased morbidity and mortality in the elderly. Immunosenescence is accompanied by pronounced age-related changes in the thymus, a primary lymphoid organ involved in T-cell development, and ultimately results in a decline in naïve T-cell production. The degeneration of the thymus marked by dramatic size reduction, termed thymic involution, remains a fundamental conundrum in immunology as it becomes apparent much earlier than other immune organs and is detrimental to the maintenance of adaptive immunity.

While thymic epithelial cells (TECs) have been well documented as the major cell type responsible for involution, very little is known about the cellular and molecular mechanisms underlying age-associated alterations in TECs with considerable effort instead focused on the identification of markers of TEC subpopulations. Due to the general paucity and heterogeneity of TECs, genome-wide transcriptome and epigenome

analyses in specific subpopulations of TECs have not been well studied to date but represent an area of intense interest in the contexts of general TEC biology and in aging. Further, despite remarkable morphological and structural changes documented in the thymic epitelium upon aging, understanding how age-associated alterations lead to the reorganization of cellular structures in TECs and how defective cell structures cause the aging phenotypes is still lacking. My thesis work was inspired by our recent pioneering work uncovering a novel mechanism by which age-associated loss of lamin-B, the major component of the nuclear structure, in *Droshophila* immune organ fat body triggers systemic inflammation and immunosenescence (Chen et al., 2014).

A better understanding of the complex mechanisms mediating thymic involution is essential to design effective therapeutic approaches to improve immune function in aged individuals. Herein I will limit my review on the mechanisms governing TEC development and their potential roles in regulating postnatal thymic homeostasis and involution. I will include outstanding questions that have not yet been resolved, with special emphasis on the role of inflammation in involution. Additionally, I will introduce the role of nuclear lamins in inflammation, tissue homeostasis and aging.

Thymic epithelial cells form niches for T-cell development

The thymus is a major site of T-cell development and is required for robust adaptive immunity in vertebrates (Anderson and Takahama, 2012). The development of the thymus is intimately linked to that of the parathyroid gland as they both arise from the same endodermal primordium in the third pharyngeal pouch during early embryogenesis (Gordon et al., 2004). Ventral-region restricted expression of the thymus-specific

transcription factor Foxn1 (Forkhead Box N1) and complementary dorsal-region expression of the parathyroid transcription factor GCM2 (Glial Cells Missing Homolog 2) defines the boundary between these two organs within the third pharyngeal pouch (Gordon et al., 2001). The importance of Foxn1 for thymus development and function is demonstrated by the severe immunocompromised phenotypes typical of athymic "nude" mice and human subjects bearing mutation alleles (Nehls et al., 1994; Palamaro et al., 2014). While Foxn1 is not required for the initial specification of thymus fate as Foxn1-null thymic rudiment exhibits some early TEC markers (Nehls et al., 1996), it is essential for proper differentiation and proliferation of TEC after fate commitment (Blackburn et al., 1996; Nowell et al., 2011). The initial seeding of hematopoietic stem cells (HSCs) in mouse thymus starts as early as embryonic day 11.5 (E11.5) (Jotereau et al., 1987) and the signals from developing thymocytes also provide essential inductive information for proper TEC development (Klug et al., 1998). The mutual interactions between TECs and developing thymocytes, termed as "cross-talk", are required for proper organization of thymic stromal architecture (Anderson and Jenkinson, 2001; Klug et al., 1998; Klug et al., 2002).

The postnatal thymus is composed of developing T cells, known as thymocytes, and non-lymphoid stromal cells that comprise the different niche microenvironments that promote the various stages of thymocyte development. Whereas the thymic stromal cells only constitute ~1% total cellularity of the thymus, they play the central role in nurturing and educating thymocyte differentiation and maturation. The thymic stromal compartment consists of thymic epithelial cells (TEC), mesenchyme, endothelial and non-lymphoid hematopoietic cells such as dendritic cell (DC) and macrophage. Among

these, TECs represent the primary stromal cell type essential for mediating distinct stages of thymocyte development (Anderson and Takahama, 2012). TECs form a complex 3-dimentional (3D) network and are organized into two discrete regions or compartments that comprise different subtypes of TECs and thymocytes (Gordon and Manley, 2011; Manley et al., 2011). The inner and outer compartments are called the medulla and cortex, respectively; and the region where they contact is the corticomedullary junction (CMJ) and is known as the site of T-cell progenitors homing and export of mature naïve T cells (Lind et al., 2001; Mori et al., 2001; Takahama, 2006). The medulla and cortex consist of two morphologically and functionally distinct TEC subsets, medullary epithelial cell (mTEC) and cortical epithelial cell (cTEC), respectively. Recent studies suggest that both mTEC and cTEC are heterogeneous and identification of detailed markers to delineate TEC subpopulations attracts extensive interest in the field (Nowell et al., 2011; Ohigashi et al., 2015; Wong et al., 2014).

T-cell development within the thymus involves extensive cell migration through the cortex and medulla, and interaction with distinct TEC-formed niches that ensure the proper selection of immuno-competent T cells (Fig. 1-1). Initial interaction with the Notch ligands expressed on cTECs specifies the T-cell fate within the early thymic progenitor (ETP) population. T-lineage specified thymocytes migrate through the cortex to reach the thymic subcapsular zone (Fig. 1-1), during which thymocytes proliferate and differentiate through $CD4^-CD8^-$ double-negative 1-4 (DN1-4) stages and transit to $CD4^+CD8^+$ double-positive (DP) stage. Several developmentally regulated chemokine receptors, including CCR7, CCR9 and CXCR4 have been identified as mediators of

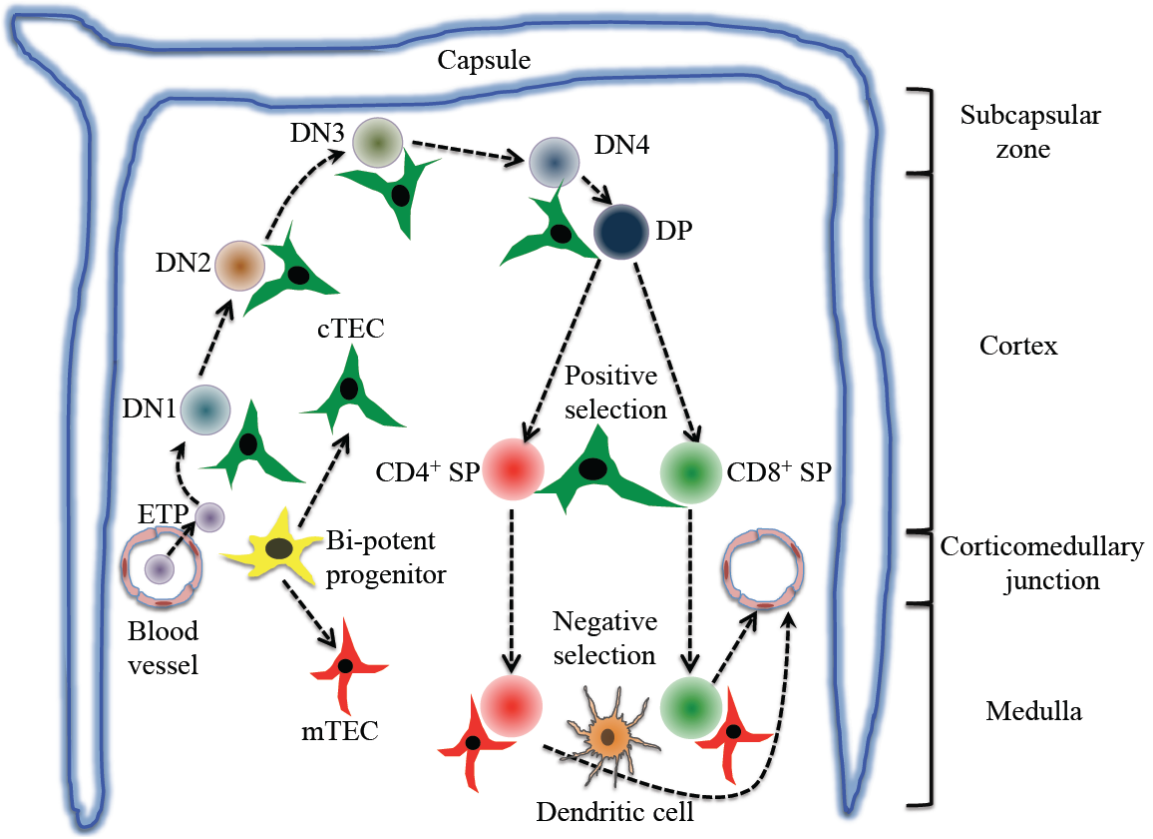

Fig 1-1. An overview of αβ T-cell development in the thymus. In the postnatal thymus, HSC-derived T-lymphoid progenitors (ETP) migrate into the thymus *via* blood vessels at the corticalmedullary junction region (CMJ). Early committed T cells lack expression of CD4 and CD8 and thus are referred to double-negative (DN) thymocytes. During migration from CMJ to subcapsular zone, DN thymocytes process through four stages with the instructive signals from cTECs (DN1, $CD44^{+}CD25^{-}$; DN2, $CD44^{+}CD25^{+}$; DN3, $CD44^{-}CD25^{+}$; DN4, $CD44^{-}CD25^{-}$). DN4 thymocytes further differentiate into $CD4^{+}CD8^{+}$ double-positive (DP) cells that express T-cell receptor (TCR) recognizing self-peptides associated with MHC (pMHC) class I (for CD8) or II (for CD4) molecules expressed on cTECs. Positive selection, which exclusively depends on cTECs, induces DP cells with functional TCRs capable of binding to pMHC to further differentiate into either $CD4^{+}$ or

$CD8^+$ single-positive (SP) thymocytes. Positively selected $CD4^+$ or $CD8^+$ SP cells then relocate into the medulla, where they are further subjected to negative selection or clonal deletion to eliminate self-reactive $CD4^+$ or $CD8^+$ SP cells. mTEC and dendritic cell (DC) are the two main cell types responsible for negative selection. Mature $CD4^+$ or $CD8^+$ T cells then emigrate to peripheral immune system *via* blood vessels at the CMJ region.

intrathymic migration of immature thymocytes (Benz et al., 2004; Misslitz et al., 2004; Plotkin et al., 2003). DP cells then migrate back from subcapsular zone towards the corticomedullary junction (Fig. 1-1), during which they are subjected to the first key selection process, often referred to as positive selection. Positive selection, which exclusively depends on cTEC, induces DP cells with functional T-cell receptors (TCRs) that bind to antigen peptide whithin MHC complex (pMHC) on antigen presenting cells (APCs) to further differentiate into either $CD4^+$ or $CD8^+$ single-positive (SP) thymocytes. More than 90% DP cells expressing non-functional TCRs die by neglect (Anderson and Takahama, 2012; Klein et al., 2009; Takahama, 2006). Successfully selected $CD4^+$ or $CD8^+$ SP cells then move cross the CMJ and relocate into the medulla, where they undergo a quality screening process known as negative selection or clonal deletion. mTEC and DC are the two main cell types responsible for negative selection, through which SP cells with high-affinity TCRs for self-pMHC are induced to die *via* apoptosis, ensuring only self-tolerant T cells survive (Klein et al., 2009). Promiscuous expression of peripheral tissue-restricted antigens (TRA) in mTEC has been demonstrated to play a central role in governing mTEC-mediated negative selection. Two key transcription factors, Autoimmune regulator (Aire) and Fezf2, function in concert to regulate distinct panels of TRA expression in mTEC to ensure immune tolerance (Anderson et al., 2002; Takaba et al., 2015). In addition to mediating clonal deletion, an intact mTEC compartment is essential for generation of $Foxp3^+$ thymic regulatory T cells (tTregs) as tTreg cells with intermediate-affinity for self-pMHC are preferentially induced for survival *via* clonal deviation but not clonal deletion in the medulla region (Aschenbrenner et al., 2007; Cowan et al., 2013). A functional thymus guarantees that only self-MHC

restricted mature T cells with no self-reactive potential are exported to establish the adaptive immune system.

Mechanisms of TEC development, maintenance and degeneration

A handful of genes and signaling pathways have been characterized in TECs and linked with the development, maintenance and involution of the thymus (Fig. 1-2). One key transcriptional factor, forkhead box protein N1 (Foxn1), has been extensively studied over the past two decades and is well documented as a regulator of TEC biology, tying together TEC development, maintenance and degeneration. Foxn1 was initially cloned from the classic athymic nude mouse mutant and functional analyses demonstrated that Foxn1 was required for proper TEC differentiation and proliferation after fate commitment, as Foxn1-null TECs were arrested at the stem/progenitor stage (Nehls et al., 1996). In contrast to its central role in embryonic TEC development, the role of Foxn1 in the postnantal thymus is much less characterized. The further regulation of Foxn1 in various TEC subsets in the postnantal thymus adds additional layers of complexity, which make it difficult to dissect the function of this important transcription factor (Nowell et al., 2011; O'Neill et al., 2016; Rode et al., 2015). Three lines of evidence suggest that Foxn1 is a key regulator of TEC maintenance and function in the postnatal thymus. First, the Manley group reported diminished Foxn1 expression in $Foxn1^{lacz/lacz}$ alleles in 1-week old postnantal thymus, resulting in accelerated thymic degeneration (Chen et al., 2009). Second, early mouse studies indicate that down-regulation of Foxn1 mRNA and protein levels in the postnatal thymus correlates with thymic involution

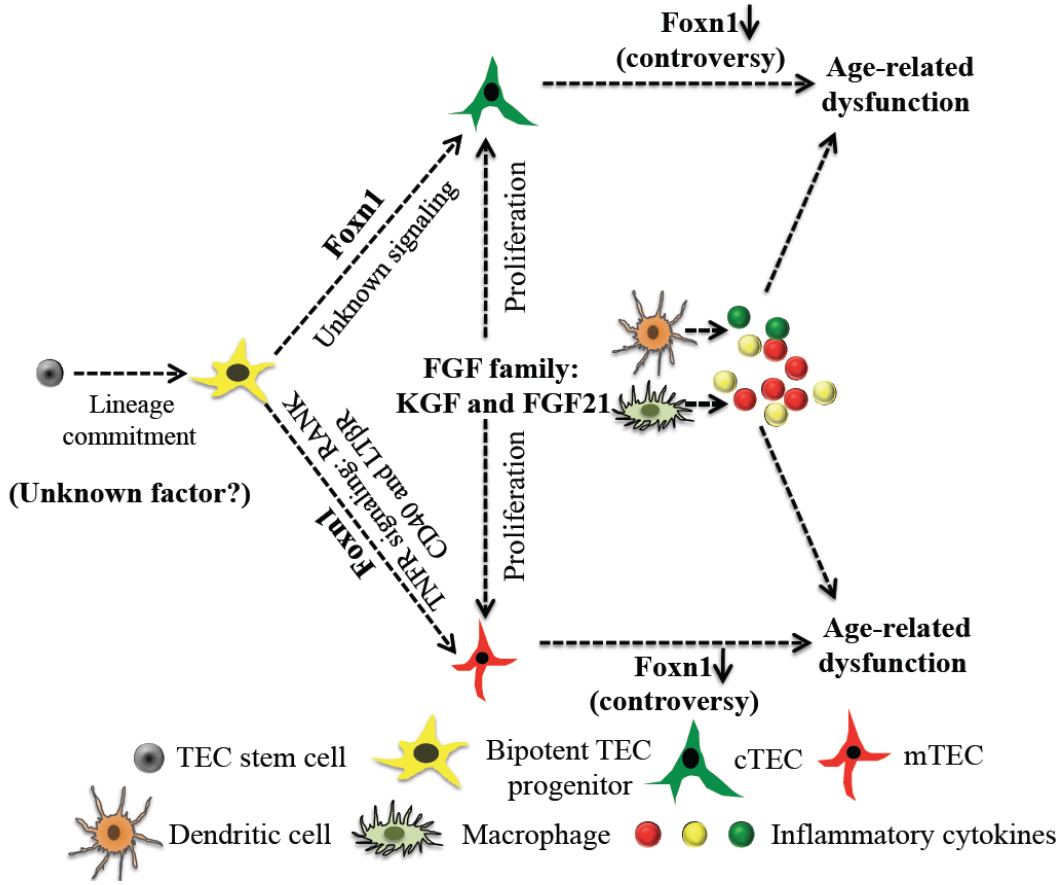

Fig 1-2. A summary of mechanisms involved in TEC development, maintenance and degeneration. While Foxn1 is not required for TEC-lineage commitment from TEC stem cells, it is essential for bipotent TEC progenitors to differentiate into either cTEC or mTEC sublineages and also plays a critical role in regulating proliferation of TEC subsets. Signaling pathways through TNF receptor (TNFR) super family members (RANK, CD40 and LTβR) play critical roles in inducing mTEC lineage development, however, it is still unknown which signaling pathway(s) derives cTEC lineage differentiation. FGF family members, such as KGF and FGF21, play a crucial role in regulating TEC proliferation in both fetal and postnatal thymus. The prevalent view suggests that down-regulation of Foxn1 expression and/or protein in TECs in the postnatal thymus triggers thymic involution, however, recent evidence fails to support this concept. Increased expression

of intrathymic inflammatory cytokines from dendritic cell and macrophage are known to play an important role in inducing age-associated alternation in TECs and leading to thymic involution.

RANK: Receptor Activator of Nuclear Factor κB; LTβR: Lymphotoxin β Receptor.

(Cheng et al., 2010; Ortman et al., 2002; Sun et al., 2010). Finally, transgenic mouse lines with overexpression of Foxn1 show 4-6 months delayed thymic involution (Zook et al., 2011), and forced TEC-specific upregulation of Foxn1 in involuted thymus leads to robust thymic regeneration characterized by increased thymopoiesis and naïve T-cell output (Bredenkamp et al., 2014). Thus, the Foxn1 expression and function is generally accepted as the prime mediator of thymus involution (Boehm and Swann, 2013). However, this notion requires a careful evaluation as several recent studies did not find a clear age-related down-regulation of Foxn1 mRNA and/or protein levels during thymic involution (Ki et al., 2014; O'Neill et al., 2016; Rode et al., 2015). For example, using a reporter, $Foxn1^{G}$ allele that is different from the one used by the Manley group, to moniter protein level of Foxn1 during embryogenesis and involution, the Blackburn group showed that there was no signicificant change of Foxn1 protein level in TEC subsets between 3-month and up to 20-month old mouse thymus, indicating that Foxn1 may not be physiologically involved in age-associated thymic involution (O'Neill et al., 2016). Since $Foxn1^{lacz/lacz}$ alleles used by Manley group resulted in artificial down-regulation of Foxn1 expression in TECs, the findings reported by $Foxn1^{G}$ allele from Blackburn group were likely to reflect bona fida expression of Foxn1 in TEC subsets during aging. Given that the thymus eventually undergoes involution even with sustained Foxn1 expression, further research is need to to identify Foxn1-independent mechanisms or pathways in thymic senescence.

Several cytokines have been shown to have thymostimulatory effects and improve thymopoiesis in aged mouse thymus. Fibroblast growth factor (FGF) family has recently received much attention as they exhibit potential for thymic regeneration. Keratinocyte

growth factor (KGF), also known as FGF7, has been well characterized in the TEC field as another key factor for thymic aging and regeneration. Signaling through the main receptor, FGF2R-IIIb, KGF has been demonstrated to play a vital role for fetal thymic organogenesis and for maintaining the integrity of the postnantal thymus *via* modulating TEC proliferation (Dooley et al., 2007; Erickson et al., 2002; Revest et al., 2001). Administration of KGF also increases thymic cellularity, enhances thymic thymopoiesis and naïve T-cell production, and accelerates T-cell functional reconstitution in aged mouse (Alpdogan et al., 2006; Min et al., 2007; Rossi et al., 2002; Rossi et al., 2007). Another FGF member, FGF21 (liver-derived metabolic hormone), has recently been identified as an immune-metabolic regulator that links metabolic and immune system to prevent T-cell immune senescence (Youm et al., 2016). Genetic overexpression of FGF21 significantly eliminates intrathymic adipocytes, restores TEC stromal architecture and augments naïve T-cell production in aged mouse thymus (Youm et al., 2016). These results suggest that approaches aimed at enhancing FGF21 signaling will lead to thymic rejuvenation and delay immune senescence, and will be of great therapeutic value.

Age-associated changes of intrathymic inflammatory cytokines have recently been documented as another category of mediators driving thymic involution. Early work analyzing human thymus samples revealed that thymic aging is associated with significantly elevated expression of proinflmamtory cytokines such as IL-6 family members, including IL-6, leukemia inhibitory factor (Lif) and oncostatin (OSM). The experimental administration of IL-6 family members induced acute thymic atrophy in murine models, suggesting an active role of inflammation in thymic senescence with aging (Sempowski et al., 2000; Sempowski et al., 2002). Global transcriptional profiling

of distinct thymic stromal cell subsets revealed that acquisition of proinflammatory features in myeloid lineage cells, sirpα^{+} DC and macrophage, represented the earliest molecular hallmarks during early thymic involution (Ki et al., 2014). This includes up-regulation of TNFα, IL-1α, IL-1β and IL-6, which have been implicated to play a role in the late stage of thymic involution. Interestingly, genetic overexpression of human TNF in mouse whole body induces a thymic atrophy phenotype with minimal effects on other immune organs/tissues, suggesting that the thymus is a sensitive immune tissue subject to inflammation insult (Liepinsh et al., 2009). Conversely, genetic ablation of components in NLRP3 inflammasome complex in macrophage to block production of IL-1β significantly delays age-related thymic atrophy and reduces intrathymic adipocytes, indicating that anti-inflammation may represent an effective means to delay or even prevent age-related thymic demise and improve T-cell mediated immune functions in the elderly (Youm et al., 2013; Youm et al., 2012). Consistent with this, anti-inflammatory Leptin has been shown to have therapeutic potential to protect against inflammation-induced murine thymic atrophy (Aschenbrenner et al., 2007). Whereas inflammatory cytokines are unambiguously involved in aged-related thymic degeneration, the direct effects of these cytokines on TECs have not determined because most research focus on intrathymic changes in the whole thymus organ (Billard et al., 2011). Since TECs are the primary cell types responsible for age-related involution and since senescence and cellular morphological changes have been well documented in the aged thymus (Aw et al., 2008; Palmer, 2013), one of the key questions remaining is how inflammatory cytokines lead to intracellular architectural changes in TECs and how defective structural changes induce TEC aging phenotypes.

Nuclear lamins link inflammation to tissue homeostasis and aging

In eukaryotic cells, the nucleus is the major organelle that stores, replicates and transcribes genetic information. The nucleus is enclosed by a double-membrane nuclear envelope, which separates cytoplasmic and nuclear compartments. The nuclear lamina (NL), a major structural meshwork underneath nuclear envelope, has recently gained more interest because mutations in components of the NL are the main causes of a spectrum of human diseases known as laminopathies (Schreiber and Kennedy, 2013). The major components of the NL are the A-type and B-type nuclear lamins, which are the type V intermediate filament (IF) proteins critically important for the structural properties of the nucleus. In mammals, *Lmna* (mouse) expresses all A-type lamins including lamin-A, lamin-C (collectively termed as lamin-A/C) and other splicing isoforms. There are two major mammalian B-type lamins: lamin-B1 and lamin-B2. They are ubiquitously expressed in somatic cells and are encoded by *Lmnb1* and *Lmnb2* (mouse), respectively. Lamin-B3 is a testis-specific lamin protein derived from *Lmnb2* by alternative splicing.

Lamins have been implicated in the regulation of numerous nuclear processes, such as nuclear assembly, DNA replication, transcriptional regulation, and chromatin organization (Burke and Stewart, 2013; Dechat et al., 2008). Consequently, B-type lamins have been assumed as housekeeping proteins necessary for basic cell viability. However, more recent studies from our lab demonstrate that mouse embryonic stem cells (mESCs) lacking all lamins can still self-renew and undergo differentiation into different cell types *in vitro* (Kim et al., 2011; Kim et al., 2013). Therefore, lamins are not required for survival at least in mESCs. B-type lamins are also reported to be dispensable for certain cell types such as the skin keratinocytes and hepatocytes *in vivo* (Yang et al.,

2011). The studies of lamins in different model organisms indicate that B-type lamins are required for proper development of some but not all organs during organogenesis (i.e., brain, diaphragm, testis) (Chen et al., 2013; Kim et al., 2011), indicating that B-type lamins may function in a cell-type dependent manner. New work from our lab further demonstrates that the assembly of each lamin into the NL and the location of other nuclear proteins depend primarily on the total lamin protein concentration present in the nucleus, suggesting that cells or tissues may exhibit different requirements for a specific lamin protein (Guo et al., 2014; Guo and Zheng, 2015). These findings provide new insights into the mechanism by which B-type lamins exhibit differential effects on the building of different organs *in vivo*.

In additional to developmental functions, lamin-B1 has recently been suggested to be involved in regulating tissue maintenance and aging. Replicative senescence of *in vitro* cultured mammalian fibroblasts has long been shown to be associated with lamin-B1 reduction, alteration of nuclear structure and chromatin organization, and increased secretion of inflammatory cytokine (Campisi, 2013; Freund et al., 2012; Kuilman et al., 2010). This senescence phenomenon is also called senescence-associated secretory phenotype (SASP) (Coppe et al., 2008). With respect to mechanism, activation of either tumor suppressor Rb or p53 is sufficient to induce lamin-B1 reduction and cellular senescence (Freund et al., 2012; Shimi et al., 2011). Further evidence suggests that lamin-B1 loss is a key trigger of global and local chromatin landscape changes that can impact gene expression in senescence (Sadaie et al., 2013; Shah et al., 2013). In addition, lamin-B1 reduction is also observed in senescence-prone cells derived from Progeria patients (premature aging) with shorten telomeres, indicating that lamin-B1 reduction may further

enhance cellular aging (Scaffidi and Misteli, 2005). Thus, lamin-B1 loss or reduction is proposed as a new biomarker of cellular senescence.

Whereas cellular senescence induced by Rb and p53 can lead to lamin-B1 reduction during cellular aging in tissue cultures, it remains largely unknown whether lamin-B1 reduction occurs *in vivo* upon aging since it is difficult to quantify lamin protein level in mammalian tissues composed of heterogeneous cell types derived from different origins. A direct link between lamin-B1 loss and tissue homeostasis and/or aging came from our lab's recent study of the role of lamin-B in the *Drosophila* immune organ called the fat body (Chen et al., 2014). Lamin-B reduction, but not A-type lamin, was apparent in cells of fat body upon aging and it induced age-associated systemic inflammation *via* up-regulation of the immune deficiency (IMD, equivalent to mammalian TNFa signaling pathway) signaling pathway, leading to increased secretion of circulating inflammatory cytokines, peptidoglaycan recognition proteins (PGRPs). Elevated circulating PGRPs in turn repress the IMD activity in the midgut and trigger overproliferation of intestinal stem cells and gut hyperplasia in aged flies (Fig. 1-3). Of interest, the immune response genes are significantly enriched in lamin-B associated chromatin domains, also known as LADs. Considering that lamins are known to repress gene expression, age-related lamin-B loss may de-repress the expression of immune genes, especially inflammatory cytokines, inducing local inflammation and tissue deterioration. While it has long been suspected that some cell-intrinsic defects may contribute to age-related chronic inflammation (inflammaging) (Franceschi et al., 2000), this study in fly provided the first line evidence by identifying a single nuclear defect, the loss of lamin-B upon aging, leading to systemic inflammation and disruption of tissue

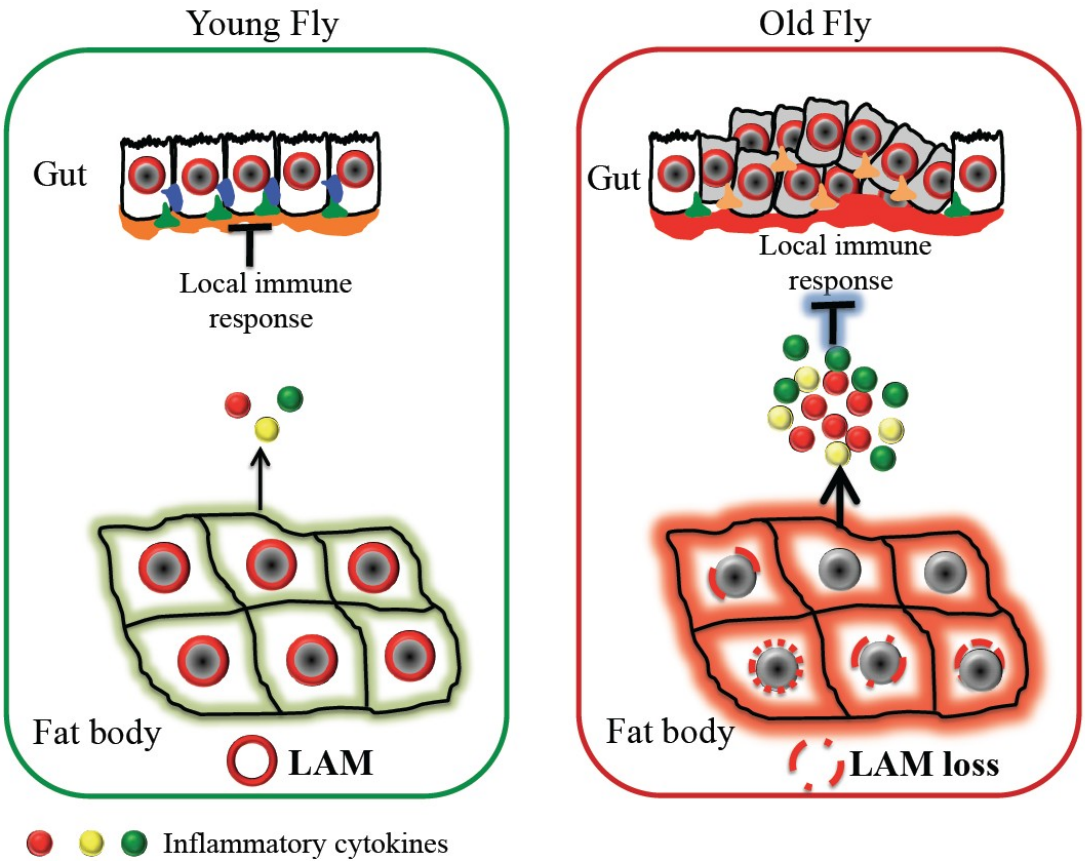

Fig 1-3. A model for age-related lamin-B loss-induced systemic inflammation in fly. Loss of lamin-B occurs in the cells in fat body in old fly, which in turn leads to derepression of inflammatory cytokines secreted into the circulation. Elevated circulating inflammatory cytokines then repress the local immune response in the midgut and result in over-proliferation and inappropriate differentiation of intestinal stem cells and gut hyperplasia. LAM: Lamin-B (fly).

homeostasis. Interestingly, lamin-B loss does not occur in all tissues in the fly upon aging, suggesting that age-associated lamin-B loss occurs in a cell-type and tissue-specific manner. Thus, a systematic examination to establish which cell/tissue type(s) undergoes age-related reduction of lamin-B in mammals would provide clues to the cause and consequence of lamin loss *in vivo*. Deciphering how aging results in lamin-B loss and the consequence of lamin-B loss should provide new insights into the mechanisms mediating human diseases that result from aging-associated tissue deterioration. One part of my thesis work has focused on using the thymic TECs as a model to investigate how lamin-B1 contributes to immune tissue homeostasis and function. A better understanding of how lamin-B1 regulates immune homeostasis will aid the identification of new therapeutic targets that improve immune function in aged individuals. In Charpter 2, I will report a new method to quantify the protein level of nuclear lamins and identification of an age-associated reduction of lamin-B1 phenotype in TECs. In Charpter 3, I will focus on characterization of lamin-B1 functions in TECs. In Charpter 4, I will talk about lamin-B1-mediated transcriptional signatures in TECs based on RNA-seq data.

II. ChIP-seq: an emerging genome-wide profiling techology

Understanding how lamins, especially lamin-B1, regulate chromatin/genome organization and gene transcription is critical to decipher the underlying mechanism by which lamin-B1 loss contributes to tissue damage and aging *in vivo*. With recent technological progress and increased affordability of the next-generation sequencing techology, Chromatin immunoprecipitation coupled with sequencing (ChIP-seq) has become a widely used approach for genome-wide mapping of transcription/chromatin

regulatory factor binding and histone modifications as it offers higher resolution, fewer artefacts and substantially improved data quality compared to its counterpart ChIP-chip (Park, 2009). Due to significant DNA loss during multiple-step manipulations (Fig. 1-4) and inefficient ligation step in library preparation, standard ChIP-seq methods generally require large amounts of starting material (~10 ng enriched DNA or $>10^6$ cells) for reliable and high-quality mapping which significantly precludes its application to rare cell populations *in vivo*, such as stem and/or progenitors cells (Furey, 2012; Park, 2009). Recently, several groups reported novel ChIP-seq protocols to minimize the required cell number and adapatation for *in vivo* application. In this section, I will briefly describe recent progress in developing new ChIP-seq methods and emphasize on their advantages and possible drawbacks.

Pre-amplication of ChIP enriched DNA (ChIPed DNA) before sequencing library preparation allows the scaling down of the initial cell number requirement to as few as 10^4 cells. LinDA-ChIP-seq (single-tube linear DNA amplification) has been applied to profiling of the oestrogen receptor-a (ERa) and histone H3K4 trimethlyation (H3K4Me3) modification using 10,000 cells (Shankaranarayanan et al., 2011). The key to this protocol is to ligate adaptors with T7 promoter to ChIPed DNA and then convert DNA to more RNA molecules throught T7 RNA polymerase-mediated linear amplification. Pre-amplifed RNAs are then converted to DNA for further sequencing library preparation. While it avoids amplification bias common in PCR-based approaches, the reproducibility of this protocol fails to meet the standard criterion for 80% precision by ENCODE project. Another method, called Nano-ChIP-seq, pre-amplifies the small amount of ChIPed DNA using a pair of custom designed hairpin-shaped primers that prevent

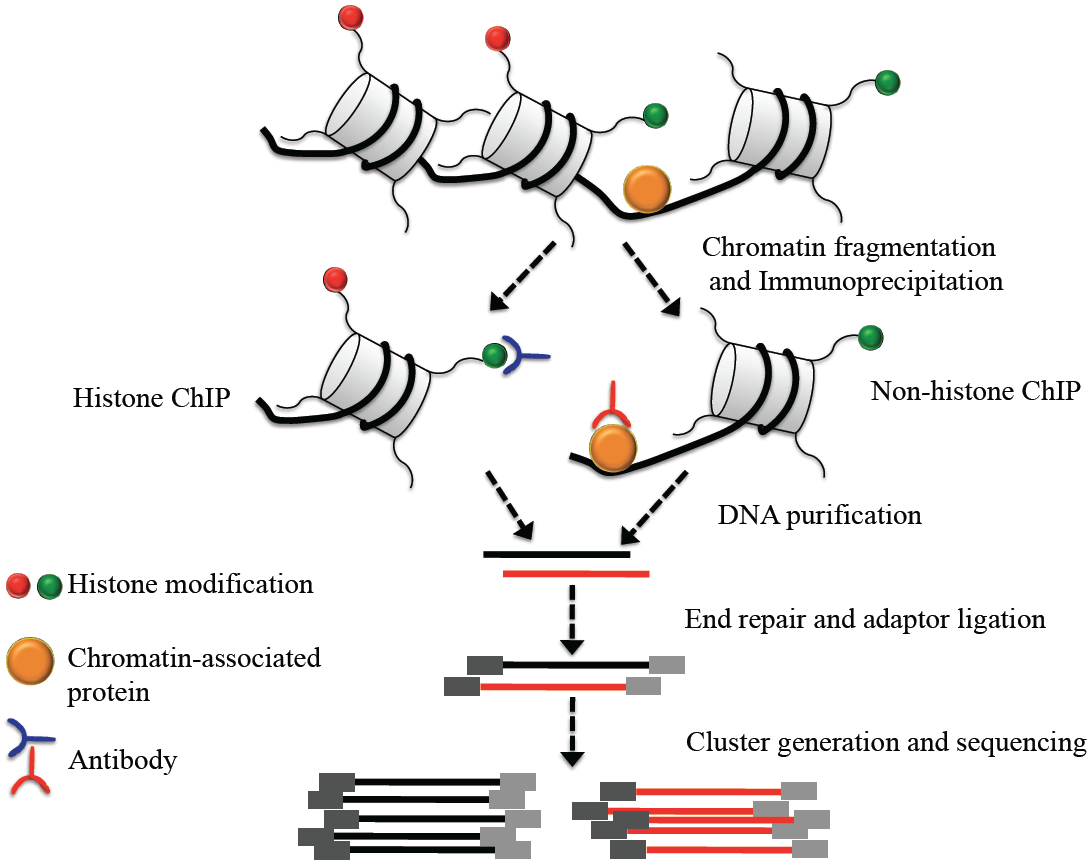

Fig 1-4. An overview of a ChIP-seq experiment. Left: profiling of histone modifications. Right: profiling of transcription factors or other chromatin-associated proteins.

self-annealing during PCR amplification (Adli et al., 2010). The hairpin primers contain a restriction site that allows ligation of illumina adaptors for direct sequencing. Although it has been applied for mapping chromatin modifications histone H3 lysine 4 trimethylation (H3K4Me3) and histone H3 lysine 27 trimethylation (H3K27Me3) in 10,000 sorted mouse bone marrow hematopoietic progenitor cells, it relies on increasing amplification cycles (4 cycles of primer extension and 5 more cycles of PCR than the Illumina standard protocol) and introduces increased amounts of mapping bias and unmapped reads in the final sequencing library. The major defect of these two protocols is failure to protect DNA loss during ChIP procedure as low-abundance ChIPed DNA may be underrepresented or lost before any kind of pre-amplication methods.

An alternative approach is to perform barcoding to first label fragmented chromatin in individual samples and then pooling of multiple chromatin-barcoded samples for ChIP in the same reaction. The first implementation of this principle, called indexing-first ChIP-seq (iChIP), reported a significant reduction of the intial cell number for ChIP-seq even down to a few hundred cells (Lara-Astiaso et al., 2014). While this protocol dramatically reduces DNA loss by sample pooling, ligation of barcoding adaptors to chromatin fragments is performed on magnetic beads, which dramatically reduces ligation efficiency. Indeed, the new work published by the same group showed that only 2-3% of chromatin fragments were added barcoding adaptors (Gury-BenAri et al., 2016), indicating that more than 97% of initial material was lost in this protocol for final ChIP-seq and thus 10,000-20,000 sorted hematopoietic stem cells (HSCs) were used in their original iChIP-seq database. Three recent publications report updated versions of this protocol, which introduce T7-promoter to barcoding adaptors to allow combination

of chromatin-barcoding pooling and T7-mediated pre-amplication of ChIPed DNA (Rotem et al., 2015; van Galen et al., 2016; Weiner et al., 2016). With the aid of new approach, the Amit group recently provided a comprenhesive genome-wide mapping of co-occurrence of 14 histone modifications in primary bone marrow derived dendritic cells (BMDC) and reported previously undescribed co-occurrence patterns such as co-existence of H3K9 monomethlyation (H3K9Me1) and H3K27 acetylation (H3K27ac) in super-enhancers (Weiner et al., 2016). While these studies are promising, a later study showed that the improved protocals only gave 7-8% recovery of T7-barcoded chromatin and still incurred more than 90% loss of chromatin (Gury-BenAri et al., 2016), preventing these approaches for general application to rare cell populations *in vivo*.

Micrococcal nuclease (MNase) is commonly used to digest uncrosslinked chromatin and is generally preferred in epigenetic profiling with a small cell number input since it removes linker DNA more efficiently than sonication, which allows more precise mapping at a single nucleosome resolution. Recently, an optimized MNase-based native Uli-NChIP-seq (Ultra-low-input Native ChIP-seq) was reported to profile genome-wide histone modifications using as few as 10^3 mESCs (Brind'Amour et al., 2015). While Uli-NChIP-seq offers acceptable mapping quality for abundant histone modifications such as H3K9Me3 and H3K27Me3 using 10^3 cells, it still suffers significant loss of ChIPed DNA and requires ~10,000 cells for reliable profiling of less abundant markers like H3K4Me3.

Despite much progress made from above mentioned approaches, a common defect from these methods is failure to consider protection of material during multiple-step processing in ChIP-seq, precluding reliable high-quality profiling in low cell number

application *in vivo*. In the last chapter of the thesis, I will report a new strategy for high-fidelity genome-wide profiling using as few as 500 cells and its application in the study of hematopoiesis.

Reference

Adli, M., Zhu, J., and Bernstein, B.E. (2010). Genome-wide chromatin maps derived from limited numbers of hematopoietic progenitors. Nat Methods *7*, 615-618.

Alpdogan, O., Hubbard, V.M., Smith, O.M., Patel, N., Lu, S., Goldberg, G.L., Gray, D.H., Feinman, J., Kochman, A.A., Eng, J.M.*, et al.* (2006). Keratinocyte growth factor (KGF) is required for postnatal thymic regeneration. Blood *107*, 2453-2460.

Anderson, G., and Jenkinson, E.J. (2001). Lymphostromal interactions in thymic development and function. Nat Rev Immunol *1*, 31-40.

Anderson, G., and Takahama, Y. (2012). Thymic epithelial cells: working class heroes for T cell development and repertoire selection. Trends Immunol *33*, 256-263.

Anderson, M.S., Venanzi, E.S., Klein, L., Chen, Z., Berzins, S.P., Turley, S.J., von Boehmer, H., Bronson, R., Dierich, A., Benoist, C.*, et al.* (2002). Projection of an immunological self shadow within the thymus by the aire protein. Science *298*, 1395-1401.

Aschenbrenner, K., D'Cruz, L.M., Vollmann, E.H., Hinterberger, M., Emmerich, J., Swee, L.K., Rolink, A., and Klein, L. (2007). Selection of Foxp3+ regulatory T cells specific for self antigen expressed and presented by Aire+ medullary thymic epithelial cells. Nat Immunol *8*, 351-358.

Aw, D., Silva, A.B., Maddick, M., von Zglinicki, T., and Palmer, D.B. (2008). Architectural changes in the thymus of aging mice. Aging Cell *7*, 158-167.

Benz, C., Heinzel, K., and Bleul, C.C. (2004). Homing of immature thymocytes to the subcapsular microenvironment within the thymus is not an absolute requirement for T cell development. Eur J Immunol *34*, 3652-3663.

Billard, M.J., Gruver, A.L., and Sempowski, G.D. (2011). Acute endotoxin-induced thymic atrophy is characterized by intrathymic inflammatory and wound healing responses. PLoS One *6*, e17940.

Blackburn, C.C., Augustine, C.L., Li, R., Harvey, R.P., Malin, M.A., Boyd, R.L., Miller, J.F., and Morahan, G. (1996). The nu gene acts cell-autonomously and is required for differentiation of thymic epithelial progenitors. Proc Natl Acad Sci U S A *93*, 5742-5746.

Boehm, T., and Swann, J.B. (2013). Thymus involution and regeneration: two sides of the same coin? Nat Rev Immunol *13*, 831-838.

Bredenkamp, N., Nowell, C.S., and Blackburn, C.C. (2014). Regeneration of the aged thymus by a single transcription factor. Development *141*, 1627-1637.

Brind'Amour, J., Liu, S., Hudson, M., Chen, C., Karimi, M.M., and Lorincz, M.C. (2015). An ultra-low-input native ChIP-seq protocol for genome-wide profiling of rare cell populations. Nat Commun *6*, 6033.

Burke, B., and Stewart, C.L. (2013). The nuclear lamins: flexibility in function. Nat Rev Mol Cell Biol *14*, 13-24.

Campisi, J. (2013). Aging, cellular senescence, and cancer. Annu Rev Physiol *75*, 685-705.

Chen, H., Chen, X., and Zheng, Y. (2013). The nuclear lamina regulates germline stem cell niche organization via modulation of EGFR signaling. Cell Stem Cell *13*, 73-86.

Chen, H., Zheng, X., and Zheng, Y. (2014). Age-associated loss of lamin-B leads to systemic inflammation and gut hyperplasia. Cell *159*, 829-843.

Chen, L., Xiao, S., and Manley, N.R. (2009). Foxn1 is required to maintain the postnatal thymic microenvironment in a dosage-sensitive manner. Blood *113*, 567-574.

Cheng, L., Guo, J., Sun, L., Fu, J., Barnes, P.F., Metzger, D., Chambon, P., Oshima, R.G., Amagai, T., and Su, D.M. (2010). Postnatal tissue-specific disruption of transcription factor FoxN1 triggers acute thymic atrophy. J Biol Chem *285*, 5836-5847.

Coppe, J.P., Patil, C.K., Rodier, F., Sun, Y., Munoz, D.P., Goldstein, J., Nelson, P.S., Desprez, P.Y., and Campisi, J. (2008). Senescence-associated secretory phenotypes reveal cell-nonautonomous functions of oncogenic RAS and the p53 tumor suppressor. PLoS Biol *6*, 2853-2868.

Cowan, J.E., Parnell, S.M., Nakamura, K., Caamano, J.H., Lane, P.J., Jenkinson, E.J., Jenkinson, W.E., and Anderson, G. (2013). The thymic medulla is required for Foxp3+ regulatory but not conventional CD4+ thymocyte development. J Exp Med *210*, 675-681.

Dechat, T., Pfleghaar, K., Sengupta, K., Shimi, T., Shumaker, D.K., Solimando, L., and Goldman, R.D. (2008). Nuclear lamins: major factors in the structural organization and function of the nucleus and chromatin. Genes Dev *22*, 832-853.

Dooley, J., Erickson, M., Larochelle, W.J., Gillard, G.O., and Farr, A.G. (2007). FGFR2IIIb signaling regulates thymic epithelial differentiation. Dev Dyn *236*, 3459-3471.

Erickson, M., Morkowski, S., Lehar, S., Gillard, G., Beers, C., Dooley, J., Rubin, J.S., Rudensky, A., and Farr, A.G. (2002). Regulation of thymic epithelium by keratinocyte growth factor. Blood *100*, 3269-3278.

Franceschi, C., Bonafe, M., Valensin, S., Olivieri, F., De Luca, M., Ottaviani, E., and De Benedictis, G. (2000). Inflamm-aging. An evolutionary perspective on immunosenescence. Ann N Y Acad Sci *908*, 244-254.

Freund, A., Laberge, R.M., Demaria, M., and Campisi, J. (2012). Lamin B1 loss is a senescence-associated biomarker. Mol Biol Cell *23*, 2066-2075.

Furey, T.S. (2012). ChIP-seq and beyond: new and improved methodologies to detect and characterize protein-DNA interactions. Nat Rev Genet *13*, 840-852.

Gordon, J., Bennett, A.R., Blackburn, C.C., and Manley, N.R. (2001). Gcm2 and Foxn1 mark early parathyroid- and thymus-specific domains in the developing third pharyngeal pouch. Mech Dev *103*, 141-143.

Gordon, J., and Manley, N.R. (2011). Mechanisms of thymus organogenesis and morphogenesis. Development *138*, 3865-3878.

Gordon, J., Wilson, V.A., Blair, N.F., Sheridan, J., Farley, A., Wilson, L., Manley, N.R., and Blackburn, C.C. (2004). Functional evidence for a single endodermal origin for the thymic epithelium. Nat Immunol *5*, 546-553.

Guo, Y., Kim, Y., Shimi, T., Goldman, R.D., and Zheng, Y. (2014). Concentration-dependent lamin assembly and its roles in the localization of other nuclear proteins. Mol Biol Cell *25*, 1287-1297.

Guo, Y., and Zheng, Y. (2015). Lamins position the nuclear pores and centrosomes by modulating dynein. Mol Biol Cell *26*, 3379-3389.

Gury-BenAri, M., Thaiss, C.A., Serafini, N., Winter, D.R., Giladi, A., Lara-Astiaso, D., Levy, M., Salame, T.M., Weiner, A., David, E.*, et al.* (2016). The Spectrum and Regulatory Landscape of Intestinal Innate Lymphoid Cells Are Shaped by the Microbiome. Cell *166*, 1231-1246 e1213.

Jotereau, F., Heuze, F., Salomon-Vie, V., and Gascan, H. (1987). Cell kinetics in the fetal mouse thymus: precursor cell input, proliferation, and emigration. J Immunol *138*, 1026-1030.

Ki, S., Park, D., Selden, H.J., Seita, J., Chung, H., Kim, J., Iyer, V.R., and Ehrlich, L.I. (2014). Global transcriptional profiling reveals distinct functions of thymic stromal subsets and age-related changes during thymic involution. Cell Rep *9*, 402-415.

Kim, Y., Sharov, A.A., McDole, K., Cheng, M., Hao, H., Fan, C.M., Gaiano, N., Ko, M.S., and Zheng, Y. (2011). Mouse B-type lamins are required for proper organogenesis but not by embryonic stem cells. Science *334*, 1706-1710.

Kim, Y., Zheng, X., and Zheng, Y. (2013). Proliferation and differentiation of mouse embryonic stem cells lacking all lamins. Cell Res *23*, 1420-1423.

Klein, L., Hinterberger, M., Wirnsberger, G., and Kyewski, B. (2009). Antigen presentation in the thymus for positive selection and central tolerance induction. Nat Rev Immunol *9*, 833-844.

Klug, D.B., Carter, C., Crouch, E., Roop, D., Conti, C.J., and Richie, E.R. (1998). Interdependence of cortical thymic epithelial cell differentiation and T-lineage commitment. Proc Natl Acad Sci U S A *95*, 11822-11827.

Klug, D.B., Carter, C., Gimenez-Conti, I.B., and Richie, E.R. (2002). Cutting edge: thymocyte-independent and thymocyte-dependent phases of epithelial patterning in the fetal thymus. J Immunol *169*, 2842-2845.

Kuilman, T., Michaloglou, C., Mooi, W.J., and Peeper, D.S. (2010). The essence of senescence. Genes Dev *24*, 2463-2479.

Lara-Astiaso, D., Weiner, A., Lorenzo-Vivas, E., Zaretsky, I., Jaitin, D.A., David, E., Keren-Shaul, H., Mildner, A., Winter, D., Jung, S.*, et al.* (2014). Immunogenetics. Chromatin state dynamics during blood formation. Science *345*, 943-949.

Liepinsh, D.J., Kruglov, A.A., Galimov, A.R., Shakhov, A.N., Shebzukhov, Y.V., Kuchmiy, A.A., Grivennikov, S.I., Tumanov, A.V., Drutskaya, M.S., Feigenbaum, L.*, et al.* (2009). Accelerated thymic atrophy as a result of elevated homeostatic expression of the genes encoded by the TNF/lymphotoxin cytokine locus. Eur J Immunol *39*, 2906-2915.

Lind, E.F., Prockop, S.E., Porritt, H.E., and Petrie, H.T. (2001). Mapping precursor movement through the postnatal thymus reveals specific microenvironments supporting defined stages of early lymphoid development. J Exp Med *194*, 127-134.

Manley, N.R., Richie, E.R., Blackburn, C.C., Condie, B.G., and Sage, J. (2011). Structure and function of the thymic microenvironment. Front Biosci (Landmark Ed) *16*, 2461-2477.

Min, D., Panoskaltsis-Mortari, A., Kuro, O.M., Hollander, G.A., Blazar, B.R., and Weinberg, K.I. (2007). Sustained thymopoiesis and improvement in functional immunity induced by exogenous KGF administration in murine models of aging. Blood *109*, 2529-2537.

Misslitz, A., Pabst, O., Hintzen, G., Ohl, L., Kremmer, E., Petrie, H.T., and Forster, R. (2004). Thymic T cell development and progenitor localization depend on CCR7. J Exp Med *200*, 481-491.

Mori, S., Shortman, K., and Wu, L. (2001). Characterization of thymus-seeding precursor cells from mouse bone marrow. Blood *98*, 696-704.

Nehls, M., Kyewski, B., Messerle, M., Waldschutz, R., Schuddekopf, K., Smith, A.J., and Boehm, T. (1996). Two genetically separable steps in the differentiation of thymic epithelium. Science *272*, 886-889.

Nehls, M., Pfeifer, D., Schorpp, M., Hedrich, H., and Boehm, T. (1994). New member of the winged-helix protein family disrupted in mouse and rat nude mutations. Nature *372*, 103-107.

Nowell, C.S., Bredenkamp, N., Tetelin, S., Jin, X., Tischner, C., Vaidya, H., Sheridan, J.M., Stenhouse, F.H., Heussen, R., Smith, A.J.*, et al.* (2011). Foxn1 regulates lineage progression in cortical and medullary thymic epithelial cells but is dispensable for medullary sublineage divergence. PLoS Genet *7*, e1002348.

O'Neill, K.E., Bredenkamp, N., Tischner, C., Vaidya, H.J., Stenhouse, F.H., Peddie, C.D., Nowell, C.S., Gaskell, T., and Blackburn, C.C. (2016). Foxn1 Is Dynamically Regulated in Thymic Epithelial Cells during Embryogenesis and at the Onset of Thymic Involution. PLoS One *11*, e0151666.

Ohigashi, I., Zuklys, S., Sakata, M., Mayer, C.E., Hamazaki, Y., Minato, N., Hollander, G.A., and Takahama, Y. (2015). Adult Thymic Medullary Epithelium Is Maintained and Regenerated by Lineage-Restricted Cells Rather Than Bipotent Progenitors. Cell Rep *13*, 1432-1443.

Ortman, C.L., Dittmar, K.A., Witte, P.L., and Le, P.T. (2002). Molecular characterization of the mouse involuted thymus: aberrations in expression of transcription regulators in thymocyte and epithelial compartments. Int Immunol *14*, 813-822.

Palamaro, L., Romano, R., Fusco, A., Giardino, G., Gallo, V., and Pignata, C. (2014). FOXN1 in organ development and human diseases. Int Rev Immunol *33*, 83-93.

Palmer, D.B. (2013). The effect of age on thymic function. Front Immunol *4*, 316.

Park, P.J. (2009). ChIP-seq: advantages and challenges of a maturing technology. Nat Rev Genet *10*, 669-680.

Plotkin, J., Prockop, S.E., Lepique, A., and Petrie, H.T. (2003). Critical role for CXCR4 signaling in progenitor localization and T cell differentiation in the postnatal thymus. J Immunol *171*, 4521-4527.

Revest, J.M., Suniara, R.K., Kerr, K., Owen, J.J., and Dickson, C. (2001). Development of the thymus requires signaling through the fibroblast growth factor receptor R2-IIIb. J Immunol *167*, 1954-1961.

Rode, I., Martins, V.C., Kublbeck, G., Maltry, N., Tessmer, C., and Rodewald, H.R. (2015). Foxn1 Protein Expression in the Developing, Aging, and Regenerating Thymus. J Immunol *195*, 5678-5687.

Rossi, S., Blazar, B.R., Farrell, C.L., Danilenko, D.M., Lacey, D.L., Weinberg, K.I., Krenger, W., and Hollander, G.A. (2002). Keratinocyte growth factor preserves normal thymopoiesis and thymic microenvironment during experimental graft-versus-host disease. Blood *100*, 682-691.

Rossi, S.W., Jeker, L.T., Ueno, T., Kuse, S., Keller, M.P., Zuklys, S., Gudkov, A.V., Takahama, Y., Krenger, W., Blazar, B.R.*, et al.* (2007). Keratinocyte growth factor

(KGF) enhances postnatal T-cell development via enhancements in proliferation and function of thymic epithelial cells. Blood *109*, 3803-3811.

Rotem, A., Ram, O., Shoresh, N., Sperling, R.A., Goren, A., Weitz, D.A., and Bernstein, B.E. (2015). Single-cell ChIP-seq reveals cell subpopulations defined by chromatin state. Nat Biotechnol *33*, 1165-1172.

Sadaie, M., Salama, R., Carroll, T., Tomimatsu, K., Chandra, T., Young, A.R., Narita, M., Perez-Mancera, P.A., Bennett, D.C., Chong, H.*, et al.* (2013). Redistribution of the Lamin B1 genomic binding profile affects rearrangement of heterochromatic domains and SAHF formation during senescence. Genes Dev *27*, 1800-1808.

Scaffidi, P., and Misteli, T. (2005). Reversal of the cellular phenotype in the premature aging disease Hutchinson-Gilford progeria syndrome. Nat Med *11*, 440-445.

Schreiber, K.H., and Kennedy, B.K. (2013). When lamins go bad: nuclear structure and disease. Cell *152*, 1365-1375.

Sempowski, G.D., Hale, L.P., Sundy, J.S., Massey, J.M., Koup, R.A., Douek, D.C., Patel, D.D., and Haynes, B.F. (2000). Leukemia inhibitory factor, oncostatin M, IL-6, and stem cell factor mRNA expression in human thymus increases with age and is associated with thymic atrophy. J Immunol *164*, 2180-2187.

Sempowski, G.D., Rhein, M.E., Scearce, R.M., and Haynes, B.F. (2002). Leukemia inhibitory factor is a mediator of Escherichia coli lipopolysaccharide-induced acute thymic atrophy. Eur J Immunol *32*, 3066-3070.

Shah, P.P., Donahue, G., Otte, G.L., Capell, B.C., Nelson, D.M., Cao, K., Aggarwala, V., Cruickshanks, H.A., Rai, T.S., McBryan, T.*, et al.* (2013). Lamin B1 depletion in

senescent cells triggers large-scale changes in gene expression and the chromatin landscape. Genes Dev *27*, 1787-1799.

Shankaranarayanan, P., Mendoza-Parra, M.A., Walia, M., Wang, L., Li, N., Trindade, L.M., and Gronemeyer, H. (2011). Single-tube linear DNA amplification (LinDA) for robust ChIP-seq. Nat Methods *8*, 565-567.

Shimi, T., Butin-Israeli, V., Adam, S.A., Hamanaka, R.B., Goldman, A.E., Lucas, C.A., Shumaker, D.K., Kosak, S.T., Chandel, N.S., and Goldman, R.D. (2011). The role of nuclear lamin B1 in cell proliferation and senescence. Genes Dev *25*, 2579-2593.

Sun, L., Guo, J., Brown, R., Amagai, T., Zhao, Y., and Su, D.M. (2010). Declining expression of a single epithelial cell-autonomous gene accelerates age-related thymic involution. Aging Cell *9*, 347-357.

Takaba, H., Morishita, Y., Tomofuji, Y., Danks, L., Nitta, T., Komatsu, N., Kodama, T., and Takayanagi, H. (2015). Fezf2 Orchestrates a Thymic Program of Self-Antigen Expression for Immune Tolerance. Cell *163*, 975-987.

Takahama, Y. (2006). Journey through the thymus: stromal guides for T-cell development and selection. Nat Rev Immunol *6*, 127-135.

van Galen, P., Viny, A.D., Ram, O., Ryan, R.J., Cotton, M.J., Donohue, L., Sievers, C., Drier, Y., Liau, B.B., Gillespie, S.M.*, et al.* (2016). A Multiplexed System for Quantitative Comparisons of Chromatin Landscapes. Mol Cell *61*, 170-180.

Weiner, A., Lara-Astiaso, D., Krupalnik, V., Gafni, O., David, E., Winter, D.R., Hanna, J.H., and Amit, I. (2016). Co-ChIP enables genome-wide mapping of histone mark co-occurrence at single-molecule resolution. Nat Biotechnol *34*, 953-961.

Wong, K., Lister, N.L., Barsanti, M., Lim, J.M., Hammett, M.V., Khong, D.M., Siatskas, C., Gray, D.H., Boyd, R.L., and Chidgey, A.P. (2014). Multilineage potential and self-renewal define an epithelial progenitor cell population in the adult thymus. Cell Rep *8*, 1198-1209.

Yang, S.H., Chang, S.Y., Yin, L., Tu, Y., Hu, Y., Yoshinaga, Y., de Jong, P.J., Fong, L.G., and Young, S.G. (2011). An absence of both lamin B1 and lamin B2 in keratinocytes has no effect on cell proliferation or the development of skin and hair. Hum Mol Genet *20*, 3537-3544.

Youm, Y.H., Grant, R.W., McCabe, L.R., Albarado, D.C., Nguyen, K.Y., Ravussin, A., Pistell, P., Newman, S., Carter, R., Laque, A.*, et al.* (2013). Canonical Nlrp3 inflammasome links systemic low-grade inflammation to functional decline in aging. Cell Metab *18*, 519-532.

Youm, Y.H., Horvath, T.L., Mangelsdorf, D.J., Kliewer, S.A., and Dixit, V.D. (2016). Prolongevity hormone FGF21 protects against immune senescence by delaying age-related thymic involution. Proc Natl Acad Sci U S A *113*, 1026-1031.

Youm, Y.H., Kanneganti, T.D., Vandanmagsar, B., Zhu, X., Ravussin, A., Adijiang, A., Owen, J.S., Thomas, M.J., Francis, J., Parks, J.S.*, et al.* (2012). The Nlrp3 inflammasome promotes age-related thymic demise and immunosenescence. Cell Rep *1*, 56-68.

Zook, E.C., Krishack, P.A., Zhang, S., Zeleznik-Le, N.J., Firulli, A.B., Witte, P.L., and Le, P.T. (2011). Overexpression of Foxn1 attenuates age-associated thymic involution and prevents the expansion of peripheral CD4 memory T cells. Blood *118*, 5723-5731.

Chapter 2: Lamin-B1 in age-associated and inflammation-mediated acute thymic involution

Summary

The nuclear lamins have recently been suggested to play important roles in tissue building, homeostasis and aging. An age-associated reduction of B-type but not A-type lamin has been reported in cells in fat body from old *Drosophila* and contributes to heterochromatin loss and derepression of immune response genes, which in turn triggers systemic inflammation and tissue dysfunction. How aging triggers cell/tissue-specific lamin-B loss is not well understood. A systematic examination to identify which cell/tissue type(s) undergoes age-related reduction of lamins should provide clues to the cause(s) of loss. To achieve this aim, I developed a novel flow cytometry based method to quantify the protein level of nuclear lamins. By applying this new tool to the thymus, the primary immune organ for T-cell development, I identified an age-associated reduction of lamin-B1 in thymic epithelial cells (TECs). I further demonstrated that macrophage- and dendritic cell-derived proinflammatory cytokines led to lamin-B1 reduction in TECs, at least in part *via* cellular senescence. This new method is readily adaptable to other cell types from any tissue/organ by incorporating cell-specific marker(s), which should open doors to further investigate how advanced age leads to lamin loss in mammalian system and how this contributes to tissue/organ dysfunction and aging.

Introduction

Much effort has been devoted to study the functions of nuclear lamins in development and tissue homeostasis since the discovery that mutations in lamins and other components of the nuclear lamina (NL) cause a spectrum of rare human diseases collectively called laminopathies (Benedetti and Merlini, 2004; Gruenbaum et al., 2005; Mounkes et al., 2003). The recent mouse and *Drosophila* genetic studies have shown that lamins are required for proper development of multiple organs during organogenesis (Chen et al., 2013; Coffinier et al., 2010; Coffinier et al., 2011; Kim et al., 2011). Further studies are needed to dissect the mechanism by which lamins function in tissue building. Interestingly, lamin-B1 reduction has recently been linked to cellular senescence, which has been implicated in tissue aging and age-related diseases (Campisi, 2013; Campisi and d'Adda di Fagagna, 2007; Childs et al., 2015). Induction of cellular senescence is accompanied by nuclear lamin-B1 reduction in cultured primary cells *in vitro*, and lamin-B1 reduction occurs upon forced expression of oncogene Ras or activation of the downstream Rb or P53 tummor suppressor, both of which trigger senescence or cellular aging (Dreesen et al., 2013a; Dreesen et al., 2013b; Freund et al., 2012; Shimi et al., 2011). These *in vitro* findings suggest that nuclear lamin-B1 may contribute to tissue degenerative process *via* cellular senescence. *In vivo,* our lab reported for the first time that lamin-B loss in the cells in *Drosophila* immune organ, the fat body, led to systemic inflammation and tissue dysfunction, providing new insights into cause and consequence of immunosenescence during aging (Chen et al., 2014). However, the relevance of this to natural aging in mammals is unknown. Due to the complexity of cellular composition in mammalian tissue/organ(s), it is intrinsically difficult to quantify alterations in lamin

expression and identify which cell type(s) lose lamins during natural aging. In addition, standard immunofluorescence (IF) and Western blotting techniques are time-consuming and are not suitable for systematic survey of cell/tissue types that undergo aging-related lamin alteration. This poses a significant impediment to deciphering how lamins function in the process of tissue maintenance and aging.

To solve the technical issues in properly quantifying lamins in specific cell types, I herein report the development of a new flow cytometry-based method using the mammalian immune system. Applying this methodology to the mouse thymus, I find a specific reduction of nuclear lamin-B1, but not lamin-B2 or Lamin-A/C, in thymic epithelial cells upon aging. The extent of lamin-B1 reduction correlates with a progressive reduction of the total cell number in the thymus, suggesting that age-associated lamin-B1 reduction in TECs contributes to thymus degeneration. I will focus on dissecting the functional roles of lamin-B1 in TECs for mediating thymic function in later chapters.

Results

Establishment of flow cytometry-based method to quantify nuclear lamins

The major issue associated with using IF to assess lamin protein levels is time-consuming due in part to the low efficacy of preparing multiple samples for cryosection slides, IF picture capture and post image processing. Western blotting also involves multiple steps and it usually takes 2-3 days to complete the whole process. To overcome these drawbacks, I adapted Biolegend's True-Nuclear Trascription Factor staining

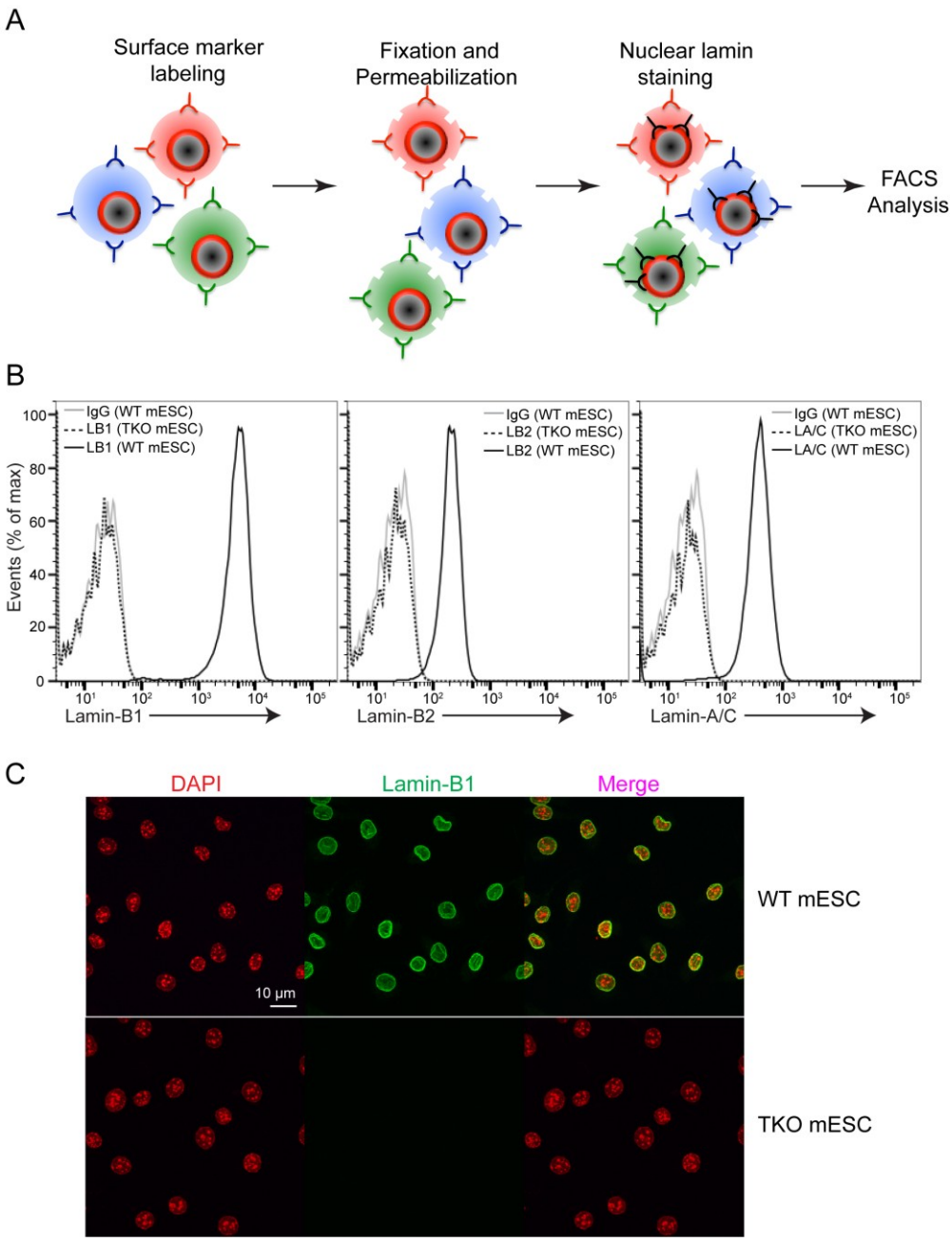

Fig 2-1. Flow cytometer-based method to quantify nuclear lamins. (A) Schematic diagram of procedure of the approach. (B) FACS histogram overlay of lamin-B1, lamin-B2 and lamin-A/C in WT mESCs (black solid line) and TKO mESCs (black dash line). Grey lines show lamin signals in IgG control. (C) Immunofluorescence images indicate lamin-B1 staining in the nuclear periphery of WT mESCs. Scale bars, 10 μm.

method for measuring nuclear lamins in individual cell types (see Materials and Methods and Fig. 2-1A). True-Nuclear Trascription Factor staining buffer has been optimized for intracellular staining with minimum effect on the surface marker staining since the method relies on different combinations of surface markers to distinguish distinct subtypes within the same tissue/organ. To validate the specificity of this assay, I first used Fluorescence-activated cell sorting (FACS) to compare fluorescence signal intensity of lamins from *Lmnb1, Lmnb2* and *Lmna* wild type (WT) and knockout (*Lmnb1*$^{-/-}$*; Lmnb2*$^{-/-}$*; Lmna*$^{-/-}$ *triple* KO or TKO) mouse embryonic stem cells (mESCs). In all tested lamin-TKO mESCs, I found fluorescence signal from the IgG control similar to background staining level (Fig. 2-1B), demonstrating the specificity of this method. To further confirm staining of lamins in the nucleus rather than non-specific binding to other components within cells, I applied FACS sorting to collect WT and TKO mESCs with lamin-B1 staining and adhered sorted mESCs to glass slides using cytospin. Then I examined the localization of lamin-B1 staining by confocal microscope. The confocal images demonstrated that this assay indeed detected the lamin-B1 at the nuclear periphery surrounding DAPI signal of DNA in the nucleus of WT mESCs (Fig. 2-1C).

Identification of lamin-B1 reduction in TECs in aged mouse thymus

Since the thymus is the first immune organ to undergo degeneration, I decided to test whether nuclear lamins play a role in this process. I first applied the lamin FACS assay to compare protein levels of all three lamins (lamin-B1/B2 and -A/C) in major cell types between 2-month-old young and 20-month-old aged wild-type (WT) mouse thymus. Preliminary analyses revealed no significant change of either lamin-B1 or lamin-B2

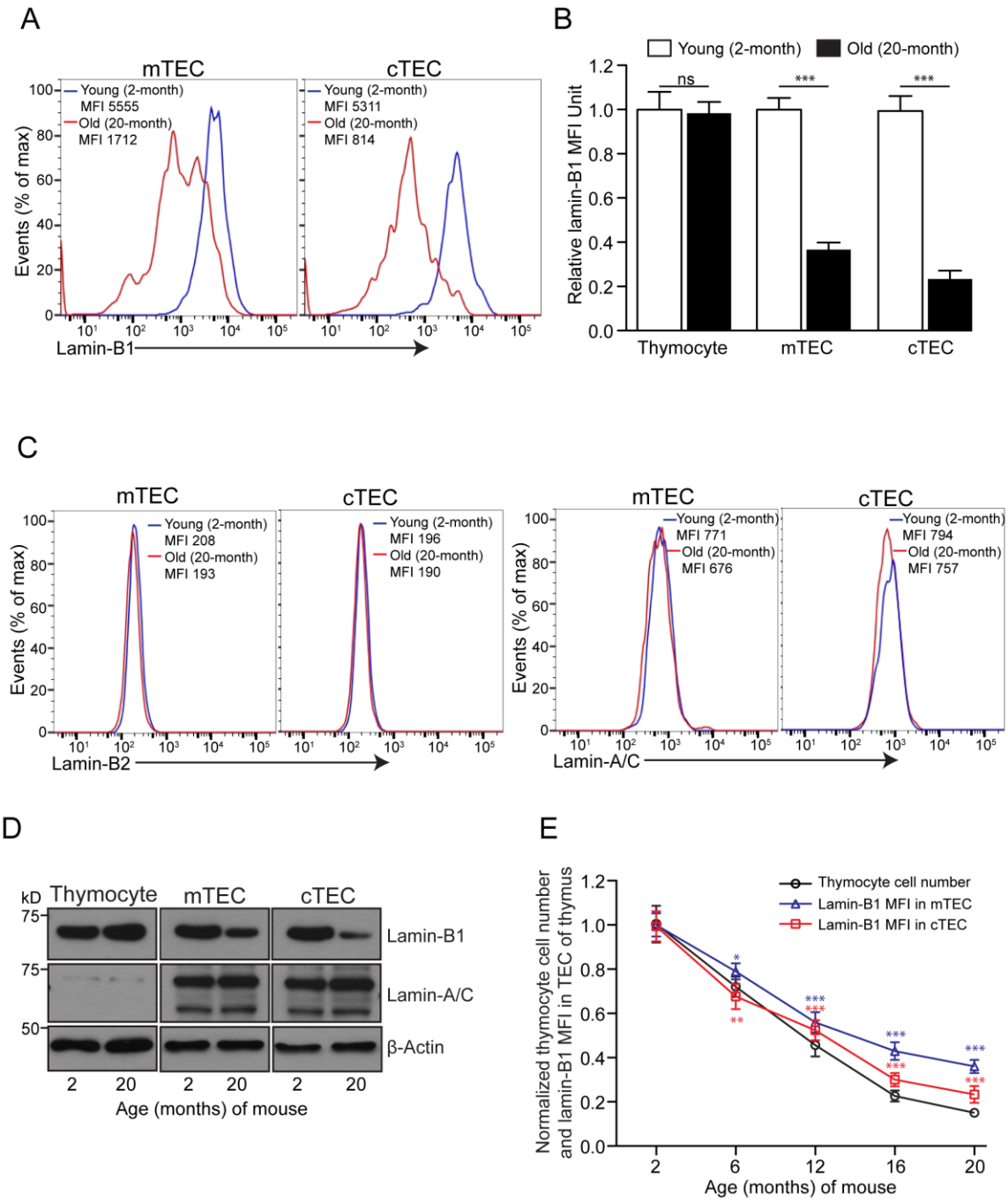

Fig 2-2. Lamin-B1 reduction in TECs correlates with thymic involution. (A) FACS histogram overlay of lamin-B1 in mTECs (left; surface markers: $CD45^{-}EpCAM^{+}Ly51^{-}$) and cTECs (right; surface markers: $CD45^{-}EpCAM^{+}Ly51^{+}$) isolated from 2-month-old young (blue line) and 20-month-old aged WT mouse thymus (red line). MFI: Mean fluorescence intensity. (B) Quantification of lamin-B1 MFI in thymocytes and TECs

between young and aged thymus from (A). MFI of lamin-B1 of thymocytes or TECs in young (2-month-old) mouse thymus is defined as 1. (C) FACS histogram overlay of lamin-B2 (left) and lamin-A/C (right) in mTECs and cTECs isolated from 2-month-old young (blue line) and 20-month-old aged WT thymus (red line). (D) Western blotting analyses of lamin-B1 and lamin-A/C in thymocytes, mTECs and cTECs from 2-month-old young and 20-month-old aged WT thymus. β-actin is used as a loading control. (E) Quantification of lamin-B1 MFI in mTECs (blue line) and cTECs (red line) in different stage thymuses, ranging from 2-month to 20-month of age. Total cell number of thymocytes (black line) shows age-related involution. Thymocyte cell number and MFI of lamin-B1 in TECs from 2-month-old thymus are defined as 1. All raw data of other time points are plotted relative to 2-month-old thymus. One representative Western blotting result of 2 independent experiments is shown for (D) and all other data shown are representative of at least 3 independent experiments. Error bars indicate SD of the mean from 3 independent experiments. Student's t test: *, $P < 0.05$; **, $P < 0.01$; ***, $P < 0.001$; ns, not significant.

protein in all examined hematopoietic stem cell (HSC) derived cells in the aged mouse thymus, including thymocyte subpopulations, macrophage and dendritic cell (DC) (data not shown; see Materials and Methods). Consistent with previous reports, I found that the expression of lamin-A/C in HSC-derived cells was significant lower compared to that of lamin-B1 or -B2. Thus, I did not include lamin-A/C analysis in HSC-derived cells in the aged thymus. Of interest, FACS analyses of mTECs and cTECs from 20-month-old aged mouse thymus showed a significant reduction of lamin-B1 in both cell types compared to that in 2-month-old young counterparts (Fig. 2-2A). I further used mean fluorescence intensity (MFI) to quantify the extent of lamin-B1 reduction. To simplify the comparison, I defined the MFI of lamin-B1 in young mouse thymus as 1. I found that there was more than 65% reduction of lamin-B1 protein in both aged mTEC and cTEC, but not in T cells (Fig. 2-2B). In order to test whether other lamins also exhibited similar reduction trends as shown in lamin-B1, I further assessed the protein levels of lamin-B2 and -A/C in both mTECs and cTECs between young and aged mouse thymus. However, I did not observe any significant change of either lamin-B2 or lamin-A/C under these conditions (Fig. 2-2C), suggesting that reduction of lamin-B1 but not lamin-B2 and -A/C specifically occurs in mTECs and cTECs in aged mouse thymus. In addition, I also applied Western blotting (Fig. 2-2D) and IF (data not shown) to assess lamin-B1 and -A/C protein levels in FACS-sorted TECs. The results of these tests further confirm the reduction of lamin-B1 in both mTECs and cTECs in the aged mouse thymus.

In order to gain more insights into the dynamics of lamin-B1 reduction in TECs and how this relates to the process of thymic involution, I further applied the lamin FACS assay to assess lamin-B1 protein levels in both mTECs and cTECs from different stages

of mouse thymus ranging from 2-month to 20-month of age. Since thymic involution leads to a reduction of thymocytes in the thymus, counts of thymocytes in different stage thymuses were used as an indicator for the degeneration process (Fig. 2-2E). I observed that the earliest time point of significant lamin-B1 reduction in both mTECs and cTECs occurred in ~6-month-old thymus, which coincided with the degeneration process of the thymus. Based on the curves of thymocyte counts and lamin-B1 levels, thymus involution trend continued with the trend of lamin-B1 reduction in TECs. This suggests that lamin-B1 reduction in TECs could be involved in thymic involution.

Age-associated increase of pro-inflammatory cytokines in the thymus leads to lamin-B1 reduction in TECs

Transcriptional profiling of thymic stromal subsets during early thymic involution revealed an augmented pro-inflammatory signature in DC subpopulation (Ki et al., 2014). Thymic macrophage has also been suggested to contribute to thymic involution *via* enhanced secretion of pro-inflammatory cytokines upon thymic aging, and genetic blockage of inflammasome activation in macrophage delays age-related thymic atrophy (Youm et al., 2012). Since inflammation in thymus appears at ~6 months, which coincides with the onset of lamin-B1 reduction in TECs and thymic degeneration (Fig. 2-2E), I reasoned that increased pro-inflammatory cytokines from thymic macrophage and DC might cause lamin-B1 reduction in TECs. In order to better understand the change of inflammation status in the thymus upon aging, I first applied FACS sorting to collect macrophage and DC subsets from the thymus at different ages (ranging from 2- to 20-month; Fig. 2-3A-D). Based on the surface expression of sirpα, I divided DC into sirpα^{+}

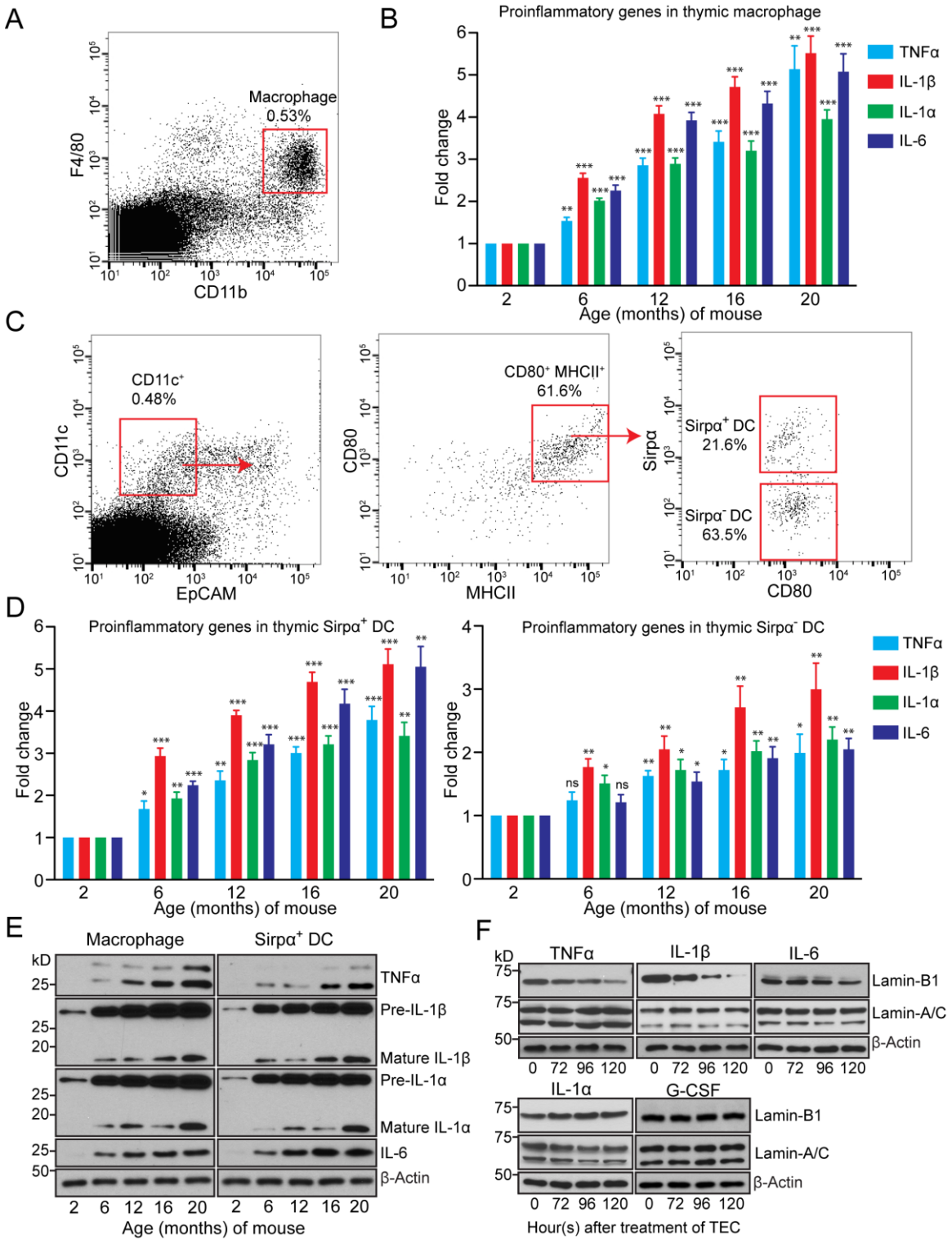

Fig 2-3. Increased proinflammatory cytokines in the thymus cause lamin-B1 reduction in TECs upon aging. (A) FACS gating strategy for sorting thymic

macrophage. Plot shows frequency of macrophage within gated total live cells. (B) qRT-PCR analyses of TNF-α, IL-1β, IL-1α and IL-6 in macrophage in different age stage thymuses. Expression is plotted relative to 2-month-old thymus. (C) FACS gating strategy for sorting thymic sirpα+ DCs and sirpα- DC subsets. (D) qRT-PCR analyses of TNF-α, IL-1β, IL-1α and IL-6 in sirpα^{+} DCs (left) and sirpα^{-} DC (right) subsets in different stage thymuses. (E) Western blotting analyses of TNF-α, IL-1β, IL-1α and IL-6 in macrophage (left) and sirpα^{+} DCs (right) in different age stage thymuses. (F) Western blotting analyses of lamin-B1 and lamin-A/C in cultured TECs treated with indicated proinflammatory cytokines. All data shown are representative of at least 3 independent experiments. Error bars indicate SEM from 3 independent experiments. Student's t test: *, $P < 0.05$; **, $P < 0.01$; ***, $P < 0.001$; ns, not significant.

and sirpα$^-$ DC subsets (Fig. 2-3C and D). I then used quantitative RT-PCR (qRT-PCR) to assess the mRNA levels of 4 key pro-inflammatory cytokines, including TNF-α, IL-1β, IL-1α and IL-6, that have been implicated in inflammation-induced thymic degeneration (Billard et al., 2011; Gruver and Sempowski, 2008; Sempowski et al., 2000; Youm et al., 2012). I observed that all these pro-inflammatory cytokines exhibited age-related increase in macrophage (Fig. 2-3B) and sirpα$^+$ DC subset (Fig. 2-3D left) beginning at 6 months, while the increase in sirpα$^-$ DC subset was relatively mild (Fig. 2-3D right; < 3 fold change even in 20-month-old thymus). This is consistent with the published microarray results (Ki et al., 2014), which showed an augmented inflammatory signature as early as 6-month, a time lamin-B1 reduction became significant in mTECs and cTECs (Fig. 2-2E).

Next, I analyzed the protein level of these pro-inflammatory cytokines by Western blotting as mRNA level does not always reflect protein level due to post-transcriptional regulation. Another reason I have to confirm protein level of these pro-inflammatory cytokines by Western blotting is that some precursor species of cytokines, such as IL-1β, have to be processed into mature form to exhibit inflammatory activity and qRT-PCR analysis cannot distinguish precursor from mature species. Western blotting analyses showed an age-associated increase in active TNF-α, IL-1β, IL-1α and IL-6 in both macrophage and sirpα$^+$ DC (Fig. 2-3E). These analyses suggest that the proinflammatory cytokines secreted from macrophage and sirpα$^+$ DC could contribute, at least in part, to an inflammatory microenvironment within the thymus upon aging.

To explore the effect of these proinflammatory cytokines on lamin-B1 in TECs, I established an *in vitro* primary TEC culture system (Jain and Gray, 2014). Upon treatment with TNF-α (10 ng/ml), IL-1β (20 ng/ml) and IL-6 (20 ng/ml), I observed a

significant reduction of lamin-B1, but not lamin-A/C, in cultured TECs within 5-day treatment (Fig. 2-3F). In contrast, IL-1α (20 ng/ml) treatment did not cause a clear lamin-B1 reduction as seen in the other 3 cytokines. Additionaly, I also found that treatment with G-CSF (20 ng/ml), which was among the top 5 up-regulated intrathymic cytokines in inflammation-induced thymic involution model (Billard et al., 2011), did not lead to lamin-B1 reduction under the same condition, suggesting that lamin-B1 reduction in TECs could be induced by selected cytokines.

Proinflammatory cytokines can induce lamin-B1 reduction in TECs *via* senescence

To address the mechanism underlying proinflammatory cytokine-induced lamin-B1 reduction in TECs, I decided to first assess whether TECs undergo apoptosis upon cytokine treatment. Caspase activation by apoptotic signals has been shown to result in cleavage of nuclear lamins (Cuvillier et al., 1998; Fraser et al., 1997; Ruchaud et al., 2002; Takahashi et al., 1996). I examined the presence of 39 or 37 kD cleaved caspase 9, which marks initiation of the apoptotic process, in TECs treated with indicated cytokines for 120 hours (Fig. 2-4A). I did not detect obvious cleaved bands of active caspase 9 even after long-time exposure, suggesting that lamin-B1 reduction is not triggered by apoptosis. To further confirm this, I performed FACS analysis for two apoptotic markers Annexin V and 7-AAD in TECs treated with indicated cytokines for 120 hours and then quantified the percentage of Annexin V^+/7-AAD^+ apoptotic cells (Fig. 2-4B). The FACS results confirmed that proinflammatory cytokine treatment did not cause significant

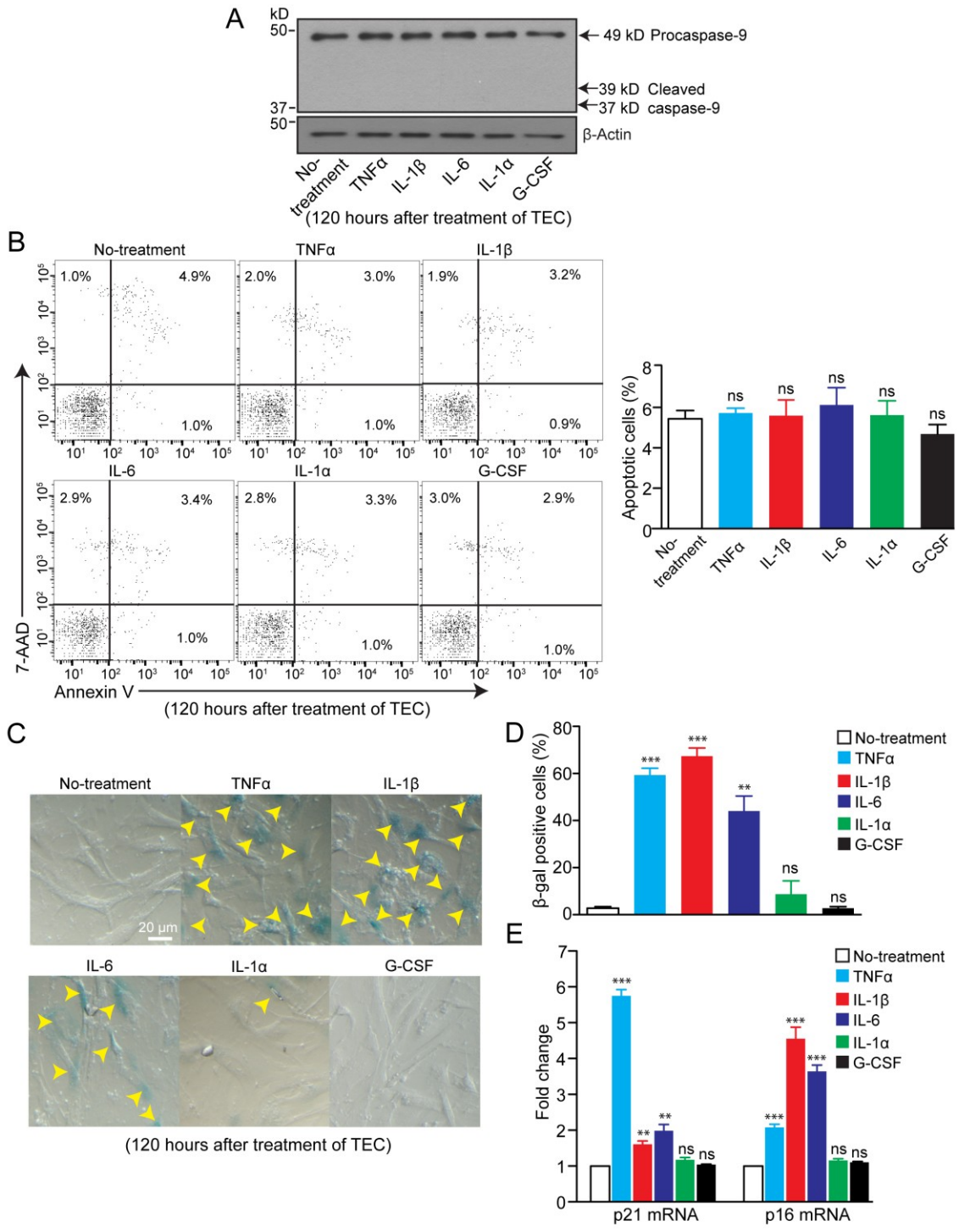

Fig 2-4. Proinflammatory cytokines can cause lamin-B1 reduction in cultured TECs *via* senescence. (A) Western blotting analysis reveals no apparent apoptosis in *in vitro* cultured TECs upon inflammatory cytokine treatment. Arrow (top) indicates 49 kD

procaspase 9; two arrows (bottom) indicate the predicated locations of 39 kD and 37 kD cleaved activated caspase 9. (B) FACS analyses of Annexin V and 7-AAD reveal no significant apoptosis between control and inflammatory cytokine groups. Left: representative FACS plots of Annexin V and 7-AAD staining of TECs; Right: quantification of apoptotic cells. (C) Increased senescence in TNF-a, IL-1β and IL-6 treated TECs as judged by β-galactosidase staining. Scale bars, 20 μm. (D) Percentage of β-galactosidase positive cells. Total 150 cells from 3 biological replicates were counted from each experimental group for quantification. (E) qRT-PCR analyses of p21 and p16 reveal different signaling pathways involved in proinflammatory cytokine-induced senescence in TECs. All data shown are representative of at least 3 independent experiments. Error bars indicate SEM from 3 independent experiments. Student's t test: *, $P < 0.05$; **, $P < 0.01$; ***, $P < 0.001$; ns, not significant.

apoptosis compared to untreated cells as less than 10% of TECs exhibited either Annexin V or 7-AAD positive signal (Fig. 2-4B right).

In addition to apoptosis, lamin-B1 loss is commonly observed in cells undergoing senescence (Freund et al., 2012). By assessing β-galactosidase activity, a known marker of senescence (Dimri et al., 1995; Itahana et al., 2007), I observed that 40-65% of TECs were positive for β-galactosidase staining after treating with TNF-α, IL-1β and IL-6 for 120 hours. By contrast, β-galactosidase activity was rarely detected in IL-1α and G-CSF groups (Fig. 2-4C and D). Senescence growth arrest is established *via* either p53 or p16-retinoblastoma protein (pRB) tumor suppressor pathway (Campisi and d'Adda di Fagagna, 2007). Due to a small number of TECs and low amount of total protein extracted from *in vitro* cultured TECs, it is not possible to assess phosphorylation of p53 and RB. Thus, I decided to use qRT-PCR assay to measure mRNA levels of p21 and p16, two key cyclin-dependent kinase inhibitors involved in p53 and pRB mediated senescence, respectively. I found that TNF-α induced a strong up-regulation of p21 expression in TECs while IL-1β and IL-6 mainly engaged in the p16-pRB signaling pathway (Fig. 2-4E). Together, these data suggested that proinflammatory cytokines could trigger lamin-B1 reduction in TECs at least in part by inducing senescence growth arrest.

Lamin-B1 reduction in TECs in thymus undergoing inflammation-mediated acute involution

Above studies suggest that age-associated elevation of inflammation in the thymus could contribute to lamin-B1 reduction in TECs. To further explore the physiopathological relevance of inflammation-induced lamin-B1 reduction *in vivo*, I

established an acute endotoxin-induced thymic involution model, which is characterized by inflammatory response with significantly elevated intrathymic expression of TNF-α (2.6 fold), IL-1β (3.5 fold) and IL-6 (37.5 fold, Top2) (Billard et al., 2011; Gruver and Sempowski, 2008; Sempowski et al., 2002). I examined whether lamin-B1 reduction in TECs occurred during inflammation-mediated thymic degeneration. 2-month-old female C57BL/6 mice were intraperitoneally (IP) injected once with Escherichia coli-derived lipopolysaccharide (LPS, 100 μg) or saline to induce thymic involution. Consistent with published data, total thymic cellularity as measured by cell number counts was significantly decreased 48 hours post induction (Fig. 2-5A left). FACS analysis of the CD4 and CD8 expression patterns revealed that distribution of thymocyte subsets was significantly altered leading to a specific loss of $CD4^+CD8^+$ DP cells within 48 hours post challenge (Fig. 2-5A right). An early study carried out transcriptome analysis of whole thymus tissue by microarray during the early stage of this acute thymic atrophy (Billard et al., 2011). Given that thymocytes comprise more than 95% of the total cellularity of the thymus, the previous transcriptome profiling should only reflect the effects of acute inflammation on thymoyctes but not on TECs. To uncover the impact of acute inflammation on TECs *in vivo*, I applied FACS sorting to isolate mTECs 48 hours post LPS challenge and then performed whole genome-wide transcriptional profiling using RNA-seq (data not shown). Due to insufficient cell number of isolated cTECs, only mTECs were used for this experiment. Interestingly, by analyzing transcriptional changes of major components of the nuclear lamina (NL), I found that lamin-B1, but not other components, was significantly reduced in mTECs during the early stage of acute thymic

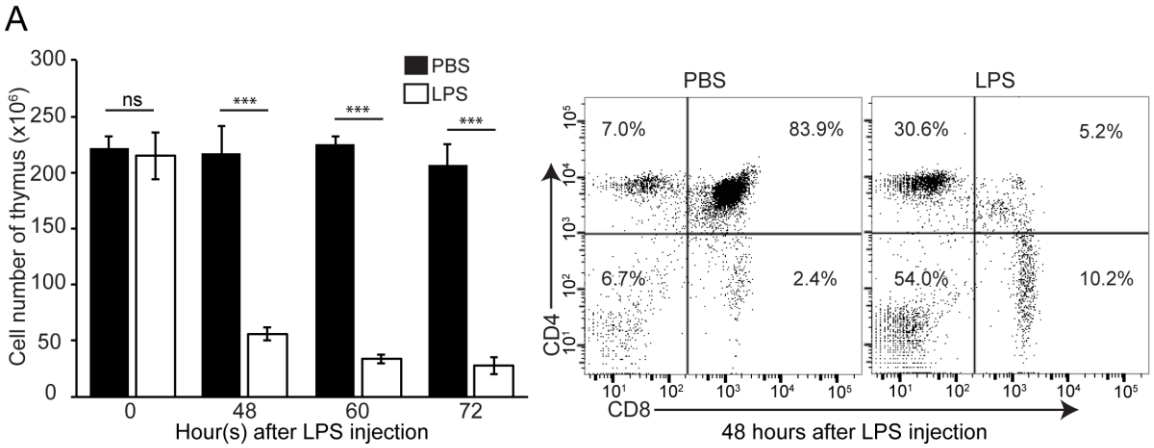

B

Up-regulation	Fold change	Down-regulation	Fold change
Sun1	1.1	Lamin-B1	-4.3
MAN1	1.2	Lamin-A	-1.5
LAP1	1.4	Lamin-B2	-1.3
Sun2	1.4	LAP2	-1.2
LBR	1.4	Emerin	-1.2
Nesprin2	1.4	Nesprin1	-1.2

mRNA levels in mTEC at 48 hours after LPS injection

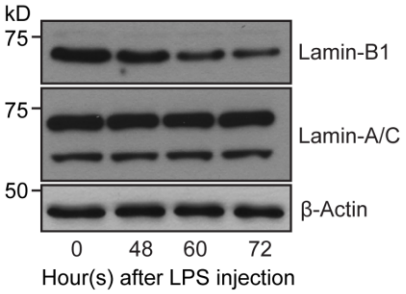

Fig 2-5. Inflammation leads to lamin-B1 reduction in TECs *in vivo* in the endotoxin-induced acute thymic involution model. (A) Total cell number of thymus at the indicated times after one-dose LPS (100 μg) challenge (left); Representative FACS plots of CD4 and CD8 staining in thymocytes from 2 independent experiments at 48 hours post LPS treatment (right). (B) RNA-seq analyses reveal selected up- and down-regulated genes in components of the nuclear lamina in mTECs in endotoxin-induced acute thymic atrophy model. (C) Western blotting analyses reveal a significant reduction of lamin-B1 but not lamin-A/C in mTECs in endotoxin-induced acute thymic atrophy model. β-actin is used as a loading control. Error bars indicate SEM from at least 3 independent experiments. Student's t test: *, $P < 0.05$; **, $P < 0.01$; ***, $P < 0.001$; ns, not significant.

atrophy (Fig. 2-5B). Using Western blotting assay, I further confirmed that more than 70% reduction of lamin-B1 in mTECs at the protein level (Fig. 2-5C), suggesting that lamin-B1 may be more sensitive to an inflammatory challenge than other NL components.

Discussion

Application of flow cytometry to analyze nuclear lamins

While flow cytometry is commonly used in the immune field with a wide variety of applications, to the best of my knowledge, it has not been applied to the study of nuclear lamins. Using the thymus as an example, I have demonstrated that flow cytometry is indeed a quick and effective tool for quantifying nuclear lamins in cells directly isolated from tissues *in vivo*. The approach I have introduced has two major advantages. First, by labeling with cell-type specific marker(s), this new method allows me to simultaneously measure lamins in different cell types from the same sample, which makes it possible to perform systematic screening of lamin loss in a mammalian tissue/organ. In the thymus study, I applied this approach to measure nuclear lamins in almost all the known cell types in this organ, including thymocytes from different developmental stages, macrophage, DC, fibroblast and TECs. It is very difficult, if not impossible, to do this kind of study using conventional methods such as Western blotting or IF. This flow cytometry-based method can be readily adapted for other tissues/organs. For example, our lab recently reported a gradual reduction of lamin-B in the brain of the aged fly based on Western blotting analysis (Tran et al., 2016). This finding raises one interesting hypothesis that loss of lamin-B may contribute to dysfunction and aging of the brain. It is not clear if this finding is reflective of a natural physiological change in the

brain or whether it might be involved in some disease conditions, such as Alzheimer. To explore this hypothesis, it is possible to apply this new method to quantify lamin protein levels in young and aged mouse brains. By labeling different fluorochrome dyes with specific antibodies recognizing four major cell types present in the vertebrate brain, including Neuna60 (neuron), GFAP (astrocyte), IBA1 (microglia) and Oligo1/2 (oligodendrocyte), it would allow one to assess whether and/or which cell type(s) undergoes lamin reduction upon aging.

Another virtue of the new method is the quantitative measurement of nuclear lamins based on the mean fluorescence intensity (MFI) of lamin signals from flow cytometry data (Fig. 2-2A). I have shown that the extent of lamin-B1 reduction in both mTECs and cTECs is well correlated with the progressive decline of total cellularity in the thymus upon aging (Fig. 2-2E), indicating that lamin-B1 may contribute to thymic degeneration. This finding is consistent with our previous study showing that lamin-B loss leads to tissue dysfunction in fly fat body (Chen et al., 2014), suggesting that lamin-B may play an evolutionary conserved role in tissue maintenance and its reduction contributes to age-associated tissue dysfunction.

The method will also allow one to more accurately reevaluate the level of other proteins, such as Foxn1 (Chen et al., 2009) and Ghrelin (Dixit et al., 2007; Taub et al., 2010; Youm et al., 2009), whose age-associated reduction has been previously proposed to contribute to thymic involution by some studies but refuted by others (Chen et al., 2009; Ki et al., 2014; O'Neill et al., 2016; Ortman et al., 2002; Sun et al., 2010). The ability to accurately measure the levels of these poteins in TECs during aging should help

to clarify the confusion regarding whether the reduction of any proteins in TECs or other cells in the thymus contributes to its involution.

Identification of age-associated lamin-B1 reduction in thymic epithelial cells

The human skin is reported to naturally exhibit an age-related loss of lamin-B1 in mammalian (Dreesen et al., 2013a; Dreesen et al., 2013b). Unfortunately, our unpublished studies did not find lamin-B1 reduciton in the skin of eyelids from elderly individuals. It still remains unclear the physiological impact of lamin-B1 loss on the aging process of the skin as deletion of both *Lmnb1* and *Lmnb2* in keratinocytes did not cause overt abnormalities in the skin and hair, even in 24-month-old mice (Yang et al., 2011). Interestingly, a recent study reported a reduction of lamin-B1 protein and a disruption of the nuclear lamina in neurons in the brain from Alzheimer's patients, indicating that lamin dysfunction may mediate neurodegenerative disorders (Frost et al., 2016). In this study, I reported the third case in mammals showing a specific reduction of lamin-B1 but not lamin-B2 and –A/C in TECs in the aged thymus. Consistent with our previous finding that not all old tissues lose lamin-B in aged fly, I did not detect any apparent change of lamin-B1 in other cell types such as thymocytes and HSC-derived myeloid lineage cells in the aged mouse thymus (data not shown). My findings raise an interesting question as to why different cell types exhibit differential regulation of lamin-B1 in the same microenvironment context. One possibility is that age-related changes in the thymic environment have distinct impacts on individual cell types and only TECs are sensitive to such environmental changes in the context of lamin-B1 reduction. For example, while IL-6 has been reported as a costimulatory molecule for T cell activation

and proliferation, my results suggests that IL-6 might induce cellular senescence of TECs and senescence-associated lamin-B1 reduction (Fig. 2-3 and 2-4). Age-associated lamin-B loss has been demonstrated to lead to heterochromatin loss and derepression of inflammatory genes (Chen et al., 2014). Since all vertebrate cells express at least one lamin protein and lamins may share some conserved functions across different species (Dechat et al., 2010), my finding indicates that loss of lamin-B1 in TECs may lead to derepression of inflammatory genes and in turn may result in intrathymic inflammation in aged thymus, which are known to play a critical role in driving the late stage thymic involution (Chinn et al., 2012; Sempowski et al., 2000). The whole genome-wide transcriptiome analyses of TECs from *Lmnb1* mutant and aged mouse thymuses will be studied to further explore the underlying mechanism and I will discuss them in Chapter 4.

Proinflammatory cytokines, lamin-B1 reduction and senescence

Proinflammatory cytokines such as TNFα and IL-6 have been implicated to play dual roles in the thymus. Physiologically optimal levels of these cytokines are essential for early T-cell development. For example, TNFα-mediated activation of NF-κb promotes the survival and development of single positive T cells in the thymus (Webb et al., 2016). Thymic differentiation of Interleukin 17 (IL-17)-producing $CD4^+$ T cell also depends upon the basal level of IL-6 (Marks et al., 2009). On the other hand, the age-associated abnormal increase of intrathymic proinflammatory cytokines is known to play a key role in exacerbating the late stage thymic degeneration. In my study, I confirmed that thymic macrophages and $sirp\alpha^+$ DC acquired a proinflammatory signature during the early stage of involution (~6-month-old thymus, Fig. 2-3) (Ki et al., 2014). and further

increase of these cytokines correlated with the progression of thymic degeneration (Fig. 2-2 and 2-3), suggesting that they may function as an initial trigger of age-associated thymic involution. Consistent with this, a recent transcriptional profiling study revealed that up-regulation of proinflammatory genes in thymic sirpα^+ DC is a key hallmark during the early thymic involution (Ki et al., 2014). How increased expression of inflammatory cytokines leads to thymic degeneration is not well understood. I showed that some of the elevated proinflammatory cytokines (TNFa, IL-1β and IL-6) induced lamin-B1 reduction in cultured TECs *in vitro* (Fig. 2-3F) and also found that lamin-B1 reduction in inflammation-induced thymic atrophy model *in vivo* (Fig. 2-5), indicating lamin-B1 as a common downstream target for these cytokine-mediated alterations in TECs. In addition, I demonstrated that proinflammatory cytokines could trigger lamin-B1 reduction in TECs at least in part *via* inducing senescence (Fig. 2-4). Interestingly, different proinflammatory cytokines engage in distinct pathways to induce TEC senescence. TNF-α-induced senescence in TECs appears to be mediated through the p53-p21 pathway, while IL-1β and IL-6 mainly engaged in the p16-RB signaling pathway (Fig. 2-4D). In agreement with my finding, increased senescence in thymic TECs was identified as one of hallmarks upon aging and contributed to architectural and morphological changes in aged mouse thymus (Aw et al., 2008). It has been reported that senescence of mammalian fibroblast is associated with lamin-B1 loss and increased secretion of inflammatory cytokine (referred to as senescence-associated secretory phenotype, SASP) and lamin-B1 depletion in proliferating cells can also trigger senescence (Coppe et al., 2008; Freund et al., 2012; Salama et al., 2014; Shah et al., 2013). Thus, age-associated reduction of lamin-B1 in TECs may contribute to the

abnormal increase of intrathymic inflammatory cytokines in aged thymus, which further accelerates degenerative process. I will dissect the role of lamin-B1 in TECs for thymic aging in Chapter 3.

Materials and methods

Mice

All mouse experiments were approved by the Institutional Animal Care and Use committee of Carnegie Institution for Science. 20-month-old female C57BL/6 mice were purchased from National Institution on Aging. Other mice in cohort experiments at the indicated ages were raised by the mouse facility of Carnegie Institution for Science. All animals were housed in specific pathogen-free conditions under a 12/12hour light dark cycle and fed *ad libitum*.

Endotoxin-induced thymic involution model

The procedure follows a detailed protocol described in (Billard et al., 2011). In brief, Escherichia coli-derived lipopolysaccharide (LPS, Sigma-Aldrich L-2880) was reconstituted at 1 mg/mL in PBS. 2-month-old female C57BL/6 mice were injected once intraperitoneally with LPS (100 μg) or saline to induce thymic involution. Thymuses were collected at indicated time points for phenotype analyses and lamin measurement.

Primary TEC isolation and culture

TECs were prepared according to a published protocol with modifications (Jain and Gray, 2014). In brief, fat and connective tissue were first removed from thymic lobes. Thymic lobes were cut into 2 mm pieces and then treated for 15 min at 37 °C with an enzymatic

mixture containing 0.25 U Liberase TM (Roche) and 0.1% DNase I (Sigma-Aldrich) in RPMI 1640. The supernatant was collected, and the digestion was repeated twice. Cells were filtered through 100μm cell strainer and spun at 1200 rpm for 5 min. The $CD45^+$ cells were depleted by CD45 microbeads (Miltenyi Biotec 130-052-301) and enriched CD45- cells were then stained with DAPI, CD45, EpCAM, Ly51, I-A/I-E (Biolegend) and UEA-1 (Vector laboratories) for 20 min at 4°C followed by sorting with FACSAria^{TM} III (BD Bioscience). The TEC subpopulations were identified as: mTEC: $CD45^-EpCAM^+UEA\text{-}1^+Ly51^-MHCII^+$; cTEC: $CD45^-EpCAM^+UEA\text{-}1^-Ly51^+MHCII^+$. FACS sorted TECs were further subjected to either downstream analyses or culture. For primary TEC culture, ~50,000 TECs were seeded in 48-well culture plates and cultured for up to 7 days in Dulbecco's modified Eagle's medium nutrient F12 (Invitrogen) supplemented with 3 μg/ml insulin (Sigma-Aldrich), 20 ng/ml epidermal growth factor (PeproTech), 100 units/ml penicillin-streptomycin, and 10% fetal bovine serum. Cultures were maintained at 37 °C and 5% CO2, and the medium was changed every two days. For pro-inflammatory cytokine treatment, TECs were cultured with above-mentioned medium supplemented with different concentrations of cytokines (10 ng/ml TNF-α, PeproTech; 20 ng/ml IL-1β, Biolegend; 20 ng/ml IL-6, PeproTech; 20 ng/ml in IL-1α, Biolegend; 20 ng/ml G-CSF PeproTech), TECs were collected at indicated time points for RNA or protein extraction.

Flow cytometry analysis of nuclear lamins

Single-cell suspension of freshly dissected thymus was prepared as described for TEC isolation without depletion of $CD45^+$ cells. Cells were first treated with TruStain fcX kit

(Biolegend) to block CD16/32 and Zombie UV™ fixable viability kit to exclude dead cells before cell surface marker staining. Surface marker staining was used to distinguish different cell types within the thymus: CD4/CD8 (T cell subsets); CD11c (DC); F4/80 (macrophage); CD31 (endothelial cell); CD140a (PDGFRα, fibroblast cells); mTEC: CD45-EpCAM^{+} UEA-1^{+}Ly51^{-}; cTEC: CD45^{-}EpCAM^{+} UEA-1^{-}Ly51^{+}. After surface marker labeling, staining of lamins follows the detailed protocol described in the True-Nuclear Trascription Factor kit (Biolegend). I use an Alexa Fluro 647 antibody labeling kit (Life technology) to prepare fluorochrome-conjugated lamin antibody. In brief, 50μg rabbit anti-lamin-B1 (Abcam), mouse anti-lamin-B2 (Invitrogen, E3), mouse anti-lamin-A/C (Active Motif) and control rabbit or mouse IgG (Santa Cruz) was labeled following the manufacturer's protocol. Fluorochrome-conjugated antibodies were reconstituted at 0.5 mg/mL in PBS and 0.1 μg of each antibody was used for staining 10^6 cells in 100μl volume. All samples were stained for 20 min at 4°C if not specifically indicated and then were immediately processed for FACS analyses by FACSAriaTM III (BD Bioscience). Data was analyzed with FlowJo software (Tree Star). All FACS antibodies were purchased from Biolegend if not indicated.

Flow cytometry analysis and sorting

Single-cell suspension of the thymus was prepared by passing minced tissue through a 40μm cell strainer. Cells were treated with TruStain fcX kit (Biolegend) to block CD16/32 before staining. All surface markers were stained for 20 min at 4°C, if not specifically indicated, and then were immediately processed for FACS analyses or sorting by FACSAriaTM III (BD Bioscience). FACS antibodies used for experiments include:

Thymocyte: CD4, CD8; macrophage: F4/80, CD11b; DC subsets: CD11c, EpCAM, CD80, I-A/I-E, Sirpα. Macrophage and DC sebsets were directly sorted into Trizol (Life technology) for RNA or Laemmli sample buffer (Bio-rad) for protein extraction. FITC Annexin V Apoptosis Detection kit with 7-AAD (BioLegend) was used to detect apoptosis of TECs. Data was analyzed with FlowJo software (Tree Star).

Immunofluorescence microscopy

mESCs stained with Alexa647-conjugated anti-lamin-B1 antibody were collected by FACS sorting and then attached to glass slides by cytospin (Shandon Cytospin 4) spun at 1200 rpm for 5 min. Attached mESCs were stained with DAPI and mounted with ProLong® Gold Antifade Mountant (Fisher Scientific). Confocal images were acquired using a laser-scanning confocal microscope (Leica SP5) with a 63X/1.4 objective. Images were processed using ImageJ.

Western blotting analysis

Whole-cell lysates were generated using Laemmli sample buffer (Bio-rad) and diluted in SDS-PAGE sample buffer. Cell lysates were separated in 10% or 15% SDS-PAGE and then transferred onto nitrocellulose membranes. The membranes were blocked with 5% milk and probed with the following antibodies: rabbit anti-lamin-B1 (1:5000, Abcam), mouse anti-lamin-A/C (1:5000, Active Motif), rabbit anti-TNF-α (1:1000, Cell Signaling), rabbit anti-IL-1β (1:1000, Cell Signaling), rabbit anti-IL-6 (1:1000, Novus biological), rabbit anti-IL-1α (1:2000, Santa cruz), mouse anti-caspase9 (1:1000, Cell Signaling) or mouse anti-β-actin (1:4000, Sigma, AC-15). Antibodies were detected with HRP-conjugated anti-mouse (1:10000) or anti-rabbit (1:10000) antibodies and West Pico

Substrate (Thermo Scientific).

Senescence-associated (SA)-β-gal assay

Senescence β-Galactosidase Staining kit (Cell Signaling, 9860S) was used to detect β-galactosidase activity at pH 6.0. In brief, *in vitro* cultured TEC cells were fixed in the fixative solution for 10 min at room temperature. The fixed cells were washed twice with PBS and then incubated with β-galactosidase staining solution containing X-gal at 37°C overnight. As the blue color developed, bright-field cell images were taken using an Axiovert 25 microscope (Carl Zeiss) connected to a Canon camera. Total 150 cells from 3 biological replicates were counted from each exprimental group for quantification.

RNA preparation and quantitative real-time PCR

TECs were isolated and enriched as described above. Total RNA was extracted following the manufacturer's protocol of Direct-zol™ RNA MicroPrep kit (Zymo Research R2060). Quantitative RT-PCR was performed using the iScript One Step RT-PCR kit (170-8892; Bio-Rad Laboratories) on a real-time PCR detection system (CFX96; Bio-Rad Laboratories). 50 ng of total RNA was reverse transcribed and amplified as follows: 50°C for 10 min, 95°C for 5 min, 95°C for 10 s, 60°C for 30 s, 72°C for 1 min. Steps 2–4 were repeated for 40 cycles. Each reaction was performed in triplicate, and the results of three independent experiments were used for statistical analysis. Relative mRNA expression levels were quantified using the ΔΔC (t) method (Pfaffl, 2001). Results were normalized to those for GAPDH, and primer sequences were listed as follows.

TNF-α: forward primer (F): CTGTAGCCCACGTCGTAGC;

Reverse primer (R): TTGAGA TCCATGCCGTTG.

IL-1β: F: TGTAATGAAAGACGGCACACC; R: TCTTCTTTGGGTATTGCTTGG.

IL-1α: F: CCGAGT TTCATTGCCTCTTT; R: ACTGTGGGAGTGGAGTGCTT.

IL-6: F: CTCTGGGAAATCGTGGAAAT; R: CCAGTTTGG TAGCATCCATC.

P21: F: GACAAGAGGCCCAGTACTTC; R: GCTTGGAGTGATAGAAATCTGTC.

P16: F: CGTACCCCG ATTCAGGTGAT; R: TTGAGCAGAAGAGCTGCTACGT.

GAPDH: F: CGACTTCAACAGCAACTCCCACTCTTCC;

R: TGGGTGGTCCAGGGTTTCTTACTCCTT.

Reference

Aw, D., Silva, A.B., Maddick, M., von Zglinicki, T., and Palmer, D.B. (2008). Architectural changes in the thymus of aging mice. Aging Cell *7*, 158-167.

Benedetti, S., and Merlini, L. (2004). Laminopathies: from the heart of the cell to the clinics. Curr Opin Neurol *17*, 553-560.

Billard, M.J., Gruver, A.L., and Sempowski, G.D. (2011). Acute endotoxin-induced thymic atrophy is characterized by intrathymic inflammatory and wound healing responses. PLoS One *6*, e17940.

Campisi, J. (2013). Aging, cellular senescence, and cancer. Annu Rev Physiol *75*, 685-705.

Campisi, J., and d'Adda di Fagagna, F. (2007). Cellular senescence: when bad things happen to good cells. Nat Rev Mol Cell Biol *8*, 729-740.

Chen, H., Chen, X., and Zheng, Y. (2013). The nuclear lamina regulates germline stem cell niche organization via modulation of EGFR signaling. Cell Stem Cell *13*, 73-86.

Chen, H., Zheng, X., and Zheng, Y. (2014). Age-associated loss of lamin-B leads to systemic inflammation and gut hyperplasia. Cell *159*, 829-843.

Chen, L., Xiao, S., and Manley, N.R. (2009). Foxn1 is required to maintain the postnatal thymic microenvironment in a dosage-sensitive manner. Blood *113*, 567-574.

Childs, B.G., Durik, M., Baker, D.J., and van Deursen, J.M. (2015). Cellular senescence in aging and age-related disease: from mechanisms to therapy. Nat Med *21*, 1424-1435.

Chinn, I.K., Blackburn, C.C., Manley, N.R., and Sempowski, G.D. (2012). Changes in primary lymphoid organs with aging. Semin Immunol *24*, 309-320.

Coffinier, C., Chang, S.Y., Nobumori, C., Tu, Y., Farber, E.A., Toth, J.I., Fong, L.G., and Young, S.G. (2010). Abnormal development of the cerebral cortex and cerebellum in the setting of lamin B2 deficiency. Proc Natl Acad Sci U S A *107*, 5076-5081.

Coffinier, C., Jung, H.J., Nobumori, C., Chang, S., Tu, Y., Barnes, R.H., 2nd, Yoshinaga, Y., de Jong, P.J., Vergnes, L., Reue, K.*, et al.* (2011). Deficiencies in lamin B1 and lamin B2 cause neurodevelopmental defects and distinct nuclear shape abnormalities in neurons. Mol Biol Cell *22*, 4683-4693.

Coppe, J.P., Patil, C.K., Rodier, F., Sun, Y., Munoz, D.P., Goldstein, J., Nelson, P.S., Desprez, P.Y., and Campisi, J. (2008). Senescence-associated secretory phenotypes reveal cell-nonautonomous functions of oncogenic RAS and the p53 tumor suppressor. PLoS Biol *6*, 2853-2868.

Cuvillier, O., Rosenthal, D.S., Smulson, M.E., and Spiegel, S. (1998). Sphingosine 1-phosphate inhibits activation of caspases that cleave poly(ADP-ribose) polymerase and lamins during Fas- and ceramide-mediated apoptosis in Jurkat T lymphocytes. J Biol Chem *273*, 2910-2916.

Dechat, T., Adam, S.A., Taimen, P., Shimi, T., and Goldman, R.D. (2010). Nuclear lamins. Cold Spring Harb Perspect Biol *2*, a000547.

Dimri, G.P., Lee, X., Basile, G., Acosta, M., Scott, G., Roskelley, C., Medrano, E.E., Linskens, M., Rubelj, I., Pereira-Smith, O.*, et al.* (1995). A biomarker that identifies senescent human cells in culture and in aging skin in vivo. Proc Natl Acad Sci U S A *92*, 9363-9367.

Dixit, V.D., Yang, H., Sun, Y., Weeraratna, A.T., Youm, Y.H., Smith, R.G., and Taub, D.D. (2007). Ghrelin promotes thymopoiesis during aging. J Clin Invest *117*, 2778-2790.

Dreesen, O., Chojnowski, A., Ong, P.F., Zhao, T.Y., Common, J.E., Lunny, D., Lane, E.B., Lee, S.J., Vardy, L.A., Stewart, C.L.*, et al.* (2013a). Lamin B1 fluctuations have differential effects on cellular proliferation and senescence. J Cell Biol *200*, 605-617.

Dreesen, O., Ong, P.F., Chojnowski, A., and Colman, A. (2013b). The contrasting roles of lamin B1 in cellular aging and human disease. Nucleus *4*, 283-290.

Fraser, A.G., McCarthy, N.J., and Evan, G.I. (1997). drICE is an essential caspase required for apoptotic activity in Drosophila cells. EMBO J *16*, 6192-6199.

Freund, A., Laberge, R.M., Demaria, M., and Campisi, J. (2012). Lamin B1 loss is a senescence-associated biomarker. Mol Biol Cell *23*, 2066-2075.

Gruenbaum, Y., Margalit, A., Goldman, R.D., Shumaker, D.K., and Wilson, K.L. (2005). The nuclear lamina comes of age. Nat Rev Mol Cell Biol *6*, 21-31.

Gruver, A.L., and Sempowski, G.D. (2008). Cytokines, leptin, and stress-induced thymic atrophy. J Leukoc Biol *84*, 915-923.

Itahana, K., Campisi, J., and Dimri, G.P. (2007). Methods to detect biomarkers of cellular senescence: the senescence-associated beta-galactosidase assay. Methods Mol Biol *371*, 21-31.

Jain, R., and Gray, D.H. (2014). Isolation of thymic epithelial cells and analysis by flow cytometry. Curr Protoc Immunol *107*, 3 26 21-15.

Ki, S., Park, D., Selden, H.J., Seita, J., Chung, H., Kim, J., Iyer, V.R., and Ehrlich, L.I. (2014). Global transcriptional profiling reveals distinct functions of thymic stromal subsets and age-related changes during thymic involution. Cell Rep *9*, 402-415.

Kim, Y., Sharov, A.A., McDole, K., Cheng, M., Hao, H., Fan, C.M., Gaiano, N., Ko, M.S., and Zheng, Y. (2011). Mouse B-type lamins are required for proper organogenesis but not by embryonic stem cells. Science *334*, 1706-1710.

Marks, B.R., Nowyhed, H.N., Choi, J.Y., Poholek, A.C., Odegard, J.M., Flavell, R.A., and Craft, J. (2009). Thymic self-reactivity selects natural interleukin 17-producing T cells that can regulate peripheral inflammation. Nat Immunol *10*, 1125-1132.

Mounkes, L., Kozlov, S., Burke, B., and Stewart, C.L. (2003). The laminopathies: nuclear structure meets disease. Curr Opin Genet Dev *13*, 223-230.

O'Neill, K.E., Bredenkamp, N., Tischner, C., Vaidya, H.J., Stenhouse, F.H., Peddie, C.D., Nowell, C.S., Gaskell, T., and Blackburn, C.C. (2016). Foxn1 Is Dynamically Regulated in Thymic Epithelial Cells during Embryogenesis and at the Onset of Thymic Involution. PLoS One *11*, e0151666.

Ortman, C.L., Dittmar, K.A., Witte, P.L., and Le, P.T. (2002). Molecular characterization of the mouse involuted thymus: aberrations in expression of transcription regulators in thymocyte and epithelial compartments. Int Immunol *14*, 813-822.

Pfaffl, M.W. (2001). A new mathematical model for relative quantification in real-time RT-PCR. Nucleic Acids Res *29*, e45.

Ruchaud, S., Korfali, N., Villa, P., Kottke, T.J., Dingwall, C., Kaufmann, S.H., and Earnshaw, W.C. (2002). Caspase-6 gene disruption reveals a requirement for lamin A cleavage in apoptotic chromatin condensation. EMBO J *21*, 1967-1977.

Salama, R., Sadaie, M., Hoare, M., and Narita, M. (2014). Cellular senescence and its effector programs. Genes Dev *28*, 99-114.

Sempowski, G.D., Hale, L.P., Sundy, J.S., Massey, J.M., Koup, R.A., Douek, D.C., Patel, D.D., and Haynes, B.F. (2000). Leukemia inhibitory factor, oncostatin M, IL-6, and stem cell factor mRNA expression in human thymus increases with age and is associated with thymic atrophy. J Immunol *164*, 2180-2187.

Sempowski, G.D., Rhein, M.E., Scearce, R.M., and Haynes, B.F. (2002). Leukemia inhibitory factor is a mediator of Escherichia coli lipopolysaccharide-induced acute thymic atrophy. Eur J Immunol *32*, 3066-3070.

Shah, P.P., Donahue, G., Otte, G.L., Capell, B.C., Nelson, D.M., Cao, K., Aggarwala, V., Cruickshanks, H.A., Rai, T.S., McBryan, T.*, et al.* (2013). Lamin B1 depletion in senescent cells triggers large-scale changes in gene expression and the chromatin landscape. Genes Dev *27*, 1787-1799.

Shimi, T., Butin-Israeli, V., Adam, S.A., Hamanaka, R.B., Goldman, A.E., Lucas, C.A., Shumaker, D.K., Kosak, S.T., Chandel, N.S., and Goldman, R.D. (2011). The role of nuclear lamin B1 in cell proliferation and senescence. Genes Dev *25*, 2579-2593.

Sun, L., Guo, J., Brown, R., Amagai, T., Zhao, Y., and Su, D.M. (2010). Declining expression of a single epithelial cell-autonomous gene accelerates age-related thymic involution. Aging Cell *9*, 347-357.

Takahashi, A., Alnemri, E.S., Lazebnik, Y.A., Fernandes-Alnemri, T., Litwack, G., Moir, R.D., Goldman, R.D., Poirier, G.G., Kaufmann, S.H., and Earnshaw, W.C. (1996). Cleavage of lamin A by Mch2 alpha but not CPP32: multiple interleukin 1 beta-converting enzyme-related proteases with distinct substrate recognition properties are active in apoptosis. Proc Natl Acad Sci U S A *93*, 8395-8400.

Taub, D.D., Murphy, W.J., and Longo, D.L. (2010). Rejuvenation of the aging thymus: growth hormone-mediated and ghrelin-mediated signaling pathways. Curr Opin Pharmacol *10*, 408-424.

Tran, J.R., Chen, H., Zheng, X., and Zheng, Y. (2016). Lamin in inflammation and aging. Curr Opin Cell Biol *40*, 124-130.

Webb, L.V., Ley, S.C., and Seddon, B. (2016). TNF activation of NF-kappaB is essential for development of single-positive thymocytes. J Exp Med *213*, 1399-1407.

Yang, S.H., Chang, S.Y., Yin, L., Tu, Y., Hu, Y., Yoshinaga, Y., de Jong, P.J., Fong, L.G., and Young, S.G. (2011). An absence of both lamin B1 and lamin B2 in keratinocytes has no effect on cell proliferation or the development of skin and hair. Hum Mol Genet *20*, 3537-3544.

Youm, Y.H., Kanneganti, T.D., Vandanmagsar, B., Zhu, X., Ravussin, A., Adijiang, A., Owen, J.S., Thomas, M.J., Francis, J., Parks, J.S., *et al.* (2012). The Nlrp3 inflammasome promotes age-related thymic demise and immunosenescence. Cell Rep *1*, 56-68.

Youm, Y.H., Yang, H., Sun, Y., Smith, R.G., Manley, N.R., Vandanmagsar, B., and Dixit, V.D. (2009). Deficient ghrelin receptor-mediated signaling compromises thymic stromal cell microenvironment by accelerating thymic adiposity. J Biol Chem *284*, 7068-7077.

Chapter 3: Characterization of lamin-B1 function in thymic epithelial cells (TECs)

Summary

Emerging evidence suggests that nuclear lamins, the type V intermediate filament proteins, play an important role linking aging-related inflammation to tissue homeostasis/aging. As described in Chapter 2, I have uncovered an age-associated lamin-B1 reduction in TECs, which correlates with the progression of age-related thymic involution. In this chapter, I investigate the potential function of lamin-B1 in TECs using a variety of mouse genetic models. I show that TEC-specific deletion of *Lmnb1,* but not *Lmnb2 or Lmna,* leads to thymic atrophy and a number of changes in the TEC compartment that are remarkably similar to reported age-related defects. Additionally, I show that lamin-B1 deficiency in TECs accelerates age-associated thymic adiposity, at least in part *via* dampening the ghrelin receptor-mediated signaling in mTECs. By using different combinations of transgenic T cell receptor (TCR) mouse models, I further demonstrate that lamin-B1 is required for proper antigen presentation in TECs and that lamin-B1 deficiency in TECs leads to inefficient positive and negative selection of T cells.

Introduction

The previous studies of nuclear lamins in different model organisms clearly demonstrated that B-type lamins are required for proper organogenesis of multiple but not all tissues/organs (Chen and Zheng, 2014; Frost et al., 2016; Kim et al., 2011). The mechanisms underlying lamin-mediated differential effects in different organs are still not well understood. In contrast to extensive studies on the role of lamins in development, the role of B-type lamins in tissue/organ homeostasis and aging remains largely unexplored. By studying the *Drosophila* immune organ, called fat body, our lab uncovered a mechanism by which lamin-B reduction in the cells of fat body upon aging induced age-associated systemic inflammation and tissue damage, suggesting that lamin-B plays a critical role in tissue homeostasis/aging and immunosenescence (Chen et al., 2014). The physiological significance of this finding needs to be further assessed in other tissue/organ(s) *in vivo* especially in the context of mammalian aging. In the preceding chapter, I reported an age-associated reduction of lamin-B1 but not lamin-B2 and -A/C in the TECs in the thymus. The reduction of lamin-B1 correlated with age-related progressive degeneration of the thymus, implying a potential role of lamin-B1 in contributing to the thymic involution.

While considerable effort has been focused on mechanisms controlling development of the thymic microenvironment essential for T-cell generation, the molecular mechanisms that mediate thymic homeostasis and involution are still not well understood (Boehm and Swann, 2013). One of the major impediments to studying thymic involution is that age-associated transcriptome analysis of TECs has only recently been studied during early involution stage (Ki et al., 2014). Therefore, the field has relied

almost exclusively on the Foxn1 to explain thymic aging for more than a decade. Whole genome-wide transcriptional profiling suggested a role for proinflammatory cytokines in initiating thymic degeneration, which was previously thought to participate in late stage of involution (Ki et al., 2014). The underlying mechanism by which elevated proinflammatory cytokines initiate thymic involution is poorly understood. In the previous chapter, my studies suggest an inflammation-mediated nuclear defect, lamin-B1 reduction in TECs, which in turn appears to be associated with thymic degeneration. Here, I describe my investigation of the role of lamin-B1 in TECs using mouse genetic models, which leads to the uncovering of several important roles of lamin-B1 in T-cell generation, thymic homeostasis and aging.

Results

TEC-specific deletion of *Lmnb1* causes thymic atrophy

To address the potential roles of nuclear lamins in TECs, I first deleted individual lamin genes in TECs by crossing *Lmnb1*$^{f/f}$, *Lmnb2*$^{f/f}$ or *Lmna*$^{f/f}$ mice with Foxn1-Cre (FN1Cre) mouse line (Gordon et al., 2007). Interestingly, while the conditional ablation of either *Lmnb2* or *Lmna* in TECs had no obvious effect on the size and total cellularity of thymus in 2-month-old mice (Fig 3-1B), depletion of *Lmnb1* in TECs resulted in apparent thymic atrophy as judged by the significantly reduced size and total cell number (~80% to 85% reduction). The degree of this atrophy is comparable to thymuses from 20-month-old mice (Fig 3-1A). Although Foxn1 is expressed in keratinocytes and hair follicles and FN1Cre can induce deletion of the corresponding genes in these cell types besides TECs, I note that none of these lamin-depleted mouse lines exhibit any obvious skin or hair phenotypes (data not shown). Since the FN1Cre allele begins to express Cre

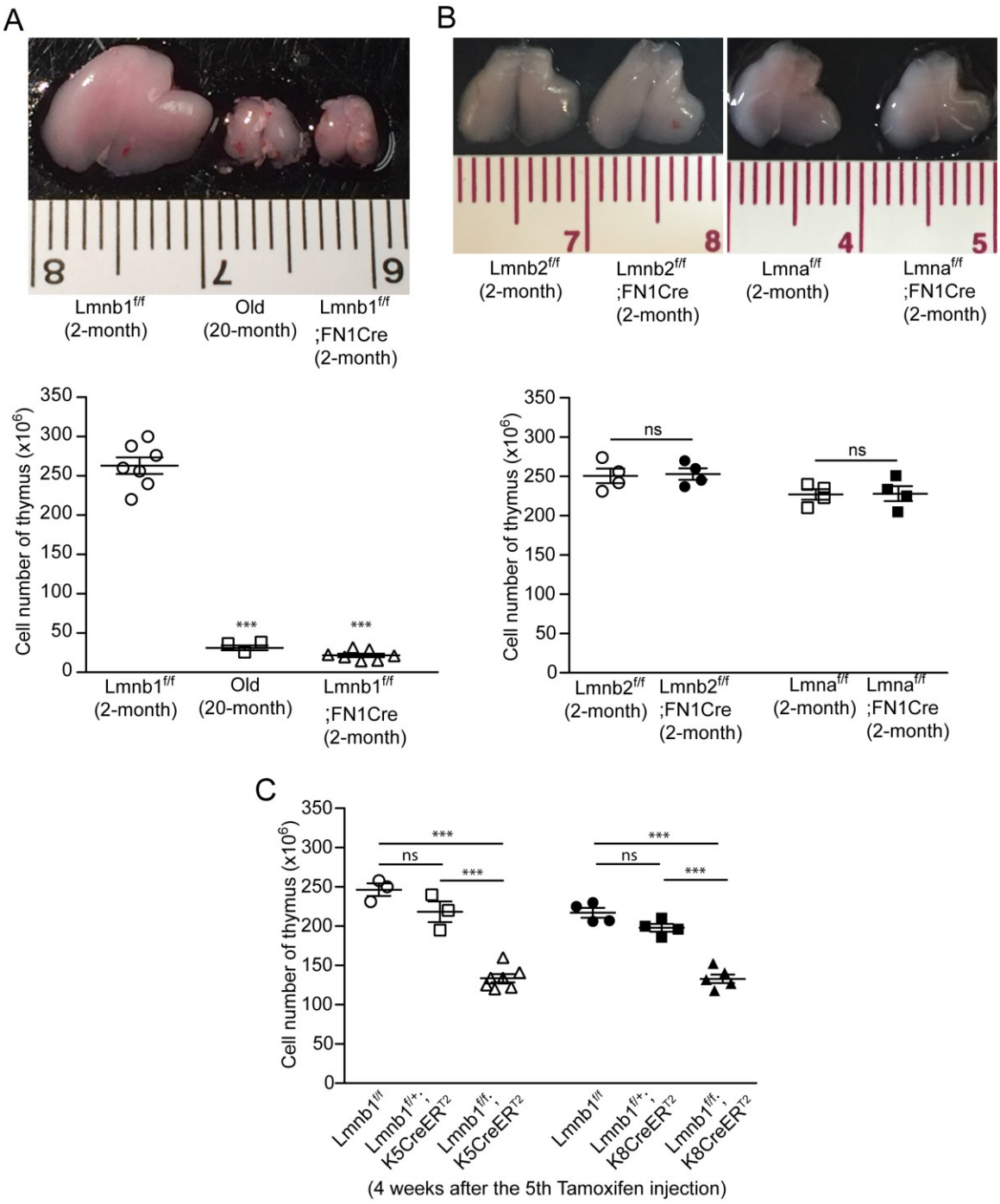

Fig 3-1. Depletion of *Lmnb1* but not *Lmnb2* and *Lmna* in TECs induces thymic atrophy. (A) Representative images of thymuses isolated from 2-month-old littermate control *Lmnb1$^{f/f}$ or Lmnb1$^{f/f}$;*FN1Cre mice and an old (20-month) wild type (WT) control (top). The total cell number counts from thymuses with indicated ages and genotypes.

Lmnb1$^{f/f}$, n=7; *Lmnb1* mutant, n=7; age, n=3. (B) Ablation of *Lmnb2* (left, n=4) and *Lmna (right,* n=4*)* in TECs do not cause obvious thymic atrophy. Top: representative pictures of thymuses; bottom: total cell number counts with indicated genotypes. (C) Quantification of total cell numbers in thymuses from mice after depletion of *Lmnb1* in either mTEC (n=7) or cTEC (n=5) by Tamoxifen (TAM) treatment. 2-month-old mice with indicated genotypes were treated with a single intraperitoneal (IP) injection of TAM (1mg/10 g body weight/day) for five successive days and with TAM (0.025 mg/ml) kept in the drinking water. Thymic phenotypes were analyzed 4 weeks after the 5th TAM injection. All data shown are representative of at least 3 independent experiments and are plotted as mean ± SEM. Student's t test: *, $P < 0.05$; **, $P < 0.01$; ***, $P < 0.001$; ns, not significant.

on embryonic day 11.5 (E11.5) in TECs, FN1Cre would drive *Lmnb1* deletion in TECs during embryonic development. To dissect the role of lamin-B1 in the adult mouse thymus, I next employed Keratin5- (K5) and Keratin8- (K8) CreER^{T2} systems to induce *Lmnb1* deletion in either mTEC or cTEC, respectively, in adult thymus following tamoxifen (TAM) injection. Preliminary results suggested that one dose of TAM (1mg TAM/10g/day, see methods) on five consecutive days resulted in a ~60% reduction of *Lmnb1* mRNA (data not shown) in both mTEC and cTEC. 4 weeks after the 5th TAM injection, the total cell number of the thymus in *Lmnb1*$^{f/f;}$ K5CreER^{T2} or *Lmnb1*$^{f/f}$; K8CreER^{T2} mice was reduced by 50-60% compared to the control groups (Fig 3-1C). Together, these results suggest that loss of lamin-B1 in TECs in adult thymus accelerates thymic degeneration.

Depletion of lamin-B1 in TECs leads to altered thymic epithelial compartments

To investigate the cellular basis for thymic atrophy upon lamin-B1 deletion, I first used hematoxylin and eosin (H&E) staining to examine the structural organization of the thymus. It has been well documented that a progressive disruption of the cortical medullary junction region (CMJ) occurs in aged thymus (Aw et al., 2008; Gray et al., 2006). H&E staining of *Lmnb1* mutant thymus revealed a clear blurring of the CMJ (Fig 3-2A). I next performed keratin immunostaining to examine the distribution and architectural organization of cTEC and mTEC compartments. In 2-month-old control thymus, K5^{+} mTECs typically form a compact medullary compartment surrounded by cortex region composed of K8^{+} cTECs (Fig 3-2B, top). In contrast, I observed a complete loss of the CMJ boundary and the presence of many small and less compacted mTEC

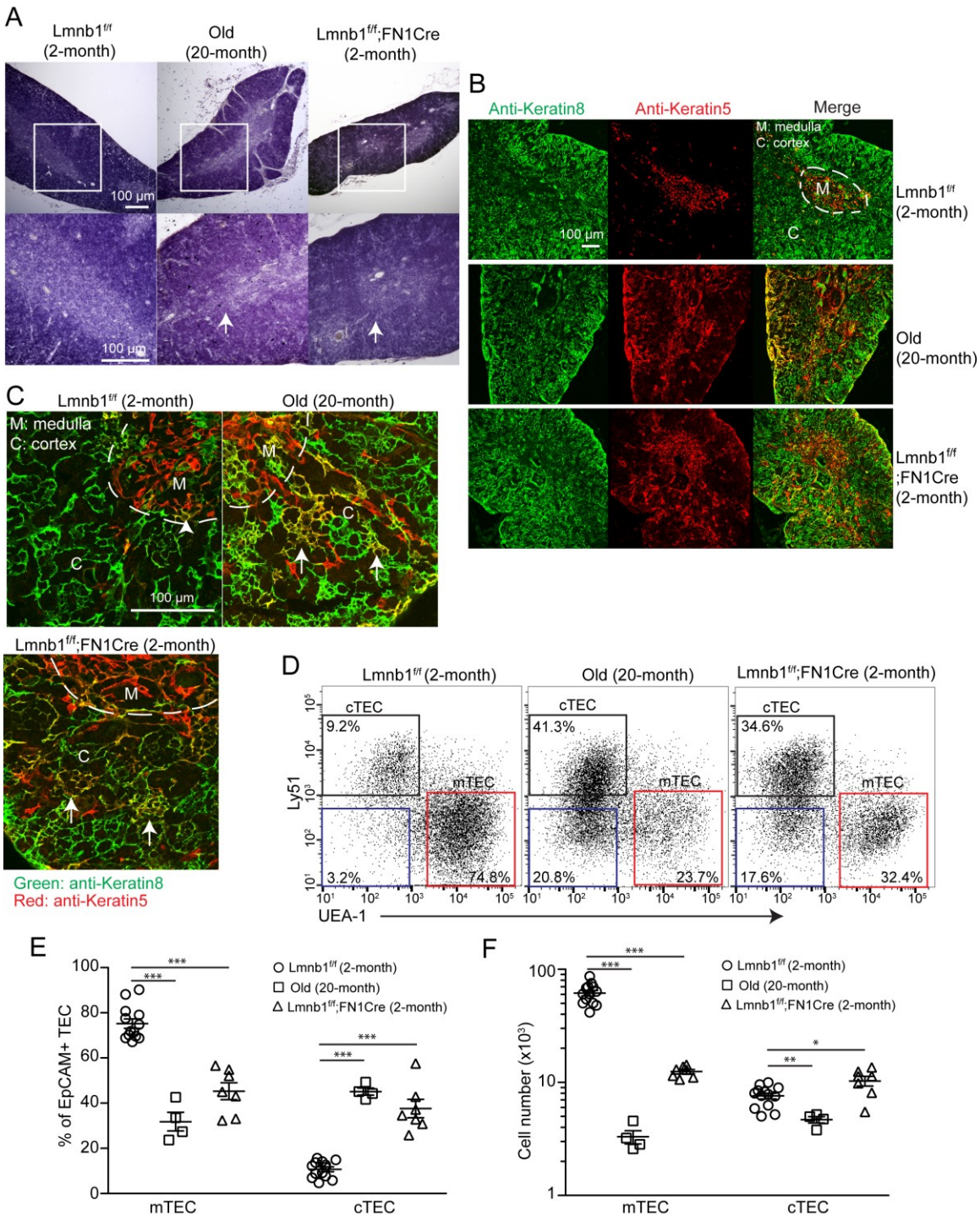

Fig 3-2. Lamin-B1 deficiency in TECs leads to altered thymic epithelial compartments. (A) Hematoxylin and eosin (H&E) staining of thymic tissue sections reveals disorganization of the TEC compartment in *Lmnb1* mutant thymus. A 20-month-

old WT involuted thymus is shown as an aged representative. The cortical medullary junction (CMJ) areas marked by white lines are enlarged at the bottom. Arrows indicate blurring of the CMJ areas in both aged and *Lmnb1* mutant thymuses. (B) Keratin staining reveals abnormal mTEC and cTEC organization in *Lmnb1* mutant and aged thymuses. A white dash line indicates intact medulla region in 2-month-old WT thymus. Green: anti-keratin8; Red: anti-keratin5. (C) High magnification images reveal K5 and K8 double-positive ($K5^+K8^+$) TECs in both aged and *Lmnb1* mutant thymuses. White dash lines indicate the CMJ regions. An arrowhead marks $K5^+K8^+$ TECs in the CMJ region in WT thymus and arrows indicate $K5^+K8^+$ TECs in cortical regions in both aged and *Lmnb1* mutant thymuses. Green: anti-keratin8; Red: anti-keratin5. (D) Flow cytometry analysis of frequency of UEA-1^+Ly51^- mTECs and UEA-1^-Ly51^+ cTECs within the gated $EpCAM^+$ TEC population. FACS plots shown are representative of at least 3 independent experiments. (E) Quantification of frequency of mTECs and cTECs in WT (n=13), *Lmnb1* mutant (n=7) and aged (n=4) thymuses. (F) Quantification of total cell number of mTECs and cTECs in WT (n=13), *Lmnb1* mutant (n=7) and aged (n=4) thymuses. All data shown are representative of at least 3 independent experiments and are plotted as mean ± SEM. Student's t test: *, $P < 0.05$; **, $P < 0.01$; ***, $P < 0.001$; ns, not significant.

islets distributed throughout the whole aged and *Lmnb1* mutant thymuses (Fig 3-2B middle and bottom). Interestingly, I also observed a much higher percentage of K5 and K8 double-positive ($K5^+K8^+$) TECs present in both aged and *Lmnb1* mutant thymuses (Fig 3-2C). The $K5^+K8^+$ TEC subset was found in the early embryonic thymus between E12.5-15.5 and was proposed as a bipotent TEC progenitor that gave rise to either mTEC or cTEC (Klug et al., 1998). This finding promoted me to further explore the alteration of TEC cellular composition in the *Lmnb1* mutant thymus.

TECs isolated from 2-month-old $Lmnb1^{f/f}$;FN1Cre mutant thymuses and control littermates were further analyzed by flow cytometry. Consistent with published results, my data confirmed that mTECs ($EpCAM^+UEA\text{-}1^+Ly51^-$) were the predominant subset (~75% to 85%) within TECs ($EpCAM^+CD45^-$) in the young WT thymus (Fig 3-2D left). However, in both aged and *Lmnb1* mutant thymuses, I observed a pronounced decrease of mTEC population, with a skew towards a cTEC dominant stromal compartment (Fig 3-2D and E). I also found that there was a remarkable increase of a TEC subpopulation ($EpCAM^+UEA\text{-}1^-Ly51^-$) that does not express canonical surface markers for either mTEC or cTEC in both aged and *Lmnb1* mutant thymuses (Fig 3-2D, marked within blue box). I refer to this population as double-negative (DN)-TEC. I suspect DN-TEC might reflect the $K5^+K8^+$ TEC subset detected in IF assay (Fig 3-2C) and additional transcriptome analysis will be needed to characterize the identity of this DN-TEC subpopulation. Furthermore, lamin-B1 deficiency in TECs led to a significant reduction in the number of mTECs but not cTECs, which is similar to the trend for mTECs observed in aged thymus (Fig 3-2F).

Loss of lamin-B1 in TECs accelerates age-related thymic adiposity

One of the hallmark changes associated with age-associated thymic involution is the gradual replacement of the TEC compartment with adipose tissue (Dixit, 2010). Lineage tracing data reveal that adipose cells are of intrathymic origin and are derived from Foxn1^{+} TECs *via* epithelial-to-mesenchymal transition (EMT) (Youm et al., 2009). In previous experiments, I observed a notable increase of perithymus fat tissue (data not shown) in the 2-month-old *Lmnb1* mutant thymus, which led me to further investigate whether or not loss of lamin-B1 in TECs promoted thymic adipogenesis. I performed a longitudinal analyses of thymic adiposity in mice up to 12-month of age and found a remarked accumulation of adipose tissue surrounding the 6- to 8-month-old *Lmnb1* mutant thymus (Fig 3-3A). Oil red staining revealed that fat cells and/or lipid-containing cells were abundant in both perithymic and intrathymic regions in *Lmnb1* mutant and aged thymus compared to the controls (Fig 3-3B). I further used neutral lipid staining to confirm the prevalence of lipid-containing cells in *Lmnb1* mutant thymus, which appeared more severe than that in 20-month-old aged thymus (Fig 3-3C). Recent studies demonstrate that the expression of Ghrelin receptor (growth hormone secretagogue receptor, or GHSR) in mTECs declines upon aging and deficiency in GHSR-mediated signaling facilitates the EMT process and thymic adipogenesis with aging (Yang et al., 2007; Youm et al., 2009). Therefore, I next measured the mRNA level of GHSR in mTECs using qRT-PCR. In agreement with previous studies, I observed a ~50% reduction in the expression of GHSR in mTECs isolated from 20-month-old aged thymus and ~65% to 70% reduction of this transcript in *Lmnb1* mutant thymus compared to the 6-month-old control thymus (Fig 3-3D). Whole genome-wide transcriptional profiling of

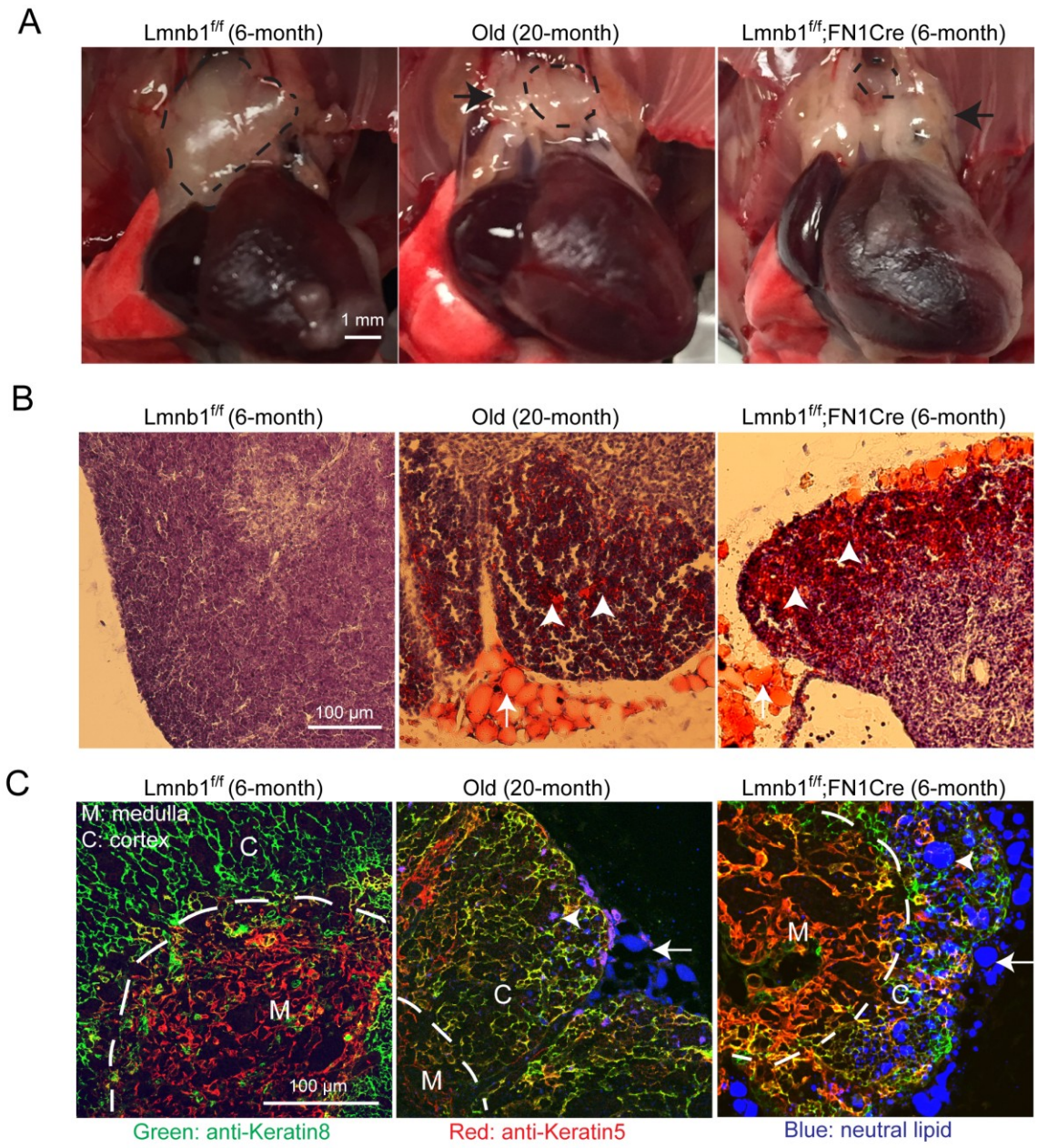
A
Lmnb1f/f (6-month)
Old (20-month)
Lmnb1f/f;FN1Cre (6-month)
1 mm
B
Lmnb1f/f (6-month)
Old (20-month)
Lmnb1f/f;FN1Cre (6-month)
100 μm
C
Lmnb1f/f (6-month)
Old (20-month)
Lmnb1f/f;FN1Cre (6-month)
M: medulla
C: cortex
C
M
100 μm
Green: anti-Keratin8
Red: anti-Keratin5
Blue: neutral lipid
D
mRNA level of Ghrelin receptor in mTEC
Fold change
1.2
1.0
0.8
0.6
0.4
0.2
0
**
***
Lmnb1f/f (6-month)
Old (20-month)
Lmnb1f/f;FN1Cre (6-month)

Fig 3-3. Deletion of *Lmnb1* in TECs accelerates age-related thymic adiposity. (A) Representative images of thymuses from 6-month-old control *Lmnb1*$^{f/f}$ and *Lmnb1*$^{f/f}$;FN1Cre mice. A 20-month-old WT thymus is shown as an aged control. Dash line marks the thymus and arrows indicate perithymic fat tissues. Scale bar, 1 mm. (B) Oil red staining reveals an increased presence of perithymic (arrow) and intrathymic (arrowhead) fat cells in *Lmnb1* mutant (6-month) and aged WT (20-month) thymus compared to the control. Scale bar, 100 μm. (C) Neutral lipid staining (Blue) reveals increased lipid-containing cells in *Lmnb1* mutant and aged thymus. Scale bar, 100 μm. (D) qRT-PCR analysis of GHSR expression in mTECs from control *Lmnb1*$^{f/f}$, *Lmnb1* mutant and aged WT thymuses. All data shown are representative of 3 independent experiments and are plotted as mean ± SEM. Student's t test: *, $P < 0.05$; **, $P < 0.01$; ***, $P < 0.001$; ns, not significant.

mTECs further confirmed this finding (in Chapter 4, data not shown). Together, these results suggested that loss of lamin-B1 in TECs accelerated age-associated thymic adiposity, at least in part, through dampening of GHSR-mediated signaling in mTECs.

Lamin-B1 deficiency in TECs impairs normal αβT cell development

There are two major T cell lineages in the thymus, αβT cells and γδT cells, defined by the types of T cell receptors (TCRs) expressed on their surface. Since TECs form distinct niche microenvironments supporting each stage of αβT-cell development, I further explored the impact of lamin-B1 loss in TECs on αβT-cell development. I first analyzed the percentage of distinct stages of developing T cells, ranging from the earliest double-negative (DN) to the final single-positive (SP) cells. I found that the frequency of both $CD4^+$ SP and $CD8^+$ SP was significantly reduced by ~50-60%, respectively, in *Lmnb1* mutant thymus compared to the control littermates (Fig 3-4A and B). Aged thymus also exhibited a similar trend but with less severity (~30-40%; Fig 3-4A and B, middle) than that in the *Lmnb1* mutant. Meanwhile, similar to aged thymus, the *Lmnb1* mutant thymus did not exhibit any obvious alterations in either DN or double-positive (DP) T cell populations with a slightly increased percentage of DP subset (Fig 3-4A and B), suggesting that lamin-B1 deficiency in TECs might cause a specific developmental defect during the DP to SP transition checkpoint. To test whether lamin-B1 loss in TECs in adult thymus leads to a similar defective T-cell development, I employed TAM-induced *Lmnb1* ablation in either mTEC ($K5CreET^{T2}$) or cTEC ($K8CreER^{T2}$) in 2-month-old adult mice. I found a pronounced reduction in both $CD4^+$ SP and $CD8^+$ SP upon *Lmnb1* deletion in either mTEC (Fig 3-4C) or in cTEC (Fig 3-4D) in adult thymus,

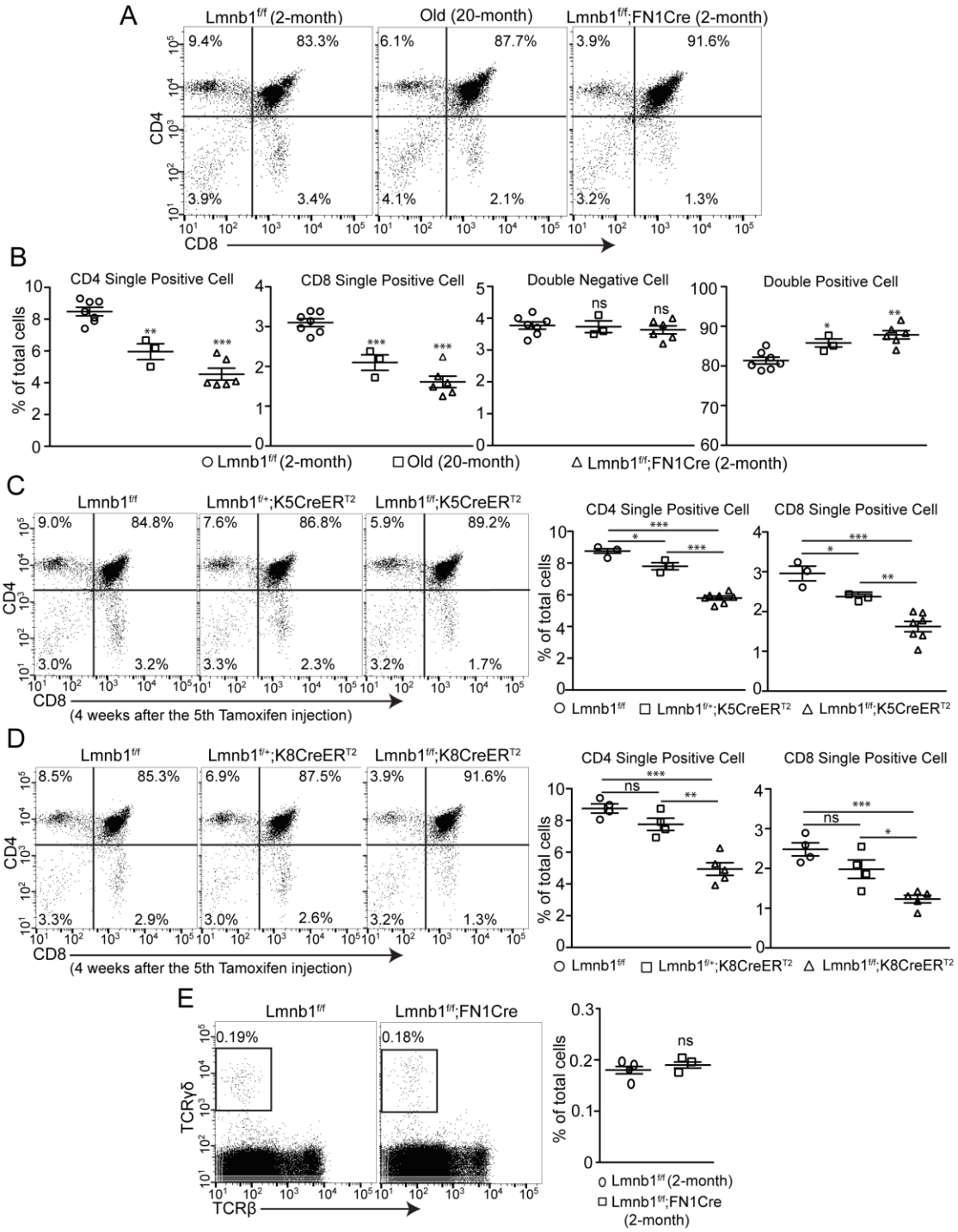

Fig 3-4. Lamin-B1 is required for TECs to support proper αβT cell development.

(A) Representative FACS dot plots of CD4 and CD8 expression of thymocytes in 2-month-old control *Lmnb1$^{f/f}$* and *Lmnb1$^{f/f}$;*FN1Cre thymus. A 20-month-old thymus is

included as an aged control. (B) Quantification of frequency of the indicated T-cell subsets described in (A). WT, n=7; *Lmnb1* mutant, n=6; Age, n=3. (C) & (D) Flow cytometry analysis of CD4 and CD8 expression reveal a reduction of both $CD4^+$ SP and $CD8^+$ SP upon *Lmnb1* depletion in mTECs by $K5CreER^{T2}$ (C, n=7) or cTEC by $K8CreER^{T2}$ (D, n=5) after TAM injection. Left: representative FACS dot plots; Right: quantification of frequency of $CD4^+$ SP and $CD8^+$ SP cells within gated live cells in the thymus. (E) Flow cytometry analysis of TCRβ and TCRγδ expression (left) and quantification of frequency of γδT cells (right) in 2-month-old control $Lmnb1^{f/f}$ and $Lmnb1^{f/f}$;FN1Cre thymus (n=3). All data shown are representative of at least 3 independent experiments and are shown as mean ± SEM. Student's t test: *, $P < 0.05$; **, $P < 0.01$; ***, $P < 0.001$; ns, not significant.

confirming that lamin-B1 plays an important role in TECs to support normal thymopoiesis.

γδT cell is another T-cell lineage arising from the early DN stage and further differentiates into effectors such as IFNγ-producing γδT1 and IL-17-producing γδT17 cells within the thymus (Bonneville et al., 2010; Fahl et al., 2014). They express a more restricted TCR repertoire and function like innate immune cells, especially in the gut-associated immune system. Unlike αβT cells, the development of γδT cells in the thymus is independent of MHC-mediated antigen presentation by TECs (Chien et al., 2014). I observed a similar percentage of γδT cells in both *Lmnb1* mutant and the littermate control thymus (Fig 3-4E), indicating that γδT cell generation is not dependent on lamin-B1 in TECs.

In order to further dissect which developmental stage(s) during αβT cell development is specially affected by lamin-B1, I subdivided thymocytes into four developmental stages based on the surface expression of TCRβ chain and CD69 (Johnson et al., 2009; Lesourne et al., 2009). Consistent with my previous findings, I did not detect any obvious change in the frequency of $TCR\beta^{-/low}CD69^{-}$ and $TCR\beta^{int}CD69^{+}$ populations (data not shown), which represent immature DN and DP subsets prior to positive selection, respectively. Instead, I found that the TEC-specific *Lmnb1* mutant thymus had a significant reduction (~50-60%) of the $TCR\beta^{high}CD69^{+}$ population, which represents thymocytes completing positive selection (Fig 3-5A and B, shown in black box). The aged thymus also exhibits a mild reduction (~30-40%) of the $TCR\beta^{high}CD69^{+}$ population (Fig 3-5A middle; Fig 3-5B, left). Collectively, these findings strongly suggest that impaired αβT-cell development caused by *Lmnb1* deletion in TECs is most likely due to

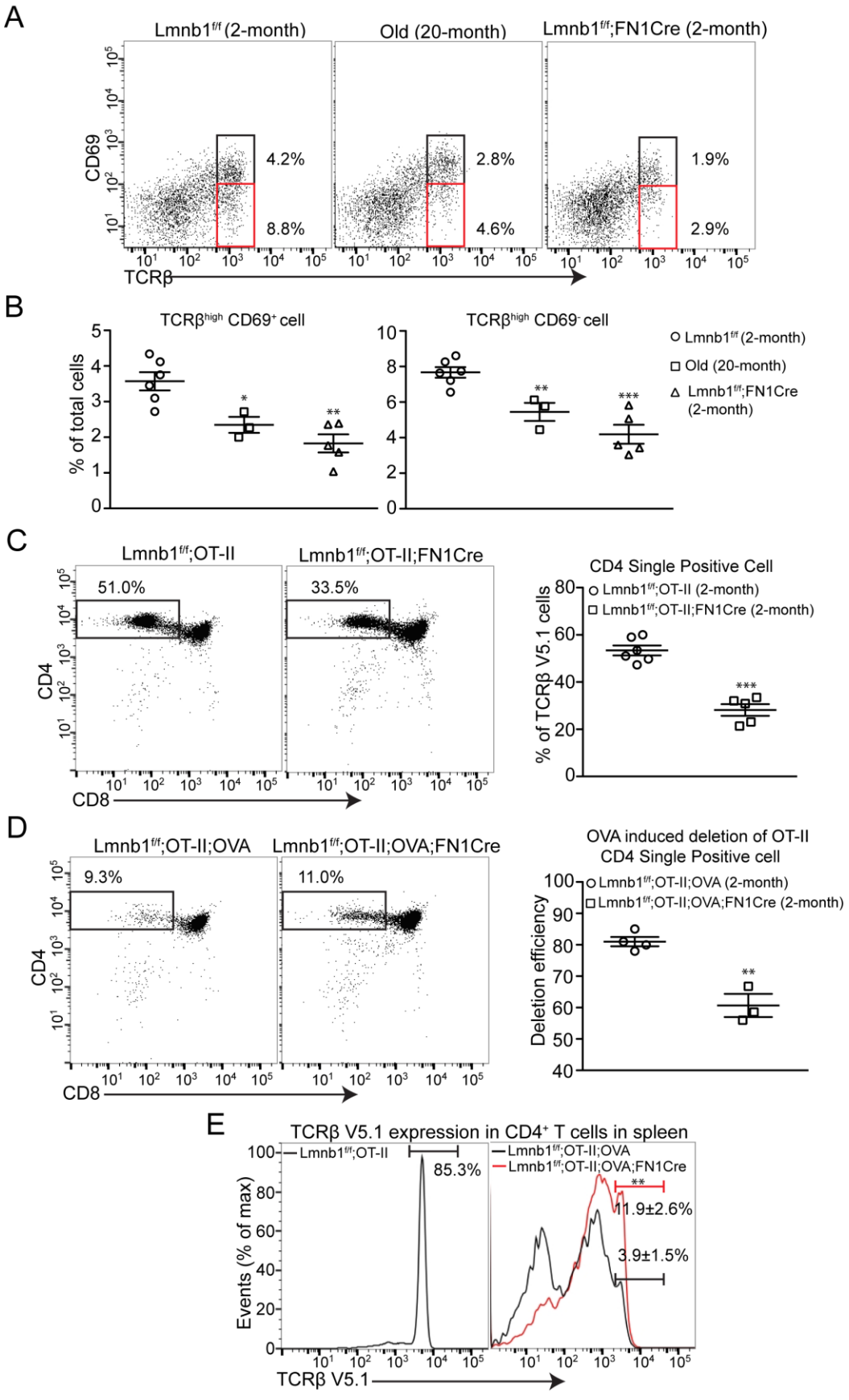
A
Lmnb1f/f (2-month)
Old (20-month)
Lmnb1f/f;FN1Cre (2-month)
CD69
TCRβ
4.2%
8.8%
2.8%
4.6%
1.9%
2.9%
B
TCRβhigh CD69+ cell
TCRβhigh CD69- cell
% of total cells
Lmnb1f/f (2-month)
Old (20-month)
Lmnb1f/f;FN1Cre (2-month)
C
Lmnb1f/f;OT-II
Lmnb1f/f;OT-II;FN1Cre
51.0%
33.5%
CD4
CD8
CD4 Single Positive Cell
% of TCRβ V5.1 cells
Lmnb1f/f;OT-II (2-month)
Lmnb1f/f;OT-II;FN1Cre (2-month)
D
Lmnb1f/f;OT-II;OVA
Lmnb1f/f;OT-II;OVA;FN1Cre
9.3%
11.0%
OVA induced deletion of OT-II
CD4 Single Positive cell
Deletion efficiency
Lmnb1f/f;OT-II;OVA (2-month)
Lmnb1f/f;OT-II;OVA;FN1Cre (2-month)
E
TCRβ V5.1 expression in CD4+ T cells in spleen
Lmnb1f/f;OT-II
Lmnb1f/f;OT-II;OVA
Lmnb1f/f;OT-II;OVA;FN1Cre
85.3%
11.9±2.6%
3.9±1.5%
Events (% of max)
TCRβ V5.1

Fig 3-5. Lamin-B1 deficiency in TECs results in defective positive and negative selection. (A) Flow cytometry analysis of TCRβ and CD69 expression of thymocyte subsets undergoing positive selection. Black box: $TCR\beta^{high}CD69^{+}$ population; red box: $TCR\beta^{high}CD69^{-}$ population. (B) Quantification of $TCR\beta^{high}CD69^{+}$ (left) and $TCR\beta^{high}CD69^{-}$ populations (right). WT, n=6; *Lmnb1* mutant, n=5; Age, n=3. (C) Flow cytometry analysis of CD4 and CD8 expression reveals a reduction of $CD4^{+}$ SP upon *Lmnb1* depletion in OT-II transgenic TCR model. Left: representative FACS dot plots; right: quantification of frequency of CD4SP within OT-II transgenic TCR thymocytes (n=5). (D) Flow cytometry analysis reveals a significant reduction of $CD4^{+}$ SP induced by OVA-mediated deletion in both control and *Lmnb1* mutant thymus (left); quantification of OVA-mediated deletion efficiency of $CD4^{+}$ SP in control and *Lmnb1* mutant thymus (right, n=3). (E) Flow cytometry analysis of surface expression of OT-II transgenic TCRβ V5.1 on $CD4^{+}$ T cells from the spleen. The left histogram shows the frequency of TCRβ $V5.1^{high}$ population in the spleen of control $Lmnb1^{f/f}$;OTII (n=3); The right histogram overlay shows the frequency of TCRβ $V5.1^{high}$ population in the spleen of control $Lmnb1^{f/f}$;OTII;OVA (black, n=4) and $Lmnb1^{f/f}$;OTII;OVA;FN1Cre mice (red, n=3). All data shown are representative of at least 3 independent experiments and are plotted as mean ± SEM. Student's t test: *, $P < 0.05$; **, $P < 0.01$; ***, $P < 0.001$; ns, not significant.

altered positive selection. In addition, the *Lmnb1* mutant thymus also exhibited a marked decrease in the frequency of mature TCRβ^{high}CD69^{-} population (Fig 3-5A, shown in red box; Fig 3-5B, right), implying either enhanced negative selection or a defective final maturation process caused by lamin-B1 deficiency in mTECs in the medulla region.

Developmental defects in T-cell selection can be assessed in mouse genetic models bearing different transgenic TCRs. Among these, the OT-II is a MHC class II-restricted TCR-transgenic mouse allele commonly used to examine positive selection. When DP cells express the OT-II transgenic TCR, ~50% of DP cells are preferentially induced towards CD4^{+} SP cells (Fig 3-5C left), thus facilitating quantitative analysis of defects in positive selection. In the thymus of *Lmnb1*$^{f/f}$; OT-II; FN1Cre mouse, I found a substantial reduction of transgenic CD4^{+} SP cells (Fig 3-4C), demonstrating that lamin-B1 plays an important role in cTEC-mediated positive selection. It is noteworthy that the FN1Cre was only expressed in ~75-80% TECs based on results from a reporter allele (Gordon et al., 2007), indicating that ~20-25% of TECs escape Cre-mediated gene deletion. I would expect more severe defects in positive selection if *Lmnb1* were completely depleted in cTECs. The milder phenotype may be due to the residual WT TECs, which can ameliorate the defects.

I next turned to the RIP-mOVA model to assess whether lamin-B1 deficiency in mTEC affected negative selection since dysfunctional negative selection also leads to alteration in CD4^{+} and CD8^{+} SP cells. The RIP-mOVA allele uses the rat insulin promoter to drive the expression of chicken ovalbumin (OVA), an antigen recognized by OVA-specific OT-II TCRs, in mTECs and preferentially induces the apoptosis of transgenic OT-II CD4^{+} SP cells (Anderson et al., 2005). In this experiment, I analyzed the

frequency of transgenic OT-II $CD4^+$ SP cells in the thymus of *Lmnb1*$^{f/f}$; OT-II; RIP-mOVA; FN1Cre and the littermate control *Lmnb1*$^{f/f}$; OT-II; RIP-mOVA. As reported in previous studies, RIP-mOVA led to a dramatic reduction of $CD4^+$ SP in both *Lmnb1* mutant and control thymus (Fig 3-5D, left). To measure the efficiency of RIP-mOVA-induced negative deletion, I first calculated the ratio of residual $CD4^+$ SP cells between the *Lmnb1*$^{f/f}$; OTII; RIP-mOVA thymus and the *Lmnb1*$^{f/f}$; OTII thymus, which indicated the percentage of surviving $CD4^+$ SP cells post negative selection. The deletion efficiency was then calculated (Equation =100%-percentage of survival) (Metzger et al., 2013). Consistent with previous reports, RIP-mOVA induced more than 80% deletion of transgenic OT-II $CD4^+$ SP cells in the control thymus, while a slightly reduced deletion (~60%) of OT-II $CD4^+$ SP was observed in *Lmnb1* mutant thymus (Fig 3-5D, right). I would expect more reduced efficiency of negative selection if *Lmnb1* were completely deleted in mTECs as the residual WT mTECs could ameliorate the defects. This suggests that lamin-B1 deficiency in mTECs results in inefficient negative selection. By staining with an antibody specific for the transgenic OT-II TCR, I further found a significant increase in the frequency of OT-II TCR Vβ5.1^{high} $CD4^+$ T cells in peripheral immune organs such as the spleen and lymphoid node (data not shown) in *Lmnb1* mutant mice (Fig 3-5E). This result indicates that an increased number of transgenic OT-II $CD4^+$ SP cells escape negative deletion in *Lmnb1* mutant thymus. Taken together, the results from transgenic TCR mouse models demonstrate that lamin-B1 is important for cTEC-mediated positive selection and mTEC-mediated negative selection processes.

I further investigated how lamin-B1 deficiency impacted the functional capacity of TECs. The processes of T-cell positive and negative selection are primarily mediated

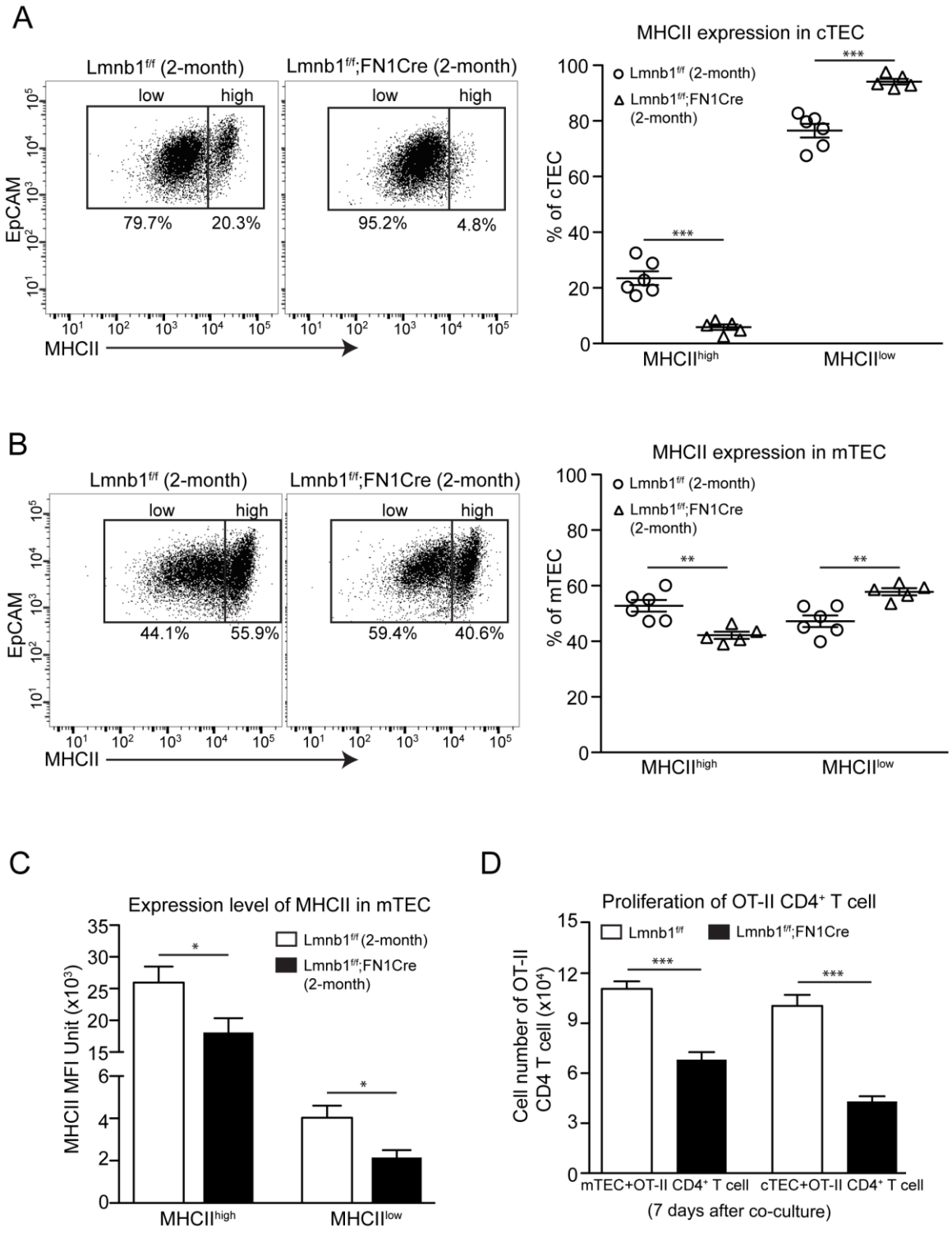

Fig 3-6. Lamin-B1 deficiency in TECs leads to reduced MHCII expression and defective antigen presentation capacity. (A) Flow cytometry analysis of MHCII reveals

a loss of MHCII^{high} cTEC subset in *Lmnb1* mutant thymus (left); quantification of percentages of MHCII^{high} and MHC^{low} cTEC subsets in control *Lmnb1*$^{f/f}$ (n=6) and *Lmnb1* mutant (n=5) thymus. (B) Flow cytometry analysis of MHCII expression reveals a reduction of MHCII^{high} mTEC subset in *Lmnb1* mutant thymus (left); quantification of percentages of MHCII^{high} and MHC^{low} mTEC subsets in control *Lmnb1*$^{f/f}$ (n=6) and *Lmnb1* mutant (n=5) thymus. (C) Summary of MHCII MFI in MHCII^{high} and MHCII^{low} mTEC subsets in control *Lmnb1*$^{f/f}$ (n=6) and *Lmnb1* mutant (n=5) thymus. (D) Proliferative response of naïve OT-II CD4^{+} T cells stimulated by purified mTEC and cTEC from 2-month-old control *Lmnb1*$^{f/f}$ and *Lmnb1* mutant thymus. The numbers of OT-II CD4^{+} T cells were counted 7 days after co-culture in the presence of 10 nM OVA 323-339 peptide. All data shown are representative of at least 3 independent experiments and are shown as mean ± SEM. Student's t test: *, $P < 0.05$; **, $P < 0.01$; ***, $P < 0.001$; ns, not significant.

by interactions between TCRs expressed on thymocytes and MHC-peptide complexes presented on TECs. Expression of MHC class II molecules on TECs plays key roles in mediating proper selections for functionally competent and self-tolerant T cells. It has been reported that both cTECs and mTECs can be defined into $MHCII^{low}$ and $MHCII^{high}$ subsets based on the expression levels of MHCII molecules and a decline in the most differentiated $MHCII^{high}$ TECs is a hallmark change in aged mouse thymus (Chinn et al., 2012; Gray et al., 2006). Strikingly, I found a nearly complete loss of $MHCII^{high}$ cTEC subpopulation in *Lmnb1* mutant thymus (Fig 3-6A), which has been suggested as the key population mediating the positive selection (Gray et al., 2006). While *Lmnb1* depletion in mTECs caused a mild reduction in frequency of $MHCII^{high}$ subset (54 ± 4% in WT and 42 ± 3% in *Lmnb1* mutant thymus; P value=0.003) (Fig 3-6B), I found a ~30% ($MHCII^{high}$ subset) and a ~50% ($MHCII^{low}$ subset) reduced expression level of MHCII molecules on *Lmnb1* mutant mTECs (Fig 3-6C), indicating a reduced capability for antigen presentation. Previous studies suggested that TEC-mediated selection was executed in a manner analogous to antigen presentation and activation of T cells for proliferation in the peripheral (Gray et al., 2006). Therefore, I purified cTECs and mTECs from WT and *Lmnb1* mutant thymus and then assessed their capacity to present cognate OVA peptide to stimulate proliferation of naïve transgenic OT-II $CD4^+$ T cells *in vitro* (see method). As expected, *Lmnb1* mutant mTECs or cTECs exhibited a poor capability to stimulate proliferation of OT-II $CD4^+$ T cells after 7-day *in vitro* co-culture (Fig 3-6D), further supporting the idea that defective positive and negative selection observed in *Lmnb1* mutant thymus was at least in part due to low efficacy in antigen presentation by lamin-B1-deficient TECs.

Discussion

In this study I further characterized the functional roles of lamin-B1 in the thymus, which showed an age-associated reduction in TECs as discussed in Chapter 2. My data demonstrated that lamin-B1 was pivotal for establishing a proper thymic niche environment to foster normal αβ but not γδ T-cell development. Using Foxn1Cre-mediated deletion, I showed that TEC-specific deletion of *Lmnb1,* but not *Lmnb2 and Lmna,* resulted in severe thymic atrophy with significantly reduced cellularity and abnormal thymic architecture. Intuitively, this suggested a lamin-B1-specific function in TECs as a recent study indicated that lamin-B1 and -B2 might have unique roles in the developing brain (Lee et al., 2014). However, since the assembly of each lamin into the NL depends primarily on the total lamin protein concentration present in the nucleus (Guo et al., 2014), another plausible explanation is that lamin-B1 is the most abundant lamin and lamin-B2 and/or -A/C cannot compensate for the defects caused by lamin-B1 deficiency in TECs. Thus, the striking phenotypes upon *Lmnb1* depletion in TECs may not simply indicate lamin-B1-specific functions in TECs. Further dissection of the role for lamin-B1 and other lamins in different cell types, or using genetic models to test rescue capability of individual lamins, should shed light on how different lamins perform specific and shared functions during tissue building and homeostasis.

Using keratin IF staining assay, I showed for the first time a significant expansion of $K5^+K8^+$ TECs in both aged and *Lmnb1* mutant thymus. Previous lineage tracing data demonstrated that a single $K5^+K8^+$ epithelial cell from an E12 embryonic thymus could differentiate into both mTECs and cTECs after transplantation into a WT fetal thymic lobe (Rossi et al., 2006). This suggests that $K5^+K8^+$ TECs present in the adult thymus

may contain precursors that give rise to both mTEC and cTEC. The expansion of putative $K5^+K8^+$ epithelial progenitors was also reported during irradiation-induced transient thymic atrophy and occurred prior to complete thymic recovery, indicating that TEC progenitors could be reactivated in the adult thymus for regeneration (Popa et al., 2007). The mechanism underlying expansion of $K5^+K8^+$ TEC precursors in aged thymus may differ from that in the irradiation-induced atrophy model as it is unlikely for TEC progenitors to be reactivated in aged thymus without injury or stress. One reasonable explanation is that accumulation of $K5^+K8^+$ TEC precursors is the result of inefficient generation of mature cTEC and mTEC from these precursors due to a defective differentiation program caused by age-associated extrinsic (e.g., inflammatory thymic environment) or intrinsic (e.g., lamin-B1 reduction) changes in aged thymus. Consistent with this, a significant reduction in most mature $MHCII^{high}$ TEC subsets is one of major changes in TEC compartment associated with aging. Interestingly, FACS analysis showed a remarkable increased percentage of a DN-TEC population ($EpCAM^+UEA\text{-}1^-Ly51^-$) in both *Lmnb1* mutant and aged thymus (Fig 3-2D), which may reflect expanded $K5^+K8^+$ TEC precursors. For the future work, keratin IF staining of FACS isolated DN-TECs will be performed to examine whether or not they are real $K5^+K8^+$ TEC precursors. If they are progenitors, further transcriptome analysis should shed light on molecular mechanism mediating age-associated thymic involution.

How does lamin-B1 deficiency in TECs promote thymic adiposity? It is well documented that adipogenic differentiation of cells is mainly induced by activation of peroxisome proliferator activated receptor gamma (PPARγ), a nuclear receptor regulating the transcriptional program required for differentiation of fat cells. Previous studies have

shown a link between the nuclear lamina (NL) and PPARγ-mediated adipogenesis. For example, over-expression of WT lamin-A or a mutant lamin-A identified in Dunnigan-type family partial lipodystrophy (FPLD) prevented differentiation of 3T3-L1 preadipocytes to adipocytes by inhibition of PPARγ2 expression (Boguslavsky et al., 2006). Furthermore, the NL protein, Emerin, was found to regulate adipogenesis by modulating the expression and activity of PPARγ (Tilgner et al., 2009). Finally, dynamic reorganization of the NL and cytoskeleton during fat cell differentiation also implies the potential role of NL in adipogenesis (Verstraeten et al., 2011). While the role of lamin-B1 in adipogenesis has not been reported, it may influence adipogenesis by regulating proper NL assembly and organization, or regulation of PPARγ in TECs. Of interest, I found a significant down-regulation of Ghrelin receptor (GHSR) in *Lmnb1* mutant mTECs, indicating enhanced PPARγ activity in mutant mTECs since GHSR-mediated signaling pathway has been demonstrated to play a key role in inhibiting activation of PPARγ signaling in TECs and preventing age-related thymic adiposity (Youm et al., 2009). While I did not detect a significant change of PPARγ at mRNA level in *Lmnb1* mutant mTECs (data not shown), further experiments will be performed to assess nuclear PPARγ activity in *Lmnb1* mutant TECs.

Interestingly, TEC-specific *Lmnb1* mutant thymus exhibited remarkably similar phenotypes to that of the aged thymus, covering almost all reported age-related alterations, such as skewing of the cTEC:mTEC ratio, a decline in the most differentiated $MHCII^{high}$ subsets, disorganization of TEC compartment and enhanced adiposity. The decline of several other proteins such as Foxn1 have been reported to contribute to thymic aging as mutant thymuses also show some of age-related phenotypes. However, to

my knowledge, the *Lmnb1* mutant thymus is the first model displaying all known age-related defects. In summary, these findings suggest that lamin-B1 may function as a novel gene regulatory node controlling thymic homeostasis. Therefore, identification of lamin-B1-regulated transcriptional program in TECs and comparative analysis with age-associated transcriptome changes should shed light on the molecular mechanism governing thymic homeostasis and aging. In the next Chapter, I will further discuss my effort to apply RNA-seq to analyze the TEC transcriptome in both aged and *Lmnb1* mutant thymus.

Materials and methods

Mice

Lmnb1$^{f/f}$ and *Lmnb2*$^{f/f}$ mice were generated by EUCOMM projects and *Lmna*$^{f/f}$ allele was generated by Dr. Youngjo Kim (Kim and Zheng, 2013). All mice were further backcrossed to the C57BL/6 background for at least 6 generations. Foxn1Cre, K5CreET^{T2} K8CreER^{T2}, OT-II and RIP-mOVA mice were purchased from Jackson Laboratory.

Tamoxifen (TAM) induced *Lmnb1* deletion

Stock solution of TAM (20 mg/ml, Sigma) was prepared by dissolving TAM powder in one volume of 100% ethanol at 55 °C for 2 min and then mixed well with 9 volumes of pre-warmed (55 °C) corn oil. To induce *Lmnb1* (exon 2) deletion, 2-month-old mice were treated with a single intraperitoneal (IP) injection of TAM (1mg/10 g body weight/day) for five successive days and with TAM kept in the drinking water (0.025 mg/ml).

Thymus phenotypes were analyzed 4 weeks after the 5th TAM injection.

Histology and Immunofluorescence Microscopy

Freshly isolated thymuses were embedded in OCT (Leica microsystems) and frozen immediately in −80°C. For H&E and Oil Red staining, 10 μm sections were fixed in 4% formaldehyde solution for 10 min and then processed according to standard protocols. For keratin staining, 10 μm sections were fixed in a 1:1 mixture of acetone and methanol at −20°C for 10 min and then washed with PBS for 3 times. After blocking, samples were stained with primary antibodies containing rat-anti-keratin8 (Troma-1, DSHB, 1:20) and rabbit-anti-keratin5 (Biolegend, 1:300) at room temperature (RT) for 1 hour, followed by Alexa488 goat anti-rat and Alexa568 goat anti-rabbit (Invitrogen) secondary antibodies Samples were then mounted with ProLong® Gold Antifade Mountant (Fisher Scientific) and allowed to dry overnight at RT before imaging. Neutral lipid staining was performed after keratin staining following the manufacturer's protocol (Life technology). Confocal images were acquired using a laser-scanning confocal microscope (Leica SP5) with a 20X or 63X objectives. Images were processed using ImageJ.

Quantitative real-time PCR

Detailed protocol was described in the 2nd chapter. Primer sequences were listed as follows. GHSR: forward primer, GGAAAACAGATATCTTCCCACG; and reverse primer, GGGACCAGAACCACAAACAG. PPARγ2: forward primer, GCCTATGAGCACTTCACAAGAA; reverse primer, TGCGAGTGGTCTTCCATCAC.

Flow cytometry analysis

Detailed protocol was described in the 2nd Chapter. The following FACS monoclonal antibodies were used for this section: CD45, EpCAM, Ly51, I-A/I-E (MHCII), CD4, CD8, TCRβ, TCRγδ, CD69, TCRβV5.1 (Biolegend) and UEA-1 (Vector laboratory). Data was analyzed with FlowJo software (Tree Star).

In vitro OTII CD4 T cell proliferation assay

Purified TEC subsets (~10,000) were co-cultured with 40,000 splenic OT-II $CD4^+$ T cells in the presence of 10 nM OVA 323-339 (GeneScript) in U-bottom 96-well plate (Gray et al., 2006). OT-II $CD4^+$ T cells were isolated using MojoSort Mouse $CD4^+$ T Cell Kit (Biolegend). Splenic dendritic cells were purified by FACS sorting and were included as a positive control. After culture for 7 days, cells were stained with PE-CD4 and counted by FACSAria™ III with 100,000 spike-in FITC-labeled BD Calibrite beads (BD bioscience). The absolute number of OT-II $CD4^+$ T cells was calculated based on the ratio of PE-CD4 vs FITC-beads.

Reference

Anderson, M.S., Venanzi, E.S., Chen, Z., Berzins, S.P., Benoist, C., and Mathis, D. (2005). The cellular mechanism of Aire control of T cell tolerance. Immunity *23*, 227-239.

Aw, D., Silva, A.B., Maddick, M., von Zglinicki, T., and Palmer, D.B. (2008). Architectural changes in the thymus of aging mice. Aging Cell *7*, 158-167.

Boehm, T., and Swann, J.B. (2013). Thymus involution and regeneration: two sides of the same coin? Nat Rev Immunol *13*, 831-838.

Boguslavsky, R.L., Stewart, C.L., and Worman, H.J. (2006). Nuclear lamin A inhibits adipocyte differentiation: implications for Dunnigan-type familial partial lipodystrophy. Hum Mol Genet *15*, 653-663.

Bonneville, M., O'Brien, R.L., and Born, W.K. (2010). Gammadelta T cell effector functions: a blend of innate programming and acquired plasticity. Nat Rev Immunol *10*, 467-478.

Chen, H., Chen, X., and Zheng, Y. (2013). The nuclear lamina regulates germline stem cell niche organization via modulation of EGFR signaling. Cell Stem Cell *13*, 73-86.

Chen, H., Zheng, X., and Zheng, Y. (2014). Age-associated loss of lamin-B leads to systemic inflammation and gut hyperplasia. Cell *159*, 829-843.

Chen, H., and Zheng, Y. (2014). Nuclear lamina builds tissues from the stem cell niche. Fly (Austin) *8*, 63-67.

Chien, Y.H., Meyer, C., and Bonneville, M. (2014). gammadelta T cells: first line of defense and beyond. Annu Rev Immunol *32*, 121-155.

Chinn, I.K., Blackburn, C.C., Manley, N.R., and Sempowski, G.D. (2012). Changes in primary lymphoid organs with aging. Semin Immunol *24*, 309-320.

Dixit, V.D. (2010). Thymic fatness and approaches to enhance thymopoietic fitness in aging. Curr Opin Immunol *22*, 521-528.

Fahl, S.P., Coffey, F., and Wiest, D.L. (2014). Origins of gammadelta T cell effector subsets: a riddle wrapped in an enigma. J Immunol *193*, 4289-4294.

Frost, B., Bardai, F.H., and Feany, M.B. (2016). Lamin Dysfunction Mediates Neurodegeneration in Tauopathies. Curr Biol *26*, 129-136.

Gordon, J., Xiao, S., Hughes, B., 3rd, Su, D.M., Navarre, S.P., Condie, B.G., and Manley, N.R. (2007). Specific expression of lacZ and cre recombinase in fetal thymic epithelial cells by multiplex gene targeting at the Foxn1 locus. BMC Dev Biol *7*, 69.

Gray, D.H., Seach, N., Ueno, T., Milton, M.K., Liston, A., Lew, A.M., Goodnow, C.C., and Boyd, R.L. (2006). Developmental kinetics, turnover, and stimulatory capacity of thymic epithelial cells. Blood *108*, 3777-3785.

Guo, Y., Kim, Y., Shimi, T., Goldman, R.D., and Zheng, Y. (2014). Concentration-dependent lamin assembly and its roles in the localization of other nuclear proteins. Mol Biol Cell *25*, 1287-1297.

Johnson, A.L., Aravind, L., Shulzhenko, N., Morgun, A., Choi, S.Y., Crockford, T.L., Lambe, T., Domaschenz, H., Kucharska, E.M., Zheng, L.*, et al.* (2009). Themis is a member of a new metazoan gene family and is required for the completion of thymocyte positive selection. Nat Immunol *10*, 831-839.

Ki, S., Park, D., Selden, H.J., Seita, J., Chung, H., Kim, J., Iyer, V.R., and Ehrlich, L.I. (2014). Global transcriptional profiling reveals distinct functions of thymic stromal subsets and age-related changes during thymic involution. Cell Rep *9*, 402-415.

Kim, Y., Sharov, A.A., McDole, K., Cheng, M., Hao, H., Fan, C.M., Gaiano, N., Ko, M.S., and Zheng, Y. (2011). Mouse B-type lamins are required for proper organogenesis but not by embryonic stem cells. Science *334*, 1706-1710.

Kim, Y., and Zheng, Y. (2013). Generation and characterization of a conditional deletion allele for Lmna in mice. Biochem Biophys Res Commun *440*, 8-13.

Klug, D.B., Carter, C., Crouch, E., Roop, D., Conti, C.J., and Richie, E.R. (1998). Interdependence of cortical thymic epithelial cell differentiation and T-lineage commitment. Proc Natl Acad Sci U S A *95*, 11822-11827.

Lee, J.M., Tu, Y., Tatar, A., Wu, D., Nobumori, C., Jung, H.J., Yoshinaga, Y., Coffinier, C., de Jong, P.J., Fong, L.G.*, et al.* (2014). Reciprocal knock-in mice to investigate the functional redundancy of lamin B1 and lamin B2. Mol Biol Cell *25*, 1666-1675.

Lesourne, R., Uehara, S., Lee, J., Song, K.D., Li, L., Pinkhasov, J., Zhang, Y., Weng, N.P., Wildt, K.F., Wang, L.*, et al.* (2009). Themis, a T cell-specific protein important for late thymocyte development. Nat Immunol *10*, 840-847.

Metzger, T.C., Khan, I.S., Gardner, J.M., Mouchess, M.L., Johannes, K.P., Krawisz, A.K., Skrzypczynska, K.M., and Anderson, M.S. (2013). Lineage tracing and cell ablation identify a post-Aire-expressing thymic epithelial cell population. Cell Rep *5*, 166-179.

Popa, I., Zubkova, I., Medvedovic, M., Romantseva, T., Mostowski, H., Boyd, R., and Zaitseva, M. (2007). Regeneration of the adult thymus is preceded by the expansion of K5+K8+ epithelial cell progenitors and by increased expression of Trp63, cMyc and Tcf3 transcription factors in the thymic stroma. Int Immunol *19*, 1249-1260.

Rossi, S.W., Jenkinson, W.E., Anderson, G., and Jenkinson, E.J. (2006). Clonal analysis reveals a common progenitor for thymic cortical and medullary epithelium. Nature *441*, 988-991.

Tilgner, K., Wojciechowicz, K., Jahoda, C., Hutchison, C., and Markiewicz, E. (2009). Dynamic complexes of A-type lamins and emerin influence adipogenic capacity of the cell via nucleocytoplasmic distribution of beta-catenin. J Cell Sci *122*, 401-413.

Verstraeten, V.L., Renes, J., Ramaekers, F.C., Kamps, M., Kuijpers, H.J., Verheyen, F., Wabitsch, M., Steijlen, P.M., van Steensel, M.A., and Broers, J.L. (2011). Reorganization of the nuclear lamina and cytoskeleton in adipogenesis. Histochem Cell Biol *135*, 251-261.

Yang, H., Youm, Y.H., Nakata, C., and Dixit, V.D. (2007). Chronic caloric restriction induces forestomach hypertrophy with enhanced ghrelin levels during aging. Peptides *28*, 1931-1936.

Youm, Y.H., Yang, H., Sun, Y., Smith, R.G., Manley, N.R., Vandanmagsar, B., and Dixit, V.D. (2009). Deficient ghrelin receptor-mediated signaling compromises thymic stromal cell microenvironment by accelerating thymic adiposity. J Biol Chem *284*, 7068-7077.

Chapter 4: Transcriptome profiling identifies lamin-B1-mediated and aged-associated signatures in TECs

Summary

Whole genome analysis of age-associated transcriptome changes in TECs is critical for the understanding of the molecular drivers of thymic involution. So far, only one study applied DNA microarray for transcriptional profiling of thymic stromal subsets during early stage of thymic involution (ranging from 1 to 6 month of age). However, similar transcriptome analysis for late stage of thymic involution is lacking and as a result, the mechanisms mediating postnatal thymic homeostasis remain largely unknown. Using RNA-seq technology, I report here, for the first time, whole genome-wide transcriptome profile of two major TEC subsets, cTEC and mTEC, from young (2-month), early-stage involution (6-month) and late-stage thymic involution (20-month). My RNA-seq data reveal a significant enrichment of genes in the inflammatory/immune response in mTECs during early involution stage, indicating that acquisition of an inflammatory signature is a hallmark of early involution. I also show that an enrichment of genes in non-TEC lineage development and functions is a common feature for both cTECs and mTECs from aged mouse thymus. Furthermore, I observed that the transcriptional alterations seen in cTECs and mTECs isolated from the 6-month-old *Lmnb1* mutant thymus were remarkably similar to those observed in the 20-month-old WT thymus, indicating that *Lmnb1* deficiency accelerates age-associated transcriptional program in TECs. Deep mining RNA-seq data should provide a conceptual framework for understanding the mechanism governing TEC homeostasis and aging.

Introduction

The recent advance in high-throughput sequencing technology has made whole genome transcriptional profiling a widely available tool to accelerate scientific progress. In line with this, transcriptome analyses of several key cell populations in the immune system by the Immunological Genome Project Consortium have generated important insights into the principles of immune system development, maintenance and function (Benoist et al., 2012). Much effort has recently been made in the TEC field to dissect transcriptional features of distinct TEC subsets using genome-wide approaches. Despite the limited number of studies, they have expanded our understanding of TEC biology (Brennecke et al., 2015; Sansom et al., 2014; St-Pierre et al., 2013). For example, transcriptional profiling of cTEC and mTEC isolated from neonatal thymus highlights substantial divergences in transcriptional landscape of these two TEC subsets (St-Pierre et al., 2013). Using single-cell RNA-seq of individual MHCII^{high} mTEC, the Hollander group shows that mTECs are capable of expressing up to 19,293 protein-coding genes, which is the highest number of expressed genes in any known cell type. This high number of expressed genes in mTECs ensures a comprehensive coverage of self-antigens in mTECs and efficiently eliminates self-reactive T cells to establish central tolerance.

Despite much progress in the understanding of TEC developmental programs, the molecular pathways that regulate age-associated involution still remain largely unknown. Until very recently, a global transcriptional profiling of thymic stromal subsets uncovered unexpected age-related transcriptional changes during early thymic involution (Ki et al., 2014). While the reduction of Foxn1 expression is generally accepted as a prime mediator of thymic involution (Chinn et al., 2012), Foxn1 was not identified as an differentially

expressed gene in mTECs during early thymic involution (6-month), arguing against the central role of Foxn1 in involution. The study concluded that the predominant transcriptional features in TECs during early thymic involution include reduced expression of cell-cycle-related genes in MHCII^{low} mTECs and E2F3 targets in cTEC and MHCII^{low} mTECs. In addition, increased expression of proinflammatory cytokines in thymic DC is another hallmark of early involution, indicating that inflammation plays a more important role than previously thought in triggering thymic involution. Due to dramatically reduced TEC cell numbers during late stage of thymic involution, transcriptome analysis of age-associated changes in TECs during late stage has not been reported. Here, I present transcriptome profiling of two major TEC subsets, cTEC and mTEC, from young (2-month), early involution (6-month) and late involution (20-month) thymuses. My RNA-seq datasets provide a valuable resource for the TEC and immunology fields to further dissect the molecular mechanism underlying age-associated thymic involution. Importantly, I show that the TEC transcriptional landscape in 6-month-old *Lmnb1* mutant thymus exhibits remarkable similarity to that in the 20-month-old aged WT thymus. Together with the TEC phenotypes observed upon *Lmnb1* depletion described in Chapter 3, these results strongly suggest that age-associated loss of lamin-B1 in TECs accelerates age-related transcriptome changes and triggers a degenerative cascade in the thymus, which ultimately leads to immune deficiency.

Results

Identification of age-associated transcriptional signatures in cTECs

To explore the molecular mechanism underlying age-related thymic involution, I decided to apply RNA-seq to profile the transcriptome of TECs isolated from different stages of WT thymuses. I chose RNA-seq rather than microarray analysis because RNA-seq offers higher sensitivity, resolution and less technical variation. To identify age-related differential expression of genes (DEGs), I applied stringent criteria for comparison and considered DEGs as those genes with fold change ≥ 2 relative to a 2-month-old WT control with adjusted false discovery rate (FDR) <0.05 and p value <0.05 (See the method section). I will first report age-associated transcriptional changes related to cTEC and then turn to mTEC later in this chapter.

While no significant age-related DEGs were reported in cTECs in early involution (Ki et al., 2014), the study used microarray for gene analysis. The lower detection sensitivity of microarray technology may mask some real DEGs. Thus, I employed RNA-seq to reassess gene expression associated with early involution in cTECs from mice at 2 and 6 months of age. I identified 74 up- and 90 down-regulated genes (Fig 4-1A) and then performed Gene Ontology (GO) term analysis to examine biological functions altered in cTECs during early involution. Consistent with the early report, no functional category related to thymic development and homeostasis was identified.

Since transcriptional profiling of TECs from late thymic involution has not been reported, I then decided to evaluate gene expression changes in cTECs from mice at 2 and 20 months of age. Using the same criteria, I identified 1486 up- and 446-down-regulated genes in aged cTECs (Fig 4-1A). Interestingly, among the up-regulated genes,

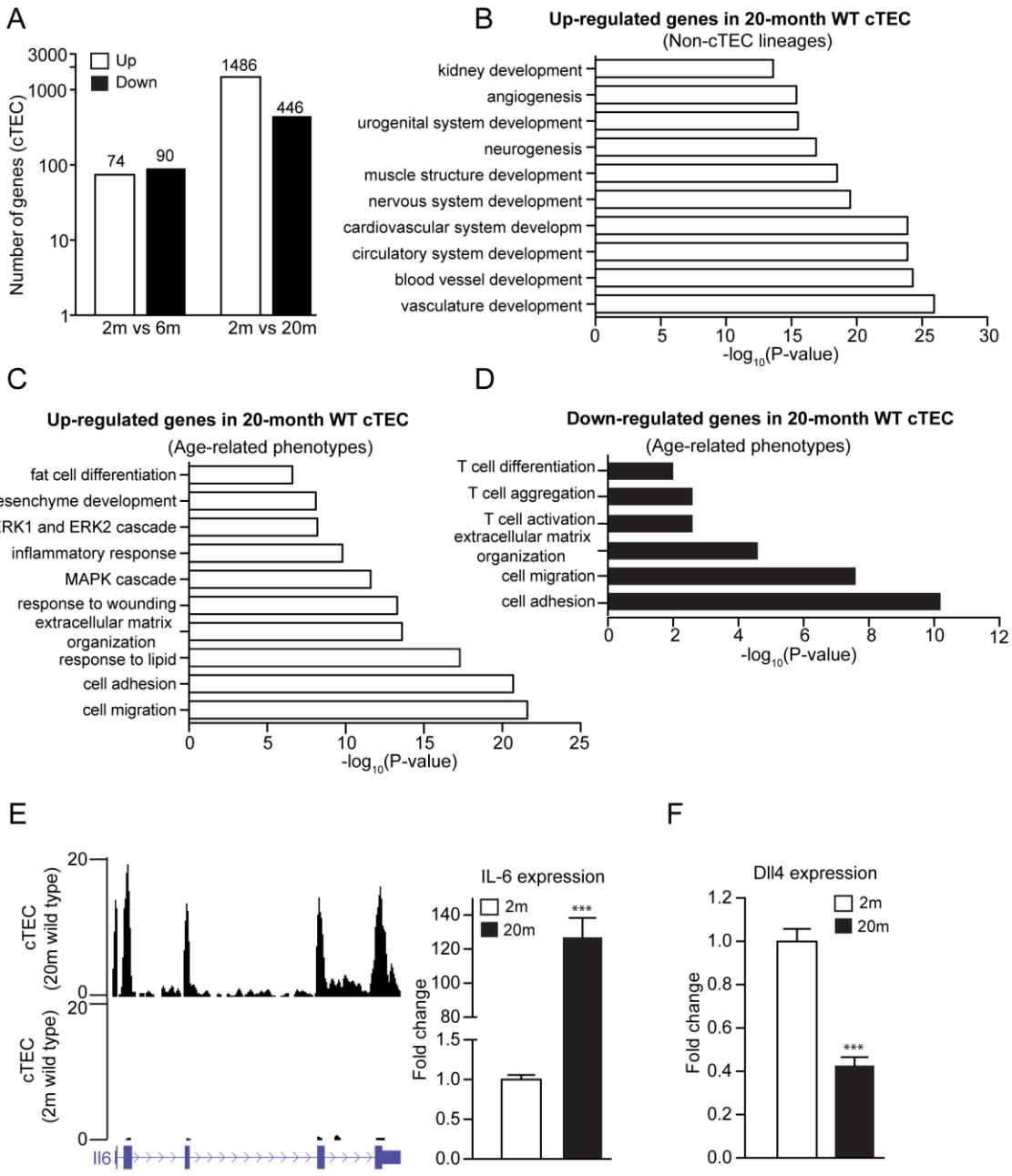

Fig 4-1. RNA-seq analysis reveals age-related transcriptional signatures in cTECs. (A) Summary of the number of up- (white) and down-regulated (black) genes (fold change ≥2) in WT cTECs during early involution (6-month) and late involution (20-month). (B) The top10 significant GO terms for the up-regulated genes are involved in development and function for the non-cTEC cells in cTECs from 20-month-old WT

thymus. (C)-(D) The top significant GO terms for up- (C) or down-regulated (D) genes with regards to age-associated phenotypes in cTECs from 20-month-old WT thymus. (E) The genome browser views show up-regulation of IL-6 expression in aged cTEC (left) and qRT-PCR analysis of IL-6 expression in young (2-month) and aged (20-month) cTECs (right). (F) qRT-PCR analysis reveals reduced expression of Dll4 in aged cTECs. All data shown are representative of at least 3 independent experiments and are plotted as mean ± SEM. Student's t test: *, $P < 0.05$; **, $P < 0.01$; ***, $P < 0.001$; ns, not significant.

GO term analysis revealed a significant enrichment of genes required for the development of many tissues and organs other than the thymus (Fig 4-1B, top10 listed). This pattern of enrichment was similar to that observed in cTECs from 6-month-old *Lmnb1* mutant thymus (Fig 4-4B, discussed in the later section). A recent study reported that cTECs from young mouse thymus express up to 84% of protein-coding genes covering nearly all peripheral tissues, which contributes to shape the maximal repertoire of self-peptides for positive selection (Sansom et al., 2014). The exact physiological meaning of up-regulation of non-cTEC lineage genes in aged cTECs is not clear, but this may interrupt the normal functions of cTECs and may lead to inefficient generation of $CD4^+$ SP and $CD8^+$ SP cells observed in aged thymus.

Additional GO term analyses further revealed up- and down-regulation of important processes involved in age-associated thymic phenotypes, respectively (Fig 4-1C and D). I first found an enrichment of genes associated with cell adhesion, migration and extracellular matrix organization (Fig 4-1C), which correlated with disruption of TEC organization and architecture in aged thymus (Fig 3-2B, Chapter 3). Consistent with enhanced adipogenesis in aged thymus, I observed a large fraction of up-regulated genes enriched in response to lipid, mesenchyme development and fat cell differentiation, providing a molecular mechanism for the possible generation of adipose cells from TECs (Fig 4-1C). Early studies demonstrated that p38 and/or ERK1/2 MAPKs played critical roles in regulating production of inflammatory cytokines such as IL-6 in cultured human thymic epithelial cells *in vitro* (Colombara et al., 2005; Mainiero et al., 2003). Whether or not the same mechanisms involved in promoting elevated inflammatory cytokines in TECs from aged mouse thymus *in vivo* is not known. GO term analyses further revealed

that up-regulated genes are highly enriched in the MAPK and ERK1/2 cascades (Fig 4-1C) and I also confirmed more than 100-fold increased production of IL-6 in cTEC from 20-month-old WT thymus (Fig 4-1E), indicating conserved mechanisms mediating inflammatory cytokine production in the mouse thymus. Further, I observed many genes involved in response to wounding and inflammation, which are in agreement with previously reported changes in the inflammation-induced thymic involution model (Billard et al., 2011) (Fig 2-5, Chapter 2). Consistent with impaired thymopoiesis upon aging, GO term analysis of down-regulated genes revealed an enrichment of genes with functions in T-cell activation, aggregation and differentiation (Fig 4-1D). Two key genes, Dll4 (Delta Like Canonical Notch Ligand 4) and Foxn1, were identified from all 3 categories. Dll4 is required for a functional thymic niche to promote survival and differentiation of early thymocyte progenitors (Koch et al., 2008). I observed a ~60% reduction in Dll4 expression in cTECs during the late stage of thymic involution (Fig 4-1F), suggesting that a decline of Notch signaling contributes to impaired thymopoiesis. The expression of Foxn1 also showed a similar reduction (~60%, data not shown) as Dll4 in cTECs, but not in mTECs, which was consistent with a recent study showing expansion of Foxn1-negative cTECs during the late thymic involution stage (O'Neill et al., 2016). Since a recent genome-wide Foxn1 Chip-seq study demonstrates that Foxn1 regulates key genes involved in antigen processing and selection for T-cell development (Zuklys et al., 2016), decreased Foxn1 expression in cTECs may further exacerbate the defective thymopoiesis seen during the late stage of thymic involution.

Age-associated transcriptional features in mTECs

A previous study concluded that down-regulation of cell-cycle related genes in mTEC subset is a key feature of early thymic involution (Ki et al., 2014). However, the study chose a one-month-old thymus as young control group, which is at a time when the thymus undergoes quick development, expansion and growth. Additionally, there were no significant changes of cell-cycle genes in mTECs between 3-month-old and 6-month-old thymus shown in the same study. Thus, the conclusions from this initial study may overestimate the contribution of cell-cycle genes to early thymic involution. To identify early thymic involution related transcriptional signatures, I compared the expression profiles of mTECs from mice at 2- and 6-month of age and initially identified 92 up- and 63 down-regulated genes (Fig 4-2A). GO term analysis of up-regulated transcripts revealed a significant enrichment of genes with functions in inflammatory/immune response, wound healing and response to IL-1 (Fig 4-2B), indicating an inflammatory signature in mTECs. Together with my early results showing increased expression of proinflammatory cytokines in sirpα^+ DC and macrophage upon aging (Chapter 2), these data strongly suggest that thymic myeloid lineage cell-derived inflammation plays a key role in triggering onset of early thymic involution.

I next evaluated the gene expression profile in mTECs from mice at 2- and 20-month of age and identified 545 up- and 754 down-regulated genes associated with late thymic involution (Fig 4-2A). GO term analysis revealed a significant enrichment of up-regulated genes with functions in non-mTEC lineage development and functions (Fig 4-2C, top10 listed), a similar pattern also observed in cTECs from aged thymus (Fig 4-1B). Among these non-mTEC lineages, I observed a ~10-fold increased expression of GCM2,

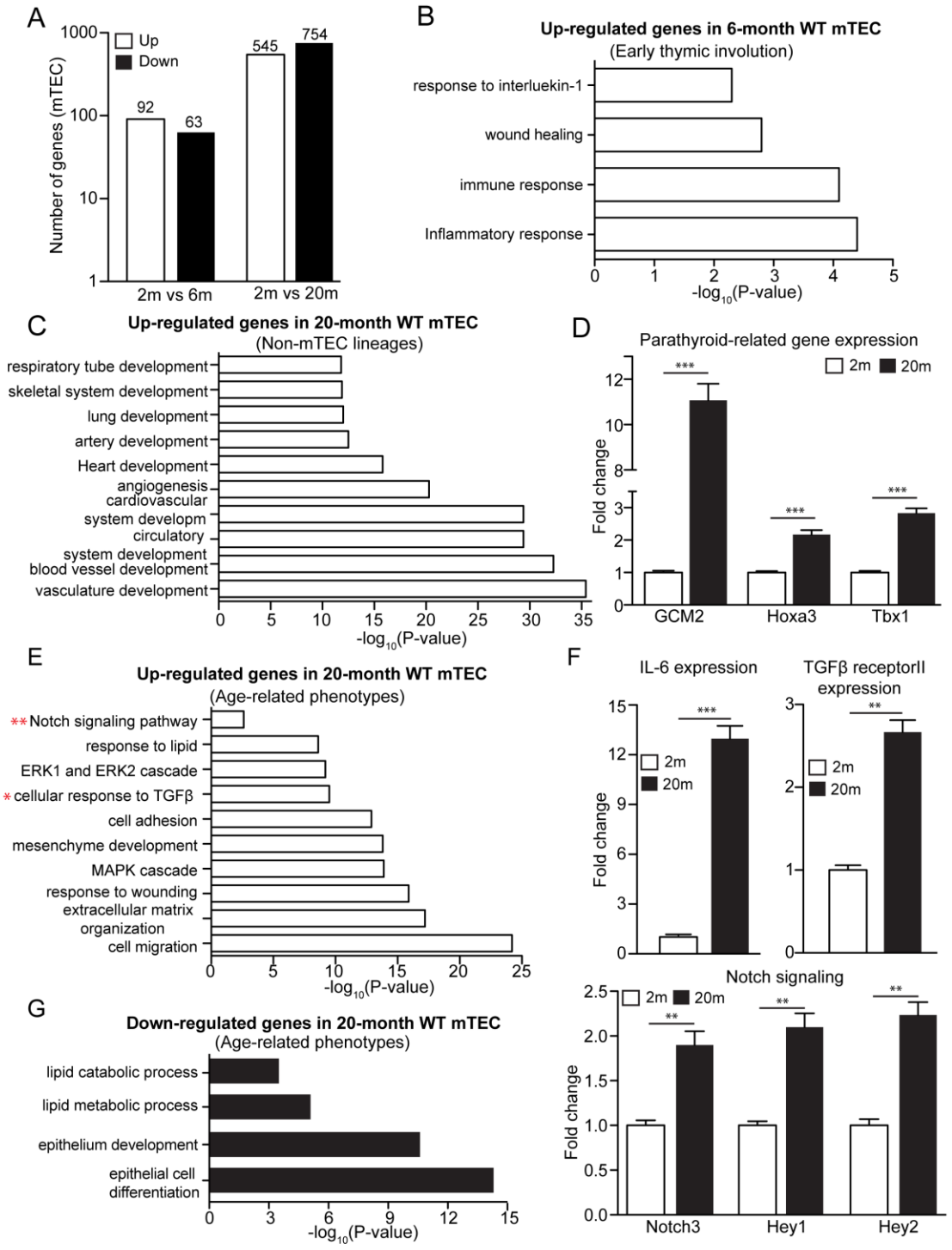

Fig 4-2. RNA-seq analysis identifies age-related transcriptional features in mTECs. (A) Summary of the number of up- (white) and down-regulated (black) genes (fold change ≥2) in WT mTECs during early involution (6-month) and late involution (20-

month). (B) The top significant GO terms for up-regulated genes in mTECs during early thymic involution (6-month). (C) The top10 significant GO terms for the up-regulated genes are involved in non-mTEC lineage development and function in mTECs from 20-month-old thymus. (D) qRT-PCR analysis of parathyroid gland related genes GCM2, Hoxa3 and Tbx1 in young (2-month) and aged (20-month) WT mTECs. (E) The top significant GO terms for the up-regulated genes with regarding to age-associated phenotypes in mTECs from 20-month-old thymus; (F) qRT-PCR analysis of selected up-regulated genes in young (2-month) and aged (20-month) mTECs: IL6 (top left); TGFβ receptor II (top right); Notch signaling (bottom). (G) The top significant GO terms for down-regulated genes with respect to age-associated phenotypes in mTECs from 20-month-old thymus. All data shown are representative of at least 3 independent experiments and are plotted as mean ± SEM. Student's t test: *, $P < 0.05$; **, $P < 0.01$; ***, $P < 0.001$; ns, not significant.

a transcriptional factor for parathyroid gland, in mTECs (not found in cTECs) from 20-month-old aged thymus. In addition, I also found increased expression of parathyroid gland related genes including Hoxa3 and Tbx1 in mTECs from aged thymus (Fig 4-2D). Given that the thymus and parathyroid gland are derived from the same primordium during early embryonic stage, these results strongly suggested that the altered transcriptional program in aged mTECs led to non-mTEC lineage differentiation and in turn interrupted appropriate functions of mTECs.

Further analysis revealed similar enrichments in functional categories observed in cTECs, including thymic structural organization, response to lipid/mesenchyme development (adiposity-related), MAPK and ERK1/2 cascades and intrathymic inflammatory reaction (Fig 4-2E). I also confirmed a more than 10-fold increased production of IL-6 in aged mTECs using qRT-PCR assay (Fig 4-2F, top left). These results suggested that age-associated changes of intrathymic environment might lead to common transcriptional alterations in both cTECs and mTECs.

A recent study demonstrated that TGFβ signaling played a negative regulatory role in the establishment and function of the thymic medulla by inhibiting differentiation and proliferation of mTECs (Hauri-Hohl et al., 2014). However, the role of TGFβ signaling in thymic aging has not been investigated. Interestingly, I observed a large number of up-regulated genes involved in the TGFβ signaling pathway and further confirmed the increased expression of TGFβ receptor II in mTECs from 20-month-old WT thymus (Fig 4-2E, marked with one red star; Fig 4-2F, top right). These data indicated that reduced proliferation and differentiation of mTECs documented in aged thymus was caused at least in part by enhanced TGFβ signaling. Interestingly, I found

many up-regulated genes enriched in the Notch signaling pathway (Fig 4-2E, marked with two red stars) and subsequent qRT-PCR analysis validated the increased expression of key Notch signaling components, such as Notch3, Hey1 and Hey2 (Fig 4-2F, bottom). While Notch signaling pathway is well studied in the T cell context, the role of Notch signaling in TEC development is largely unknown. A recent study reported that Notch signaling was active in cTECs and/or early immature mTEC subset and that repression of Notch signaling in early immature mTEC subset was required for efficient differentiation and maturation of mTECs (Goldfarb et al., 2016). Thus, enhanced Notch signaling in mTECs upon aging may interrupt the normal differentiation program and partially prevent immature mTEC from progressing to a mature stage. Consistent with this, GO term analysis of down-regulated genes also revealed an enrichment of genes with functions in epithelial cell differentiation and development (Fig 4-2G). I also found a significant expansion of $K5^{+}K8^{+}$ TEC progenitors based on keratin IF assay and a remarkable increase of a DN-TEC population ($EpCAM^{+}UEA\text{-}1^{-}Ly51^{-}$) in both natural aged and *Lmnb1* mutant thymuses (Chapter 3, Fig 3-2 B-D). Additionally, an enrichment of lipid metabolic and catabolic process was also observed in down-regulated genes and might contribute to age-related ectopic adiposity in the thymus (Fig 4-2G).

Depletion of *Lmnb1* in TECs accelerates age-associated transcriptional program

Since a TEC-specific ablation of *Lmnb1* caused phenotypes similar to those observed in the aged WT thymus, I next explored the transcriptional changes in TECs from 2- and 6-month-old *Lmnb1* mutant thymus and examined whether these transcriptional changes mirrored age-related alterations. For this analysis, I will first

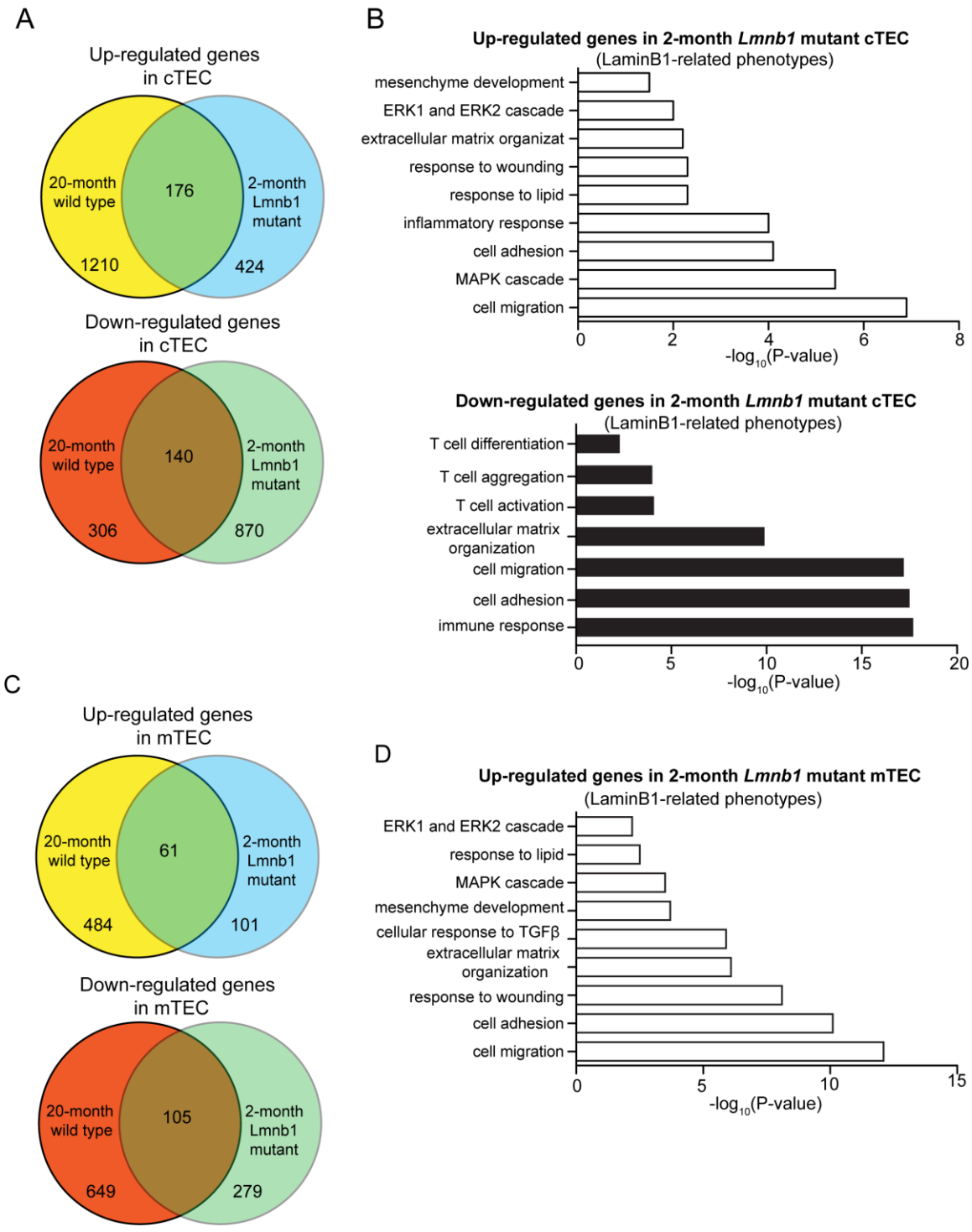

Fig 4-3. Transcriptional signatures of *Lmnb1* mutant TECs from 2-month-old thymus revealed by RNA-seq. (A) Graphs show the overlap of up- (top) or down-regulated (bottom) genes (fold change ≥2) between aged (20-month) WT and *Lmnb1*

mutant (2-month) cTECs. (B) The top significant GO terms for up- (top) or down-regulated (bottom) genes with regards to lamin-B1-mediated phenotypes in cTECs from 2-month-old mutant thymus. (C) Graphs summarize the overlap of up- (top) or down-regulated (bottom) genes between aged (20-month) WT and *Lmnb1* mutant (2-month) mTECs. (D) The top significant GO terms for down-regulated genes related to lamin-B1-mediated phenotypes in mTECs from 2-month-old mutant thymus.

report transcriptional profile for the 2-month-old *Lmnb1* mutant cTEC and mTEC and then turn to 6-month-old *Lmnb1* mutant cTEC and mTEC. Using a 2-fold cut off, I found that the transcriptional profiles of TECs from 2-month-old *Lmnb1* mutant thymus were not remarkably similar (~12% to 29%, shared numbers of DEGs compared to 2-month-old WT thymus) to that observed in 20-month-old aged TECs (Fig 4-3A and C). In cTECs, the *Lmnb1 mutant* only shared 176 up- and 140 down-regulated genes with aged group, respectively. Despite relatively few genes in each category, GO term analysis of altered genes in 2-month-old *Lmnb1* mutant cTECs still revealed some similar functional categories as shown in aged cTECs. They also included thymic structural organization, response to lipid/mesenchyme development (adiposity-related), MAPK and ERK1/2 cascades and intrathymic inflammatory response in up-regulated genes and down-regulation of T-cell activation/differentiation (Fig 4-3B, 2-month-old *Lmnb1* mutant cTECs; Fig 4-1C and D, 20-month-old cTECs). For up-regulated DEGs in *Lmnb1* mutant mTECs, I observed an enrichment of similar functional categories as those shown in the aged group (Fig 4-3D, 2-month-old *Lmnb1* mutant mTECs; Fig 4-2E, 20-month-old mTECs). Unlike the 20-month aged group, Notch signaling was not identified in GO term analysis in 2-month-old *Lmnb1* mutant mTECs because it did not meet 2-fold increase criterion. However, several components in Notch signaling pathway including Notch3/4, Hey1 and Hey2 did show increased expression (ranging from 1.3 to 1.5 fold) in *Lmnb1* mutant mTECs (data not shown), indicating enhanced Notch signaling as a result of *Lmnb1* depletion in mTECs in 2-month-old mutant thymus.

Next I decided to perform transcriptional profiling of cTECs and mTECs isolated from 6-month-old *Lmnb1* mutant thymus. Strikingly, *Lmnb1* mutant cTECs and mTECs

from 6-month-old thymus exhibited a highly similar transcriptional profile to those in 20-month-old WT thymus. I will first describe data analysis for cTECs and then discuss mTECs. Using the same criteria (2-fold cut off), I initially found that 6-month *Lmnb1* mutant cTECs shared 968 up- and 191 down-regulated genes with 20-month-old aged group (total 1486 up- and 446 down-regulated DEGs), respectively. These results were striking as DEGs in 6-month-old *Lmnb1* mutant thymus shared ~65% of up-regulated genes and ~45% down-regulated genes observed in the 20-month-old age group while 6-month-old WT controls exhibited less than 10% commonly altered genes with 20-month-old age group (data not shown). GO term analysis of up-regulated genes further revealed a highly significant enrichment of non-cTEC lineage development and functions (Fig 4-4B, top10 listed), reflecting a trend that was similar to that identified in cTECs from 20-month-old WT thymus (Fig 4-4B and Fig 4-1B). For up-regulated genes, GO term analysis also identified very similar functional categories as observed in aged cTECs including thymic structural organization, response to lipid/mesenchyme development/fat cell differentiation (adiposity-related), MAPK and ERK1/2 cascades and intrathymic inflammatory reaction (Fig 4-4C and Fig 4-1C). Of interest, a large number of up-regulated genes exhibited similar level of change. For example, cTECs from 20-month-old aged thymus exhibited ~127 fold increased expression of IL6 (Fig 4-1E) and *Lmnb1* mutant cTECs from 6-month-old thymus expressed ~112 fold increase of IL-6 transcripts (Fig 4-4E). For down-regulated genes, similar enrichments were observed such as T-cell activation, aggregation and differentiation. While Dll4 was not identified as a DEG in 6-month *Lmnb1* mutant cTECs, the expression of Foxn1 in *Lmnb1* mutant cTECs showed a similar ~60% reduction as that in cTECs from 20-month-old WT thymus (data not

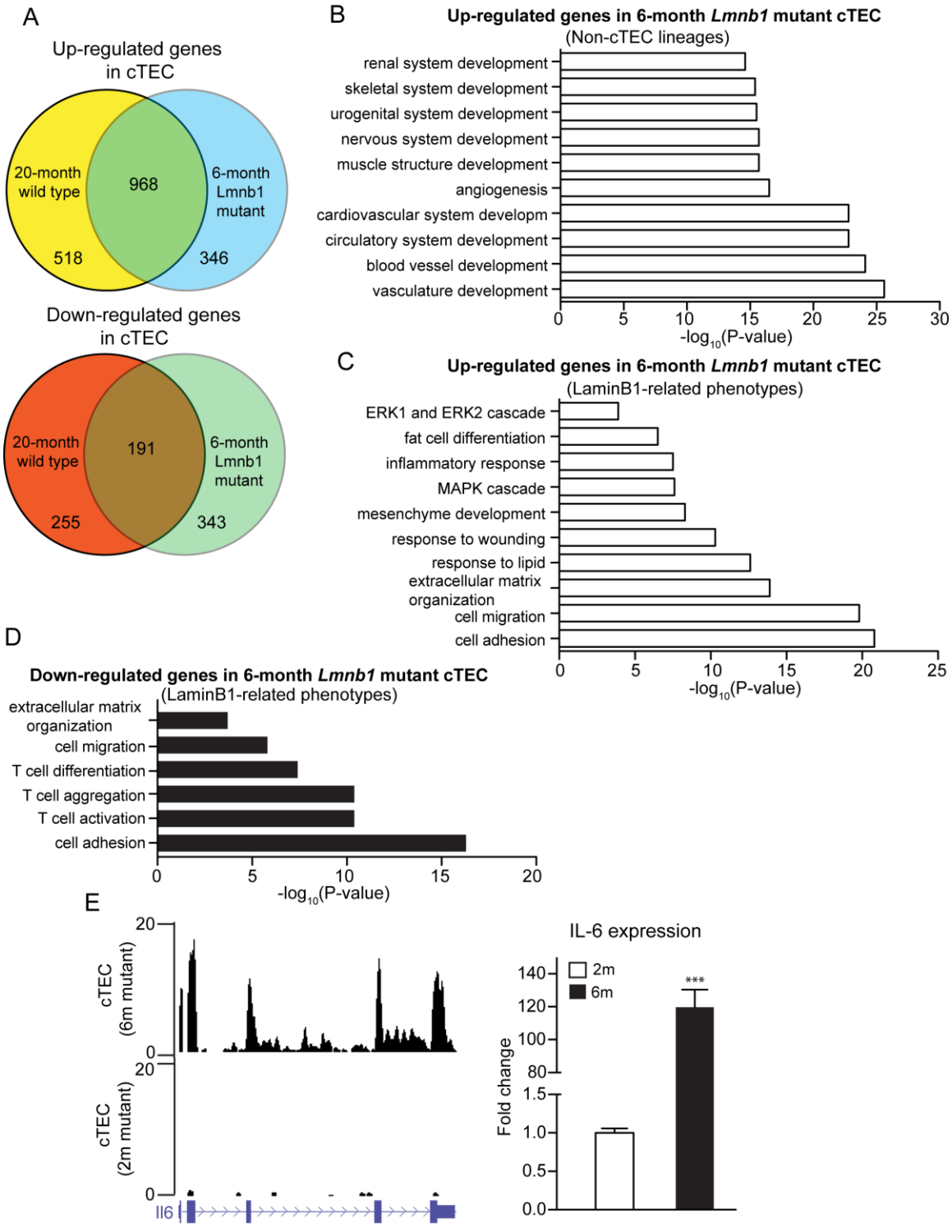

Fig 4-4. Accelerated age-associated transcriptional program in *Lmnb1* mutant cTECs from 6-month-old mutant thymus revealed by RNA-seq. (A) Graphs show the overlap of up- (top) or down-regulated (bottom) genes (fold change ≥2) between aged

(20-month) WT and *Lmnb1* mutant (6-month) cTECs. (B) The top10 significant GO terms for up-regulated genes in non-cTEC lineage development and function in *Lmnb1* mutant cTECs from 6-month-old thymus. (C)-(D) The top significant GO terms for up- (C) or down-regulated (D) genes with regards to lamin-B1-mediated phenotypes in cTECs from 6-month-old mutant thymus. (E) The genome browser views show up-regulation of IL-6 expression in *Lmnb1* mutant (6-month) cTECs (left); qRT-PCR analysis of IL-6 expression in *Lmnb1* mutant cTECs from 2- and 6-month-old thymuses (right). All data shown are representative of at least 3 independent experiments and are plotted as mean ± SEM. Student's t test: *, $P < 0.05$; **, $P < 0.01$; ***, $P < 0.001$; ns, not significant.

shown), which might lead to similar global transcriptional changes that result in defective thymopoiesis.

For mTEC, I first found that mTECs from 6-month-old *Lmnb1* mutant thymus shared 411 up-regulated genes with aged WT controls (411 out of total 545), covering as high as ~75% of the up-regulated genes seen in the aged WT group (Fig 4-5A, top). Less dramatically, the 6-month *Lmnb1* mutant mTEC shared ~55% of down-regulated genes with 20-month-old aged group (Fig 4-5A, bottom; 417 out of total 754). GO term analysis again revealed a significant and similar enrichment of up-regulated genes with functions in non-mTEC lineage development and functions (Fig 4-5B, top10 listed; Fig 4-2C for 20-month-old aged controls). I also observed a very similar increased expression of parathyroid gland-related genes, such as GCM2, Hoxa3 and Tbx1, in *Lmnb1* mutant mTECs from 6-month-old thymus (Fig 4-5C; Fig 4-2D for 20-month-old aged controls). Further analysis revealed more similar enrichments in functional categories observed in aged mTECs including thymic structural organization, response to lipid/mesenchyme development (adiposity-related), MAPK and ERK1/2 cascades, cellular response to TGFβ and intrathymic inflammatory reaction (Fig 4-5D). Using qRT-PCR assay, I validated the increased expression of IL-6, TGFβ receptor II and Notch signaling components including Notch3, Hey1 and Hey2 in 6-month *Lmnb1* mutant mTEC (Fig 4-5E), and showed that the altered levels were similar to those seen in 20-month aged WT mTECs (Fig 4-2F). GO term analysis of down-regulated genes identified a similar enrichment of genes as that in aged group with functions in epithelial cell differentiation and lipid catabolic/transport process (Fig 4-5F), consistent with the ectopic adiposity appearing in 6-month-old *Lmnb1* mutant thymus (Chapter 3, Fig 3-3C). Together, my

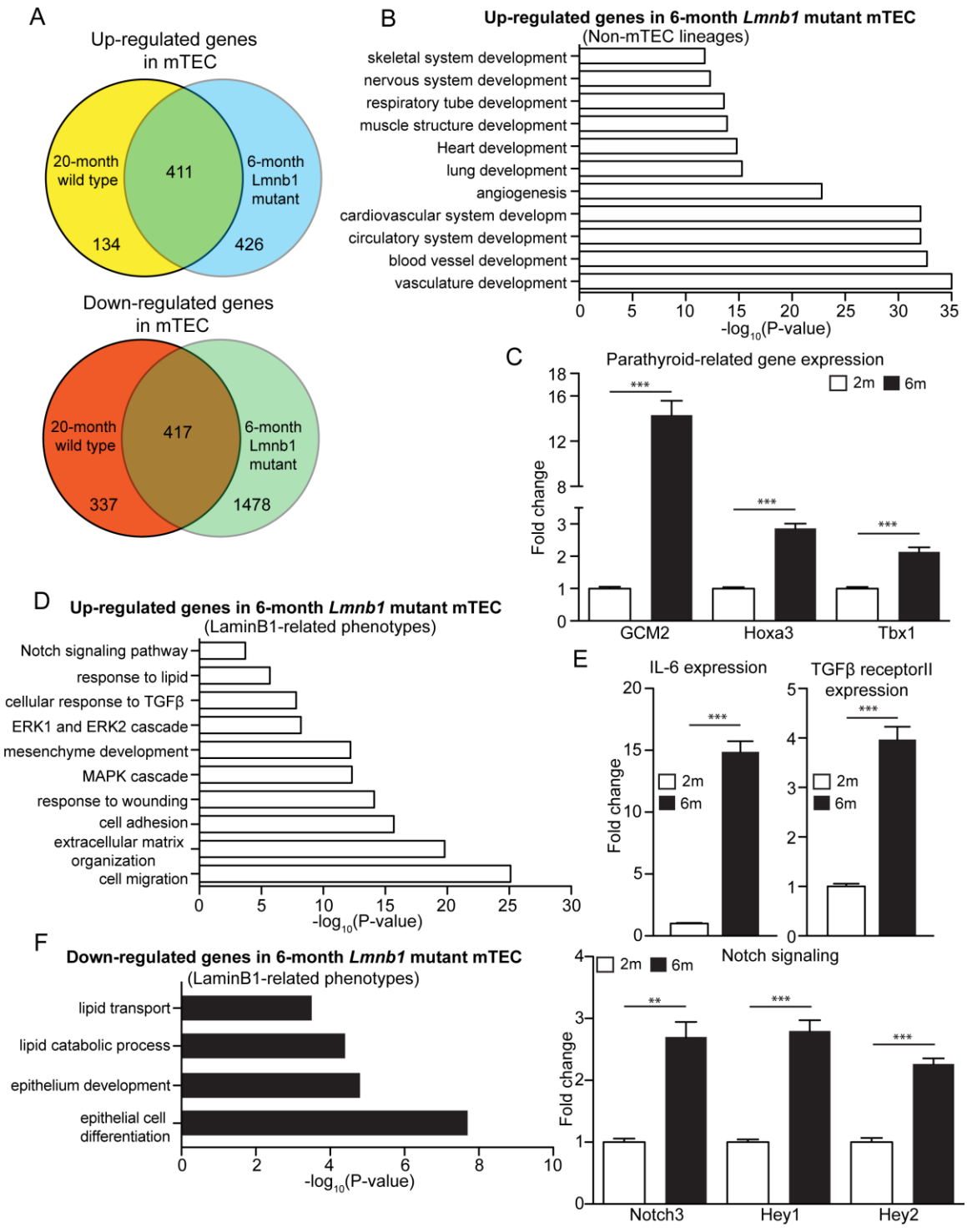

Fig 4-5. RNA-seq analysis reveals accelerated age-related transcriptional program in *Lmnb1* mutant mTECs from 6-month-old mutant thymus. (A) Graphs show the overlap of up- (top) or down-regulated (bottom) genes (fold change ≥2) between aged

(20-month) WT and *Lmnb1* mutant (6-month) mTECs. (B) The top10 significant GO terms for up-regulated genes in non-mTEC lineage development and function in 6-month *Lmnb1* mutant mTECs. (C) qRT-PCR analysis of parathyroid gland-related genes GCM2, Hoxa3 and Tbx1 in 2- and 6-month *Lmnb1* mutant mTECs. (D) The top significant GO terms for up-regulated genes with regards to lamin-B1-mediated phenotypes in mTECs from 6-month-old mutant thymus. (E) qRT-PCR analysis of select up-regulated genes in 2- and 6-month *Lmnb1* mutant mTECs: IL6 (top left); TGFβ receptor II (top right); Notch signaling (bottom). (F) The top significant GO terms for down-regulated genes with regards to lamin-B1-mediated phenotypes in mTECs from 6-month-old mutant thymus. All data shown are representative of at least 3 independent experiments and are plotted as mean ± SEM. Student's t test: *, $P < 0.05$; **, $P < 0.01$; ***, $P < 0.001$; ns, not significant.

data strongly suggest that *Lmnb1*-loss-mediated transcriptome change contributes, at least in part, to the age-associated change in the transcriptional program in TECs and that this in turn leads to the observed degenerative phenotypes.

Discussion

In this study, I present global gene expression data for two main TEC subsets, cTEC and mTEC, covering young stage (2-month), early involution (6-month) and late involution (20-month). To my knowledge, this is the first whole genome-wide transcriptome profiling of TECs at the late stage of thymic involution. Nonetheless, I have to emphasize one caveat before discussing my findings. While I chose standard surface markers to isolate cTECs and mTECs, they are still heterogeneous and can be subdivided into distinct subsets. For example, mTECs can be grouped into $MHCII^{low}$ and $MHCII^{high}$ subpopulations based on MHCII expression. As the frequency of TEC subsets is not maintained during aging, it is critical to compare transcriptional profiles of individual TEC subsets. However, due to the low cell number of TECs collected from pooled aged thymuses, it is technically challenging to separate individual cTEC and mTEC subpopulations for RNA-seq analyses in this study. With the help of new low-cell number RNA-seq and the single-cell RNA-seq technologies, future experiments will use more defined TEC subsets for whole genome-wide transcriptional profiling. Nevertheless, my RNA-seq data provide novel insight into the age-associated transcriptional landscape changes in TECs and will be a valuable resource for the whole TEC research community.

While decreased Foxn1 expression is commonly accepted as a major factor contributing to thymic involution (Chinn et al., 2012), Foxn1 was not identified as a DEG

in mTECs in my RNA-seq and in a recently published microarray study (Ki et al., 2014) during early thymic involution (6-month). It is possible that Foxn1 is reduced at the protein level, without a significant change at mRNA level, in mTECs during early involution. However, using a novel Foxn1^{G} reporter allele, a newly published study found that there was no significant change of Foxn1 protein level in mTECs between 3-month-old and 24-month-old thymus (O'Neill et al., 2016). This new evidence strongly argues against the central role of Foxn1 in driving early thymic involution. Consistent with the previous microarray data, my GO term analysis revealed a significant enrichment of up-regulated genes in inflammatory/immune response, wound healing and response to IL-1 in mTECs during early involution (Fig 4-2B), indicating that acquisition of an inflammatory signature in mTECs is a hallmark of early stage of thymic involution. Considering that other groups and my study above (Chapter 2) reported increased expression of proinflammatory cytokines in sirpα^{+} DC and macrophage in thymus upon aging (Ki et al., 2014; Youm et al., 2012), these data strongly suggest that thymic myeloid cell-derived inflammation plays a key role in initiating thymic degeneration.

Surprisingly, GO term analysis also revealed a significant enrichment of up-regulated genes with functions in non-TEC lineage development and functions in both aged cTECs and mTECs. A recent TEC transcriptome profiling showed that both cTECs and mTECs expressed peripheral tissue-restricted antigens (TRA), commonly referred to as promiscuous gene expression (PGE) (Sansom et al., 2014). The study estimated that TECs from young mouse thymus were able to express up to 19,293 protein-coding genes. The optimal expression level of these TRAs shapes the maximal repertoire of TCR available for the positive and negative selection of developing thymocytes. Dysregulation

of the PGE program due to age-associated defects in TECs may result in up-regulation of some non-TEC lineage genes at the cost of others and may disrupt normal thymopoiesis. For example, one interesting case is the ectopic expression of parathyroid specific transcription factor GCM2 in aged mTECs (Fig 4-2D), implying that the aged thymus may exhibit some features of parathyroid gland. As the main function of the parathyroid is to regulate calcium homeostasis with no reported role for supporting thymopoiesis, it is reasonable to speculate that ectopic expression of GCM2 in aged mTECs would interfere with normal negative selection of auto-reactive T cells and contribute at least in part to increased autoimmunity risk during aging (Prelog, 2006).

The early studies have shown that both $CD4^+$ and $CD8^+$ T cells produced by the aged mouse thymus had impaired functions (Maue et al., 2009). These T-cell defects were mainly attributed to the impact of an aged thymic microenvironment, but not from aged T-cell progenitors because functional T cells were generated when HSCs from aged mouse were transplanted into young mouse thymus. GO term analyses revealed for the first time a deterioration of the intrathymic microenvironment at the transcriptional level, affecting thymic structural organization and ectopic adiposity, all of which contributed to defective thymopoiesis in aged mouse thymus. One key feature uncovered by RNA-seq analysis is an enhanced inflammatory environment within the aged mouse thymus. I found more than 100-fold increased production of IL-6 in aged cTECs and 10-fold increased expression of IL-6 in aged mTECs, respectively. In Chapter 2, I showed that pro-inflammatory cytokines such as IL-6 were able to induce lamin-B1 reduction in cultured TECs *in vitro*. Therefore, increased production of IL-6 from TECs and myeloid lineage-derived macrophage and DC in aged mouse thymus may further accelerate lamin-

B1 loss in TECs. Interestingly, *Lmnb1* mutant TECs exhibited remarked similar phenotypes and transcriptional changes as aged TECs (Fig 4-4 and 4-5), including increased production of IL-6 (Fig 4-4E and 4-5E). This raises the possibility that IL-6 may play a central role in exacerbating degeneration of aged thymus *via* positive feedback loop, which may help to prevent or reduce the chance of producing too many defective naïve T cells within inflammatory microenvironment and may be a beneficial aspect of thymic involution.

One interesting observation from this study is the enhanced Notch signaling in both aged and *Lmnb1* mutant mTECs. According to the prevailing view, both cTECs and mTECs originate from bipotent progenitors. The current model for TEC differentiation suggests that bipotent progenitors can either progress "by default" to mature cTECs or acquire an mTEC fate in response to other signals, during which repression of Notch signaling in early immature mTECs is required for efficient mTEC differentiation and progression towards a mature $MHCII^{high}$ stage. In line with this, overexpression of Notch1 in TECs resulted in thymic hypoplasia with impaired mTEC maturation (Goldfarb et al., 2016). Enhanced Notch signaling in mTECs from aged mouse thymus may partially prevent immature mTECs from progressing to a mature stage, which in turn interrupts appropriate negative selection and final maturation of native T cells. In agreement with this, I observed an expansion of $K5^{+}K8^{+}$ TEC progenitors and a remarkable increase of a DN-TEC population ($EpCAM^{+}UEA\text{-}1^{-}Ly51^{-}$) in both natural aged and *Lmnb1* mutant thymus (Chapter 3, Fig 3-2).

Interestingly, I found that both cTECs and mTECs isolated from 6-month-old *Lmnb1* mutant thymus exhibited remarkably similar transcriptional changes as these

shown in the 20-month-old WT thymus. How could lamin-B1 loss affect global transcriptome in TECs? Lamins, especially lamin-B1, have long been suggested to have a role in maintaining heterochromatin and gene regulation (Dechat et al., 2010). Using the fly immune organ fat body as a model, our lab reported that depletion of lamin-B led to a loss of heterochromatin and depression of a large number of immune responsive, inflammatory genes and retrotransposons (Chen et al., 2014; Chen et al., 2016). GO term analysis also revealed that age-associated lamin-B loss in the fly fat body mainly affected genes related to immune, metabolism, cell fates and cell-cell adhesion. I observed a very similar enrichment of functional categories in up-regulated genes in *Lmnb1* mutant cTECs and mTECs, such as inflammatory response, strongly suggesting that lamin-B1 might play an evolutionarily conserved role in maintaining tissue homeostasis and functions. Given that an age-associated lamin-B1 reduction occurs in TECs upon aging, it is plausible that loss of lamin-B1 leads to global transcriptome and epigenome changes in TECs and triggers a degenerative cascade in the thymus. In the next chapter I will describe my effort to develop a novel low-cell number ChIP-seq technology, which will be applied to further dissect how lamin-B1 regulates TEC epigenetic landscape and gene expression in my future study.

Materials and methods

Quantitative real-time PCR

Primer sequences were listed as follows.

Dll4: F: AGGTGCCACTTCGGTTACAC; R: GGAGAGCAAATGGCTGATA.

GCM2: F: GATACCCTGTCACCAACTTCTG; R: GAAGCCATCTGTCTCTTGAGG.

Hoxa3: F: TCAAGGCAGAACACTAAGCAG; R: ACTCCTTCTCCAGCTCTACC.

Tbx1: F: TGGGACGAGTTCAATCAGC; R: TGTCATCTACGGGCACAAAG.

Notch3: F: TTCCCCGTGTCGTAATGGTG; R: TCGAAGCCAGGAAGGCAAG

Hey1: F: TGAGAAGCAGGGATCTGCTAAG; R: GCATTCCCGAAACCCCAAAC.

Hey2: F: ACAGGGGGTAAAGGCTACTTTG; R: AGATGAGAGACAAGGCGCAC

Whole-Transcriptome Shotgun Sequencing (RNA-seq)

Total RNA was extracted following the manufacturer's protocol of Direct-zol™ RNA MicroPrep kit (Zymo Research). Poly-A selected mRNA was purified and sequencing libraries were built using Illumina TruSeq RNA sample prep kit V2 (Illumina). Libraries were sequenced by single end 50-bp reads on Illumina HiSeq-2000.

Bioinformatics

For RNA-seq, low-quality reads (quality score below 20) were trimmed and reads shorter than 36 bp after trimming were filtered out. The remaining reads were further mapped. RNA-seq fastq files were generated by the Illumina pipeline (Casava 1.8). The reads were then mapped to mouse genome (mm9) by Tophat2 (Kim et al., 2013). Splicing junctions are from RefSeq annotation. Number of reads falling into each gene was counted using custom scripts. Then differentially expressed genes were called using edgeR (Robinson et al., 2010)(fold change ≥ 2 and FDR < 0.05). GO term analyses of DEGs were performed by DAVID (Huang da et al., 2009)

Reference

Benoist, C., Lanier, L., Merad, M., Mathis, D., and Immunological Genome, P. (2012). Consortium biology in immunology: the perspective from the Immunological Genome Project. Nat Rev Immunol *12*, 734-740.

Billard, M.J., Gruver, A.L., and Sempowski, G.D. (2011). Acute endotoxin-induced thymic atrophy is characterized by intrathymic inflammatory and wound healing responses. PLoS One *6*, e17940.

Brennecke, P., Reyes, A., Pinto, S., Rattay, K., Nguyen, M., Kuchler, R., Huber, W., Kyewski, B., and Steinmetz, L.M. (2015). Single-cell transcriptome analysis reveals coordinated ectopic gene-expression patterns in medullary thymic epithelial cells. Nat Immunol *16*, 933-941.

Chen, H., Zheng, X., and Zheng, Y. (2014). Age-associated loss of lamin-B leads to systemic inflammation and gut hyperplasia. Cell *159*, 829-843.

Chinn, I.K., Blackburn, C.C., Manley, N.R., and Sempowski, G.D. (2012). Changes in primary lymphoid organs with aging. Semin Immunol *24*, 309-320.

Colombara, M., Antonini, V., Riviera, A.P., Mainiero, F., Strippoli, R., Merola, M., Fracasso, G., Poffe, O., Brutti, N., Tridente, G.*, et al.* (2005). Constitutive activation of p38 and ERK1/2 MAPKs in epithelial cells of myasthenic thymus leads to IL-6 and RANTES overexpression: effects on survival and migration of peripheral T and B cells. J Immunol *175*, 7021-7028.

Dechat, T., Adam, S.A., Taimen, P., Shimi, T., and Goldman, R.D. (2010). Nuclear lamins. Cold Spring Harb Perspect Biol *2*, a000547.

Goldfarb, Y., Kadouri, N., Levi, B., Sela, A., Herzig, Y., Cohen, R.N., Hollenberg, A.N., and Abramson, J. (2016). HDAC3 Is a Master Regulator of mTEC Development. Cell Rep *15*, 651-665.

Hauri-Hohl, M., Zuklys, S., Hollander, G.A., and Ziegler, S.F. (2014). A regulatory role for TGF-beta signaling in the establishment and function of the thymic medulla. Nat Immunol *15*, 554-561.

Huang da, W., Sherman, B.T., and Lempicki, R.A. (2009). Bioinformatics enrichment tools: paths toward the comprehensive functional analysis of large gene lists. Nucleic Acids Res *37*, 1-13.

Ki, S., Park, D., Selden, H.J., Seita, J., Chung, H., Kim, J., Iyer, V.R., and Ehrlich, L.I. (2014). Global transcriptional profiling reveals distinct functions of thymic stromal subsets and age-related changes during thymic involution. Cell Rep *9*, 402-415.

Kim, D., Pertea, G., Trapnell, C., Pimentel, H., Kelley, R., and Salzberg, S.L. (2013). TopHat2: accurate alignment of transcriptomes in the presence of insertions, deletions and gene fusions. Genome Biol *14*, R36.

Koch, U., Fiorini, E., Benedito, R., Besseyrias, V., Schuster-Gossler, K., Pierres, M., Manley, N.R., Duarte, A., Macdonald, H.R., and Radtke, F. (2008). Delta-like 4 is the essential, nonredundant ligand for Notch1 during thymic T cell lineage commitment. J Exp Med *205*, 2515-2523.

Mainiero, F., Colombara, M., Antonini, V., Strippoli, R., Merola, M., Poffe, O., Tridente, G., and Ramarli, D. (2003). p38 MAPK is a critical regulator of the constitutive and the beta4 integrin-regulated expression of IL-6 in human normal thymic epithelial cells. Eur J Immunol *33*, 3038-3048.

Maue, A.C., Yager, E.J., Swain, S.L., Woodland, D.L., Blackman, M.A., and Haynes, L. (2009). T-cell immunosenescence: lessons learned from mouse models of aging. Trends Immunol *30*, 301-305.

O'Neill, K.E., Bredenkamp, N., Tischner, C., Vaidya, H.J., Stenhouse, F.H., Peddie, C.D., Nowell, C.S., Gaskell, T., and Blackburn, C.C. (2016). Foxn1 Is Dynamically Regulated in Thymic Epithelial Cells during Embryogenesis and at the Onset of Thymic Involution. PLoS One *11*, e0151666.

Prelog, M. (2006). Aging of the immune system: a risk factor for autoimmunity? Autoimmun Rev *5*, 136-139.

Robinson, M.D., McCarthy, D.J., and Smyth, G.K. (2010). edgeR: a Bioconductor package for differential expression analysis of digital gene expression data. Bioinformatics *26*, 139-140.

Sansom, S.N., Shikama-Dorn, N., Zhanybekova, S., Nusspaumer, G., Macaulay, I.C., Deadman, M.E., Heger, A., Ponting, C.P., and Hollander, G.A. (2014). Population and single-cell genomics reveal the Aire dependency, relief from Polycomb silencing, and distribution of self-antigen expression in thymic epithelia. Genome Res *24*, 1918-1931.

St-Pierre, C., Brochu, S., Vanegas, J.R., Dumont-Lagace, M., Lemieux, S., and Perreault, C. (2013). Transcriptome sequencing of neonatal thymic epithelial cells. Sci Rep *3*, 1860.

Youm, Y.H., Kanneganti, T.D., Vandanmagsar, B., Zhu, X., Ravussin, A., Adijiang, A., Owen, J.S., Thomas, M.J., Francis, J., Parks, J.S.*, et al.* (2012). The Nlrp3 inflammasome promotes age-related thymic demise and immunosenescence. Cell Rep *1*, 56-68.

Zuklys, S., Handel, A., Zhanybekova, S., Govani, F., Keller, M., Maio, S., Mayer, C.E., Teh, H.Y., Hafen, K., Gallone, G.*, et al.* (2016). Foxn1 regulates key target genes

essential for T cell development in postnatal thymic epithelial cells. Nat Immunol *17*, 1206-1215.

Chapter 5: Development of a low-cell-number epigenome profiling method

This work has been published and I am listed as a co-first author.

Zheng, X., Yue, S., Chen, H., Weber, B., Jia, J., and Zheng, Y. (2015). Low-Cell-Number Epigenome Profiling Aids the Study of Lens Aging and Hematopoiesis. Cell Rep *13*, 1505-1518.

Summary

Understanding how chromatin modification regulates development and disease can be limited by available material. Despite recent progress, balancing high quality and reliable mapping using chromatin-immunoprecipitation-based deep sequencing (ChIP-seq) remains a challenge. We report two techniques, Recovery via Protection (RP)-ChIP-seq and favored amplification RP-ChIP-seq (FARP-ChIP-seq), that provide reproducible mapping in as few as 500 cells. FARP-ChIP-seq accurately mapped histone H3 lysine 4 trimethylation (H3K4me3) and histone H3 lysine 27 trimethylation (H3K27me3) in long-term hematopoietic stem cells (LT-HSCs), short-term HSCs (ST-HSCs), and multi-potent progenitors (MPPs) from one mouse. These datasets indicate a lack of H3K4me3/H3K27me3 bivalency on hematopoietic genes in HSCs.

Introduction

Mapping of epigenome modifications or chromatin regulator/transcription factor binding in a pure cell population is critical for basic and translational research. The ability to map epigenome changes in a cell population during development can shed light on the steps by which different cell lineages establish their transcriptional programs. Mapping the epigenome in a few cells isolated from diseased or healthy tissues may allow the discovery of specific disease-associated changes. Unfortunately, since ChIP-seq requires multi-step manipulations, DNA loss due to irreversible absorption or degradation has made it difficult to reliably obtain high quality mapping in only a few cells (Park, 2009).

ChIP-seq using standard methods requires nanograms of DNA: equal or greater than 10^6 cells are needed for reliable and high quality ChIP-seq (Park, 2009). Various strategies have been developed to reduce the cell number needed. One method is to amplify the cells derived from tissues *in vitro*. Although this is applicable for progenitor/stem cell populations, it is not useful for dissected post-mitotic cells. Culturing and proliferation *in vitro* may also change progenitor/stem cells, potentially making the genome-wide studies unrepresentative of cells *in vivo*. Several methods have been developed to facilitate ChIP-seq using thousands or tens of thousands of cells. One of them relies on increasing DNA amplification cycles (Adli et al., 2010; Ng et al., 2013; Shankaranarayanan et al., 2012; Shankaranarayanan et al., 2011), which may introduce bias as low abundance ChIP DNA may be underrepresented or lost. Another method utilizes carrier proteins, chemicals, and/or mRNA during ChIP (Zwart et al., 2013), but

the absence of carrier during post-ChIP processing still leads to significant DNA loss, thereby compromising ChIP-seq quality.

A third method, called indexing-first ChIP-seq (iChIP-seq) (Lara-Astiaso et al., 2014), uses barcoding and pooling of multiple samples to study the epigenome in multiple hematopoietic lineages. Although the method reduces DNA loss by sample pooling, relying on sorting of fixed cells and sequential ChIP may still lead to DNA loss. Additionally, the on-bead ligation of adapters to chromatin fragments may reduce efficiency. Indeed 10-20K sorted hematopoietic cells were used in these iChIP-seq datasets (Lara-Astiaso et al., 2014). Finally, micrococcal nuclease (MNase)-base native ChIP (ultra-low-input micrococcal nuclease-based native ChIP, ULI-NChIP) was also used for epigenetic mapping (Brind'Amour et al., 2015). While the quality of ULI-NChIP-seq for some epigenetic modifications is reasonable, other modifications were not mapped, indicating that the loss of ChIP DNA during manipulations could have resulted in variable outcomes. Here we report a new ChIP-seq method for high fidelity genome-wide profiling using as few as 500 cells, and report its applications.

Results

Recovery via Protection (RP)-ChIP-seq for 500 cells

An effective way to protect DNA from loss during ChIP-seq is to use agents that behave like DNA and which co-purify with chromatin or the DNA of interest during ChIP and library building. This would prevent the loss of DNA due to non-specific irreversible absorption and degradation by residual contaminating DNAses. One straightforward means is to use chromatin as a protection agent. Although this would

A

	Drosophila Genome	Mouse Genome	Human Genome
Drosophila	100%	50,684 (0.002%)	101,745 (0.003%)
S.cerevisiae	331 (0.0002%)	891 (0.00003%)	1,202 (0.00004%)
E.coli	0	0	8 (0.0000003%)
Synthetic biotin-DNA	0	0	0

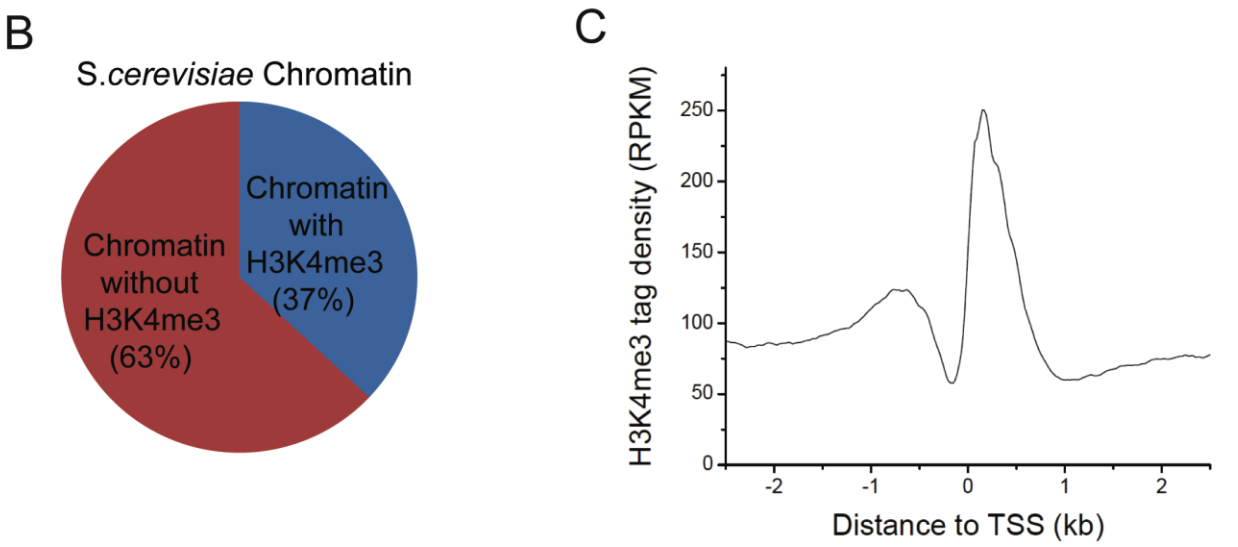

Figure 5-1. Analyses of carrier DNAs. (A) Whereas *Drosophila* genomic DNA sequences can be mapped to many regions in the *Mus musculus* (mouse) or *Homo sapiens* (human) genome, a very small number of *S. cerevisiae* or *E. coli* genomic sequences can be mapped to the genomes of *Drosophila*, mouse, or human. Synthetic biotin-DNA sequences are designed to not match to these genomes. (B) Analyses of yeast chromatin with H3K4me3. (C) The normalized H3K4me3 densities are plotted within the 2.5 Kb up- and downstream of TSS in yeasts.

result in the presence of carrier DNA in the sequencing library, the carrier DNA sequences can be easily filtered out computationally after deep-seq if they do not map to the genome of interest. We compared various genomes, including mouse, human, *Drosophila*, yeast, and bacteria with one another. We generated artificial reads by scanning the genome using a 50 base pair (bp) sliding window. Using Bowtie (Langmead et al., 2009) and allowing 3 mismatches, we mapped the *Drosophila* sequences to other genomes.

Due to sequence conservation, many short reads derived from the *Drosophila* genome mapped broadly to mammalian genomes (Figure. 5-1A), so chromatin from *Drosophila* and mammalian genomes cannot be used as protection agents for one another. However, very few reads from *S. cerevisiae* (yeast) and *E. coli* were mapped to human, mouse, or *Drosophila* genomes (Figure. 5-1A). Importantly, over 90% of the few short mapped reads are in rDNA or simple repeat regions of target genomes. Since ~30% of yeast chromatin carries histone H3 lysine 4 trimethylation (H3K4me3) (Figure. 5-1B and C) and since commercial antibodies can successfully ChIP H3K4me3 from yeasts to human, as proof of principle, we used yeast chromatin as a carrier in the ChIP-seq of H3K4me3 in a small number of mouse embryonic stem cells (mESCs). We refer to this ChIP-seq as Recovery via Protection (RP)-ChIP-seq.

We mixed formaldehyde cross-linked yeast (~$5x10^7$) with either 500 or 2000 cross-linked mESCs. Following sonication, antibody to H3K4me3 was used to ChIP both the yeast and mESC chromatin using standard ChIP and library building procedures. The similar patterns of H3K4me3 distribution around the transcriptional start sites (TSS) between the ChIP-seq datasets from 500 or 2000 mESCs and the dataset from the

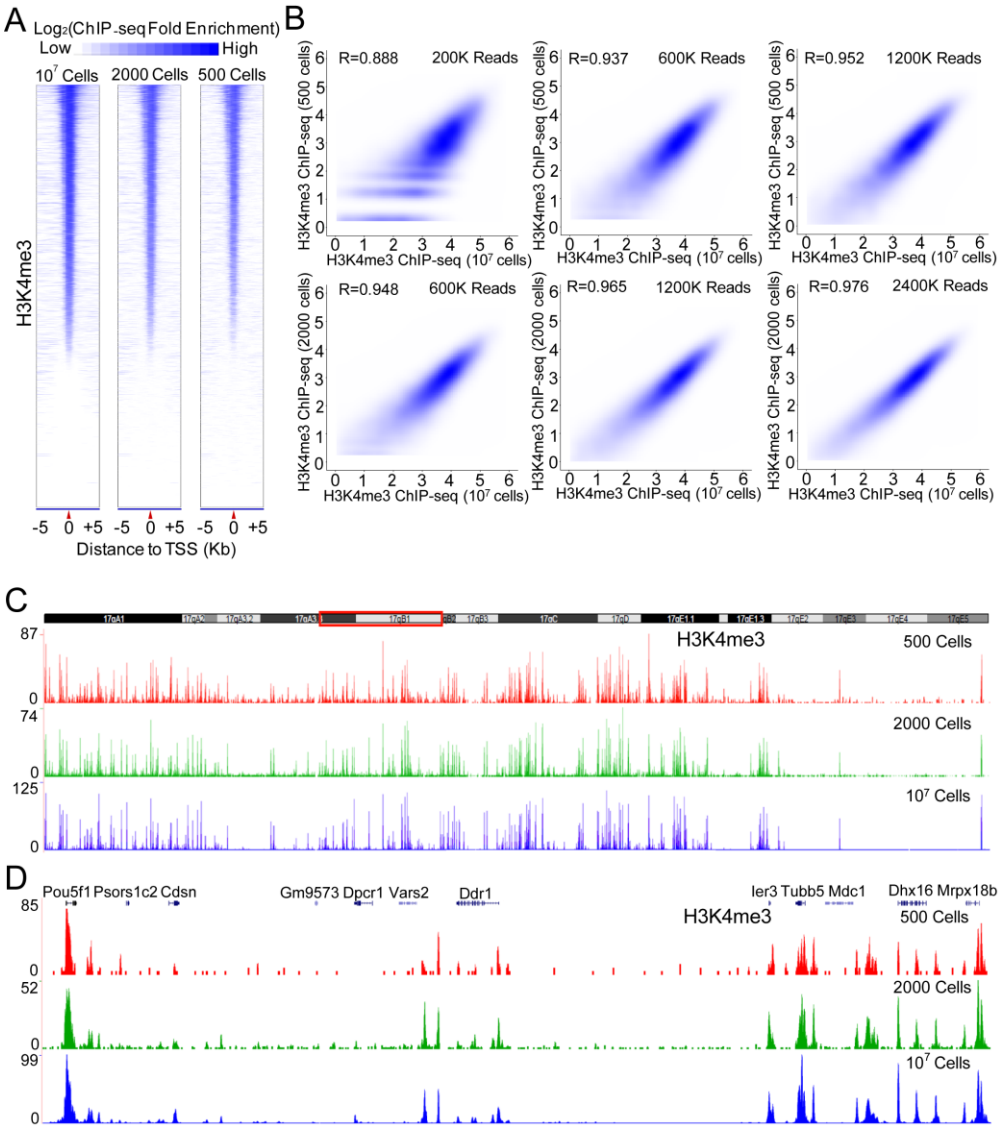

Figure 5-2. RP-ChIP-Seq. (A) Heatmaps of H3K4me3 on 5 Kb upstream and downstream of TSS in 10^7, 2000, or 500 mESCs, rank ordered based on H3K4me3 in 10^7 mESCs. (B) Contour plots (Spearman correlation coefficient, R) of H3K4me3 on promoters by RP-ChIP-seq in 500 or 2000 mESCs at the indicated mouse reads and the standard ChIP-seq in 10^7 mESCs at 163 million reads. (C)-(D) Plots of H3K4me3 peaks on chromosome 17 (C) or the enlarged region boxed in red in C using 500, 2000, and 10^7 mESCs (D).

standard ChIP-seq of 107 mESCs (Jia et al., 2012) (Figure. 5-2A), show that RP-ChIP-seq successfully mapped H3K4me3 in 500 or 2000 mESCs. Importantly, increasing read depth resulted in further improvements of RP-ChIP-seq quality as indicated by increased correlation between RP-ChIP-seq and standard ChIP-seq of 107 cells (Figure. 5-2B). With 2.4 and 1.2 million mapped mouse reads, the correlation coefficient between the standard ChIP-seq of 107 mESCs and RP-ChIP-seq for 2000 and 500 mESCs reached R=0.976 and 0.952, respectively (Figure. 5-2A). Analyses of specific chromatin regions also showed that RP-ChIP-seq uncovered H3K4me3 peaks reliably (Figure. 5-2C and D).

Favored Amplification RP-ChIP-seq (FARP-ChIP-seq) reduces read depth and is applicable to all mapping needs

The RP-ChIP-seq described above effectively preserved the chromatin of interest, but it requires a substantial increase of total reads to obtain sufficient reads of the DNA of interest. It is not universally applicable for ChIP-seq mapping of other epigenomes and transcription-factor binding since yeast chromatin does not share all epigenetic modifications as animal genomes. We thus used a biotinylated synthetic DNA (biotin-DNA) to replace the yeast chromatin. We designed 210-bp biotin-DNA that does not map to *Drosophila*, mouse, or human genomes. Since only a few endogenous biotinylated proteins have been found and none or few of them are associated with chromatin (Jia et al., 2012; Kim et al., 2009; Rybak et al., 2005), by mixing the biotin-DNA with chromatin, it was possible to recovery the biotin-DNA and the chromatin of interest using streptavidin beads and antibody-coupled protein G beads, respectively. To inhibit amplification of biotin-DNA during library building, a PCR amplification blocker oligo

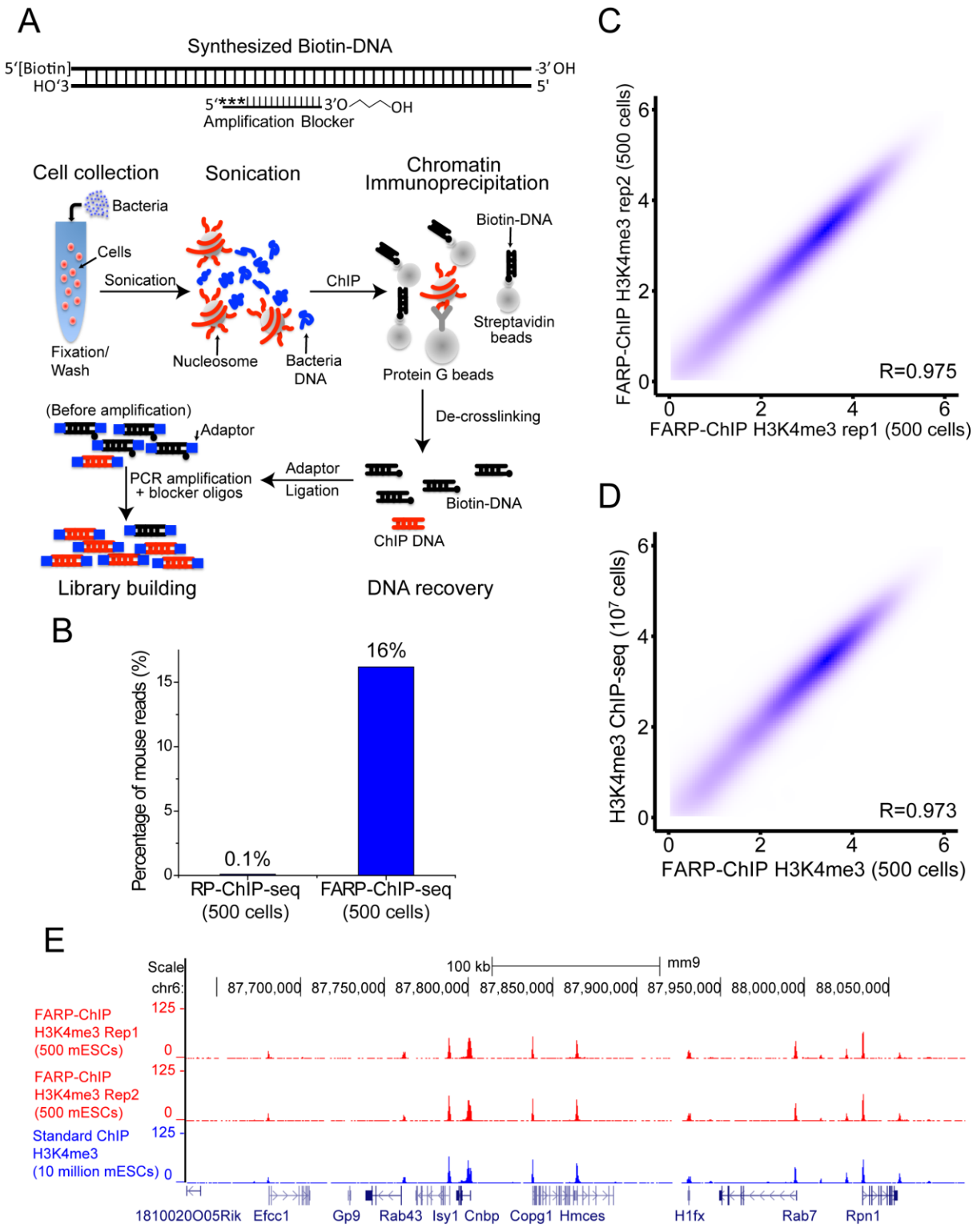

Figure 5-3. Favored amplification (FA) RP-ChIP-seq (FARP-ChIP-seq). (A) Top: the biotin-DNA carrier annealed to the blocker oligo carrying a 3' modified 3-carbon

spacer and 5' 3 phosphorothioate modifications (asterisks). Bottom: cells of interest (red) were mixed with bacteria (blue), fixed, washed, and sonicated. Biotin-DNA bound to strepavidin beads and antibody-bound protein G beads were added for ChIP. (B) FARP-ChIP-seq resulted in increased ratios of mapped mouse reads to total reads. (C)-(D) Contour plots (as $\log_2$ of the average read density within 2 Kb upstream and downstream of TSS. Spearman correlation coefficient, R) between two biological replicates of FARP-ChIP-seq in 500 mESCs (C) or between 500 mESC FARP-ChIP-seq and the 10^7 mESCs standard ChIP-seq (D). (E) Enrichment at the indicated genes on chromosome 6 were mapped by the indicated methods.

complementary to the biotin-DNA was designed to contain phosphorothioate modification of the first 3 nucleotides at the 5'-end to resist the exonuclease activity of the PCR enzyme while a modified nucleotide carrying 3-carbon spacer at the 3'-end was designed to inhibit extension of the oligonucleotide by PCR (Figure. 5-3A). Indeed, when added at 0.25 μM during library amplification, the blocker oligo reduced the amplification of the biotin-DNA by over 99% (data not shown). We refer to this method as favored amplification RP-ChIP-seq (FARP-ChIP-seq).

We mapped H3K4me3 in 500 mESCs using FARP-ChIP-seq. Since H3K4me3 exhibits sharp peaks near promoters, the total chromatin marked by H3K4me3 is lower compared to other histone modifications, which leads to difficulty in library building using low cell numbers. Indeed, the ULI-NChIP method obtained a H3K27me3 library from ~1000 mESCs but was unsuccessful for H3K4me3 mapping using the same cell number (Brind'Amour et al., 2015). Successful H3K4me3 mapping indicates that our method is also applicable for other histone modifications. To efficiently recover the small number of mESCs and their chromatin, we added ~$5x10^8$ bacteria as cell carrier to 500 mESCs followed by fixation, wash, and sonication (Figure. 5-3A). After ChIP using biotin-DNA-bound Steptavidin beads and protein G beads coupled to H3K4me3 antibodies, blocker oligos were added during library building (Figure. 5-3A). FARP-ChIP-seq resulted in a ~160-fold increase of mouse genomic DNA reads compared to RP-ChIP-seq at the same read depth for 500 mESCs (Figure. 5-3B). The biological replicates were highly consistent (Figure. 5-3C). The blocker oligo did not affect the quality of the FARP-ChIP-seq data because the biological replicates were highly correlated (Spearman correlation coefficient, R) with one another and with the standard

ChIP-seq of 10^7 mESCs (Figure. 5-3C and D). The genome browser view also shows a high correlation (Figure. 5-3E).

FARP-ChIP-seq offers the highest quality H3K4me3 map to date in hematopoietic stem cell subtypes sorted from one mouse

Next we tested whether FARP-ChIP-seq could accurately map the epigenome of sub-types of hematopoietic stem cells (HSCs) sorted from one mouse. HSCs support life-long production of all blood cells. Very little is known about genome-wide epigenetic regulation during early hematopoiesis because of the small numbers of cells that can be sorted from bone marrow (BM). For example, only ~0.1% of BM cells are HSCs, which are defined as Lineage-negative (lin$^-$: CD3$^-$, CD4$^-$, CD8$^-$, B220$^-$, CD11b$^-$, Gr1$^-$, Nk1.1$^-$, and Ter119$^-$), Sca1-positive (Sca1$^+$), and c-Kit$^+$ (LSK HSCs). The LSK HSCs (~30,000/mouse) consist of three functionally distinct subpopulations: long-term HSCs (LT-HSCs), short-term HSCs (ST-HSCs), and multi-potent progenitors (MPPs), which represent 0.007% (~2000/mouse), 0.04% (~12000/mouse), and 0.05% (~15000/mouse) of total BM cells, respectively (Yang et al., 2005). Three studies have mapped the HSC epigenome. The Nano-ChIP-seq mapped H3K4me3, H3K27me3, and H3K36me3 in 20000 mixed-population LSK HSCs (Adli et al., 2010). Of the two recent studies, one mapped H3K4me3, H3K27me3, and H3K36me3 in subpopulations of LSK HSCs pooled from many mice using standard ChIP-seq (Sun et al., 2014), while the other mapped H3K4me1, H3K4me2, H3K4me3 and H3K27ac in LT-HSCs, ST-HSCs, and MPPs pooled from 6 mice ranging from 8-12 weeks old using iChIP-seq (Lara-Astiaso et al., 2014).

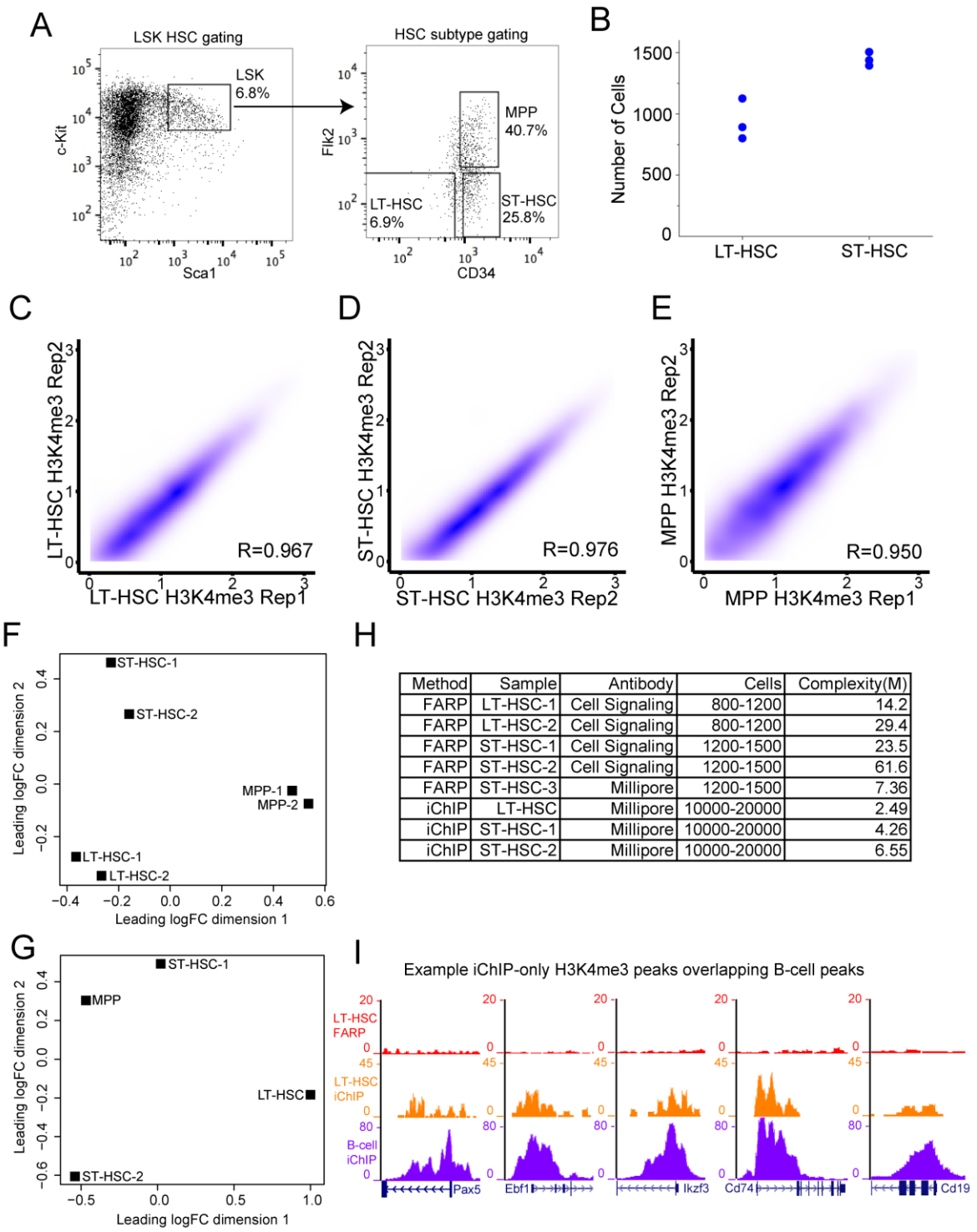

Method	Sample	Antibody	Cells	Complexity(M)
FARP	LT-HSC-1	Cell Signaling	800-1200	14.2
FARP	LT-HSC-2	Cell Signaling	800-1200	29.4
FARP	ST-HSC-1	Cell Signaling	1200-1500	23.5
FARP	ST-HSC-2	Cell Signaling	1200-1500	61.6
FARP	ST-HSC-3	Millipore	1200-1500	7.36
iChIP	LT-HSC	Millipore	10000-20000	2.49
iChIP	ST-HSC-1	Millipore	10000-20000	4.26
iChIP	ST-HSC-2	Millipore	10000-20000	6.55

Figure 5-4. FARP-ChIP-seq of HSC subtypes. (A) FACS plots with the markers and gating used for sorting LSK HSCs, LT-HSCs, ST-HSCs, and MPPs. (B) The number of

sorted LT-HSC and ST-HSC used in FARP-ChIP-seq determined by low-depth genome sequencing. (C)-(E) Contour plots (Spearman coefficient, R) between H3K4me3 on promoters obtained (plotted as $\log_2$ of the average read density within 2 Kb upstream and downstream of TSS) by FARP-ChIP-seq in two biological replicates of LT-HSCs (C), ST-HSCs (D), and MPPs (E). (F)-(G) MDS-plot of FARP-ChIP-seq (F) or iChIP-seq (G) H3K4me3 maps in LT-HSCs, ST-HSCs, and MPPs. Distances between biological replicates (-1 and -2) within and between HSC subtypes show the similarity/differences among the datasets. iChIP-seq of LT-HSCs and MPPs have no biological replicate, while the ST-HSCs biological replicates (-1 and -2) do not cluster together. (H) A summary of FARP-ChIP-seq and iChIP-seq of H3K4me3 in LT-HSCs and ST-HSCs with the cell numbers, antibody sources, and library complexities. (I) Genome-browser view of representative iChIP-only H3K4me3 peaks in LT-HSCs that overlaps with the iChIP H3K4me3 peaks in B cells, but are absent from the FARP-ChIP-seq of LT-HSCs.

Assuming that all the reported ChIP-seq qualities are high, the epigenome maps obtained by pooling sub-populations of HSCs from several mice at different ages or using mixed LSK HSCs may not accurately determine the epigenome of LT-HSCs, ST-HSCs, or MPPs. We thus applied FARP-ChIP-seq to map H3K4me3 and H3K27me3 in LT-HSCs, ST-HSCs, or MPPs sorted from one 8-week old C57BL/6J mice. To avoid cross contamination of HSC subtypes, we gated stringently during sorting and based on the estimated cell numbers by flow cytometry, ~1500 LT-HSCs, ~6000 ST-HSCs, and ~10000 MPPs could be sorted from one mouse (Figure. 5-4A). Since flow cytometry cannot accurately count the relatively rare LT-HSCs and ST-HSCs in one mouse, we developed a method that accurately determined the number of these cells in the input samples for FARP-ChIP-seq to be 800-1200 LT-HSCs and 1200-1500 ST-HSCs (Figure. 5-4B). For MPPs, we used one fourth of the total sorted cells for one FARP-ChIP-seq, which corresponded to 2000-2500 cells.

We found highly consistent FARP-ChIP-seq maps for H3K4me3 between biological replicates in the three HSC subtypes (Figure. 5-4C-E). A multi-dimension scaling plot (MDS-plot) showed good clustering of replicates (Figure. 5-4F), indicating that the H3K4me3 peaks are distinct in LT-HSC, ST-HSC, and MPPs. The only reported maps of H3K4me3 in LT-HSC, ST-HSC, and MPPs utilized iChIP-seq, in which the BM cells pooled from several 8-12 week-old mice were first labeled, fixed, and then sorted for the three HSC subtypes. iChIP-seq was performed using 10,000-20,000 sorted LT-HSC, ST-HSC, or MPPs. Since the iChIP-seq used the same markers to sort LT-HSC, ST-HSC, and MPPs, we compared our FARP-ChIP-seq maps to those of iChIP-seq.

We first determined whether the iChIP H3K4me3 dataset could distinguish LT-HSCs, ST-HSCs, and MPPs. Only one sample for LT-HSCs and MPPs were available in the iChIP study. Nonetheless, the MDS-plot revealed that the two biological replicates for ST-HSC iChIP-seq failed to cluster, whereas the biological replicates of the FARP-ChIP-seq datasets clustered well (Figure. 5-4F-G). Consistent with the MDS plot, no differential H3K4me3 peaks were identified among the iChIP-seq H3K4me3 datasets obtained for LT-HSCs, ST-HSCs, and MPPs, whereas hundreds of differential peaks were found in the FARP-ChIP-seq datasets.

We next used the 'preseq' software package (Daley and Smith, 2013) to estimate the iChIP-seq H3K4me3 library complexity based on the deposited datasets (Lara-Astiaso et al., 2014). The iChIP library complexities for LT-HSCs, ST-HSCs, and MPPs are 2.5-6.5M (million reads) (Figure. 5-4H). If the recovery rates of ChIP DNA were constant for different numbers of input cells, this would translate to 250-650K library complexity for 1000 cells, which would suggest that iChIP-seq might not perform well using low cell numbers. By contrast, our FARP-ChIP-seq library complexities for the HSC subtypes ranged from 14M to 60M using 800-1500 input cells (Figure. 5-4H). Since we used an H3K4me3 antibody different from that in the iChIP study, we repeated the FARP-ChIP-seq using the same antibody used by iChIP-seq. The library complexity obtained using 1500 ST-HSCs was 7.3M, which was higher than the highest complexity of 6.4M obtained by iChIP-seq of 10,000-20,000 cells (Figure. 5-4H). This indicates that FARP-ChIP-seq offers more accurate epigenome mapping in fewer cells.

To ensure high recovery of live-sorted rare HSC subtypes during fixation and washes, we used bacteria as cell carriers in FARP-ChIP-seq, whereas a large number of

labeled BM cells were fixed, washed, and sorted for HSC subtypes in iChIP-seq. Although fixing and washing large numbers of BM cells prevents cell loss, fixation changes the fluorescence of cell surface labels and is also not compatible with propidium iodide (PI) or DAPI staining used for dead cell exclusion. Thus fixation could result in increased impurity of the sorted cells. We reasoned that lineage-signature based on H3K4me3 could allow us to assess cell purity used in iChIP-seq and FARP-ChIP-seq. By comparing the H3K4me3 datasets for LT-HSCs, we found 10,718 shared, 1,252 FARP-ChIP-only, and 4,963 iChIP-only peaks. GO-term analyses of the FARP-ChIP-only peaks showed no significant enrichment of genes belonging to any terms, whereas the iChIP-only peaks were enriched for genes involved in B-cell activation and proliferation, including key B-cell regulators such as *Pax5*, *Ebf1*, *Ikzf3*, *Cd74*, and B-cell marker genes such as *Cd19* (Figure. 5-4I), suggesting a potential B-cell contamination of the LT-HSCs in the iChIP-seq. Next, we compared the iChIP-only H3K4me3 peaks in LT-HSCs to the total iChIP-seq H3K4me3 peaks determined for B cells in the same study (Lara-Astiaso et al., 2014). Among the top 20% highest LT-HSCs iChIP-only peaks, which are unlikely resulted from random noise, 95% overlapped with the B-cell H3K4me3 peaks (data not shown). Similar analysis suggests that one of the ST-HSC samples used in iChIP-seq also have B-cell contamination. These analyses demonstrate that FARP-ChIP-seq allows high quality epigenome mapping in a low number of sorted pure HSC subtypes because it does not rely on the sorting of fixed cells and it ensures the recovery of very low amounts of ChIP DNA.

High quality H3K4me3 mapping by FARP-ChIP-seq offers a resource for studying HSC subtypes

Since the broadest H3K4me3 peaks often mark genes important for the function and identity of a given cell type (Benayoun et al., 2014), we further mined the H3K4me3 maps obtained by FARP-ChIP-seq for LT-HSCs, ST-HSCs, and MPPs. GO-term analysis showed that all broad H3K4me3 peaks in LT-HSCs, ST-HSCs, and MPPs were enriched in hematopoietic functions. For example, genes important for HSC regulation such as *Meis1*, *Hlf,* and *Erg,* all exhibited broad H3K4me3 peaks (Figure. 5-5A) in all three HSC subtypes. Thus, by looking for genes with broadest H3K4me3 peaks in our datasets, one may identify new candidate regulators of HSC for further functional studies.

By comparing ST-HSCs and LT-HSCs, we identified 725 up- and 788 down-regulated H3K4me3 peaks (fold change>1.5, FDR<0.05). Among the genes exhibiting increased H3K4me3 peaks in ST-HSCs, we found those involved in cell-cycle regulation and DNA replication such as *E2f8*, *Smc2*, and *Chek1* (Figure. 5-5B). Consistently, previous RNA-seq showed an increased expression of genes that belong to these functional groups (Cabezas-Wallscheid et al., 2014). Interestingly, we found that multiple regulators of chromatin organization such as *Cbx5* and *Suv39h1* exhibited increased H3K4me3 (Figure. 5-5B), suggesting that ST-HSC may have more condensed chromatin structure than LT-HSC. GO-term analysis of differential promoter H3K4me3 peaks between LT-HSC and ST-HSC also supports the functional differences in cell cycle and chromatin organization in these two HSC subtypes (Figure. 5-5C).

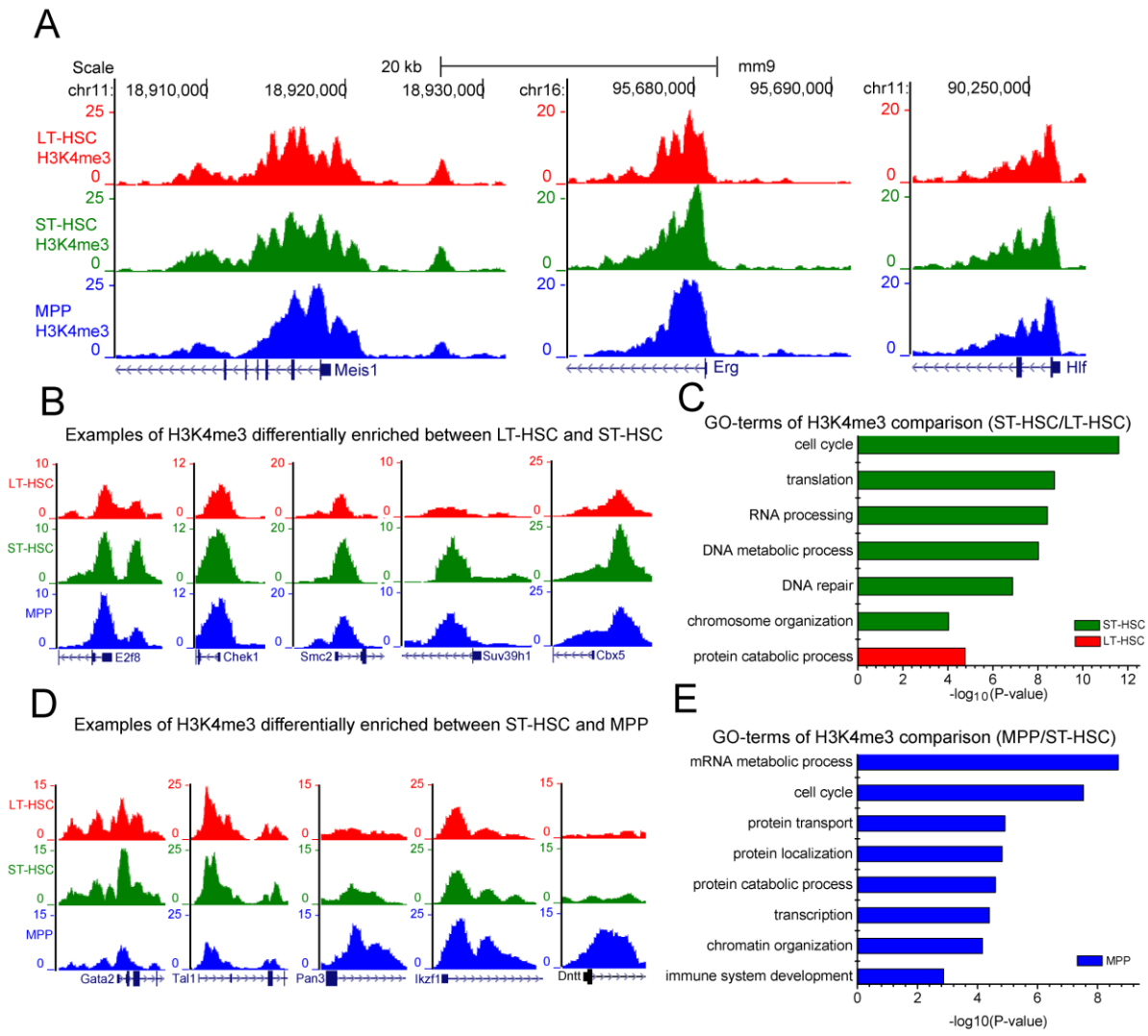

Figure 5-5. Comparison of H3K4me3 between HSC subtypes. (A) Genome browser view of common broad H3K4me3 peaks on genes in the HSC subtypes. (B)-(E) Genome browser view of H3K4me3 differences on genes in the HSC subtypes (B, D) and GO-term of genes with significant changes of promoter H3K4me3 between indicated HSC subtypes (C, E). Green, red, or blue bars, ST-HSC or LT-HSC, or MPP enriched GO-terms, respectively. No ST-HSC enriched GO-terms were found.

When the H3K4me3 datasets between ST-HSCs and MPPs were compared, we identified 878 up- and 881 down-regulated peaks (fold change>1.5, FDR<0.05) in MPPs. Among the genes with down-regulated H3K4me3, we found known regulators of HSC generation, maintenance, or survival, such as *Gata2* and *Tal1* (Figure. 5-5D) (Porcher et al., 1996; Tsai and Orkin, 1997), had the broadest peaks in LT-HSC and ST-HSC. This suggests that H3K4me3 changes on these genes are responsible for preparing MPPs for multi-lineage differentiation. However, genes such as *Ikzf1* and *Dntt* that are known to be required for lymphoid lineage functions exhibited an increase in H3K4me3 in MPPs (McCaffrey et al., 1975; Reynaud et al., 2008). Interestingly, GO-term analysis of differential promoter H3K4me3 peaks further revealed enrichment of genes required for mRNA metabolism and cell cycle in MPPs (Figure. 5-5E). Taken together, the high quality H3K4me3 maps obtained by FARP-ChIP-seq provide useful resources for the study of LT-HSCs, ST-HSCs, and MPPs.

A general lack of H3K4me3/H3K27me3 bivalency in HSCs on genes required for hematopoietic differentiation

The marking of genes required for lineage specification and development by both H3K27me3 and H3K4me3 on their promoters was first discovered in mESCs (Bernstein et al., 2006). This so-called bivalent epigenetic mark is implicated in poising developmental regulators for rapid up- or down-regulation, and is thus considered to be important for lineage differentiation (Bernstein et al., 2006). Several studies have suggested the existence of bivalent genes in other stem/progenitor cells, but the co-existence of these marks on the same promoter within one cell has been firmly

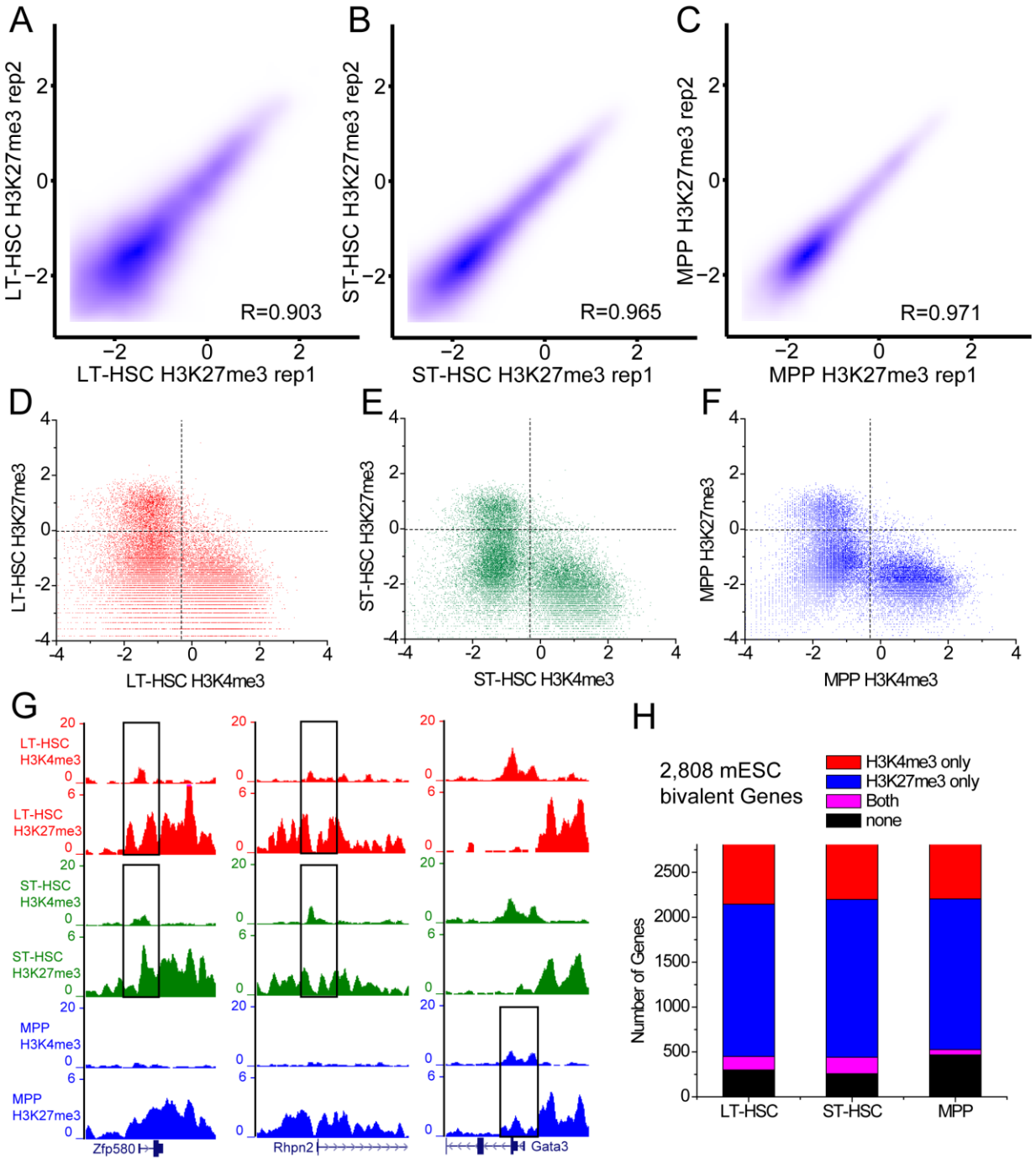

Figure 5-6. **Genes for hematopoietic lineage differentiation are not generally marked by H3K4me3/HK27me3 bivalency in HSCs.** (A)-(C) Contour plots (Spearman correlation coefficient, R) between H3K27me3 (plotted as $\log_2$ of the average read

density within 5 kb upstream and downstream of TSS) on promoters obtained by FARP-ChIP-seq in biological replicates of the HSC subtypes. (D)-(F). Scatter plots of H3K4me3 and H3K27me3 enrichment (plotted as $\log_2$ of the average read density within 2 Kb upstream and downstream of TSS) based on FARP-ChIP-seq in the HSC subtypes. (G) Genome browser view of bivalent genes found by FARP-ChIP-seq in the HSC subtypes and by previous studies. Rectangles outline the bivalent promoters. (H) Bar plot showing how bivalent genes found in mESCs are resolved in HSC subtypes mapped by FARP-ChIP-seq.

established only in mESCs (Voigt et al., 2012). Whether the reported bivalency for other stem/progenitor cells reflects true dual marking or cell heterogeneity remains unclear.

The studies that reported bivalent genes in HSCs used total LSK HSCs or purified sub-populations of LSK HSCs (Adli et al., 2010; Sun et al., 2014; Weishaupt et al., 2010). Overall, ~740-2260 bivalent genes were found in HSCs or its subtypes. Since the biological replicates of FARP-ChIP-seq maps of H3K27me3 were highly consistent (Figure. 5-6A-C), we analyzed H3K27me3/H3K4me3 bivalency using our datasets. We found that LT-HSCs, ST-HSCs, and MPPs had only 302, 376, and 117 bivalent genes, respectively (Figure. 5-6D-F). Among these, *Rhpn2*, *Zfp580*, *Rassf5*, and *Gata3*, were reported as bivalent genes previously (Sun et al., 2014; Weishaupt et al., 2010) (Figure. 5-6G). When analyzing how many of the known mESC bivalent genes were resolved in the three HSC subtypes, we found that 605-662 and 1677-1757 of them became H3K4me3-only or H3K27me3-only genes, respectively. Whereas 58-184 of the mESC bivalent genes remained bivalent, 257-468 of them had neither modification in the three HSC subtypes (Figure. 5-6H). Importantly, the bivalent genes uncovered by FARP-ChIP-seq are not implicated in regulating hematopoietic lineage development and GO-term analysis revealed no significant enrichment of pathway genes. Moreover, when all bivalent genes were combined in the three HSC subtypes, the 562 total bivalent genes identified by FARP-ChIP-seq were still smaller than the number previously reported for HSCs.

To confirm whether H3K4me3/H3K27me3 bivalency is not used to mark the genes required for differentiation of HSCs, we analyzed the bivalent genes reported

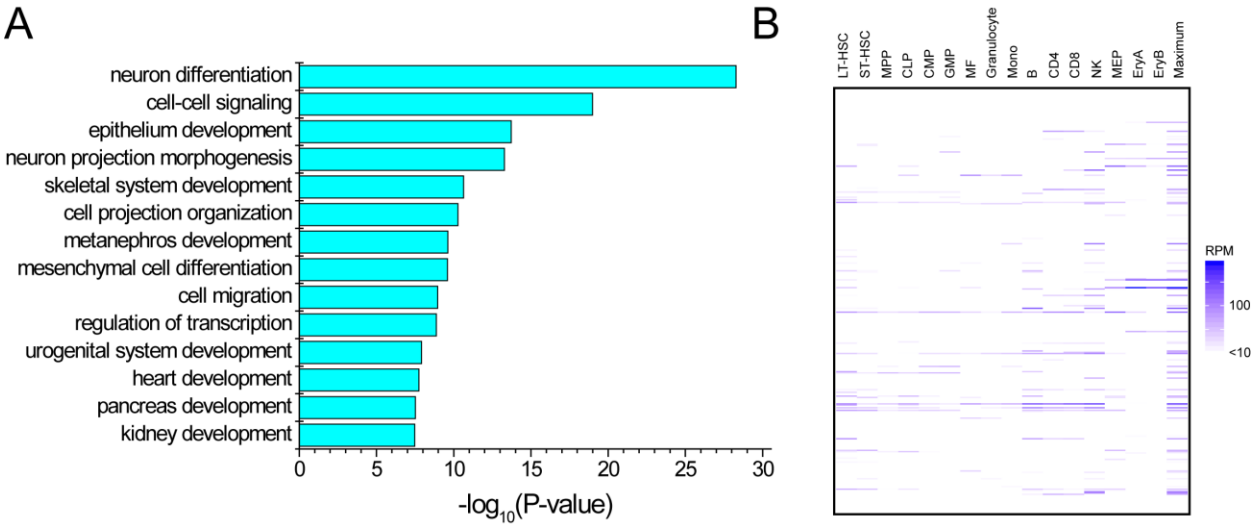

Figure 5-7. Analyses of H3K4me3 and H3K27me3 bivalent genes found in SP-CD150^{+}-LSK HSCs. (A) GO-term analysis of the H3K4me3 and H3K27me3 bivalent genes. (B) Heatmap showing the 3'-RNA-seq reads (reads per million, RPM) of the top 300 H3K4me3-enriched bivalent genes in the SP-CD150^{+}-LSK HSCs. Each row represents a gene and each column represents the RNA-seq for the indicated cell type. Only 72 out of 1940 genes were expressed in at least one of the 16 cell types. The last column shows the maximum expression of these genes.

previously by focusing on the dataset obtained for a sub-population of LSK HSCs defined as SP (side population) and $CD150^+$ (SP-$CD150^+$-LSK HSCs) (Sun et al., 2014). Since no bivalent gene list was provided in the mapping of the SP-$CD150^+$-LSK HSCs (Sun et al., 2014), we first used our criteria to identify bivalent genes in the published dataset. We found 1940 promoters with both H3K4me3 and H3K27me3 enrichment in SP-$CD150^+$-LSK HSCs, similar to the reported number of bivalent genes (Sun et al., 2014). Among these, 210 overlapped with the bivalent genes found in our dataset, whereas the remaining genes had only H3K27me3 enrichment (91.7%, 1587 of 1730) in our dataset. Strikingly, GO-term analyses revealed that the 1940 bivalent genes were not enriched for hematopoietic differentiation or development, but were instead enriched for the differentiation/development of nervous system followed by epithelia, skeletal system, kidney, mesenchymal cells, urogenital system, heart, pancreas, and kidney (Figure. 5-7A). Among the 1940 bivalent genes, we selected 300 with the strongest H3K4me3 and compared them to the available RNA-seq datasets of the hematopoietic lineages and found that only 72 were expressed in at least one lineage (Figure. 5-7B) (Lara-Astiaso et al., 2014). This is consistent with the idea that genes required for non-hematopoietic lineage development are silenced in HSCs and the differentiated hematopoietic lineages. Based on our dataset, most of the 1940 bivalent genes are marked only by the repressive H3K27me3, so these analyses further confirm that H3K4me3 and H3K27me3 are not used to mark the poised state of genes required for hematopoietic lineage differentiation in HSCs.

Discussion

The ChIP-seq method reported here is based on the idea that if a rare cell population is not lost during the initial fixation and wash steps, and if chromatin loss is minimized during ChIP and library building, it should be possible to uncover low abundance DNA without increasing DNA amplification cycles. Although we report only epigenome mapping using FARP-ChIP-seq, the general principle of using synthetic DNA as carrier is applicable to all ChIP-seq, genomic DNA-seq, and RNA-seq needs when a single cell or a small number of cells are used. The presence of bacteria DNA and bio-DNA in the final sequencing library calls for ~5-fold increase in read depth for FARP-ChIP-seq of 500 cells, and read depth is decreased as cell number used increases. Considering that FARP-ChIP-seq offers the highest fidelity mapping compared to all other methods for low cell numbers, this modest increase in sequencing depth justifies its application.

Various carrier approaches have been employed to ensure the recovery of small amounts of DNA or RNA in different applications. In the specific case of ChIP-seq, we show that DNA or chromatin carrier ensures co-purification of carriers with the DNA of interest in each step. Since the carrier has the same characteristics to the DNA of interest, it can effectively occupy non-specific and irreversible DNA binding sites present on all surfaces and they can also saturate contaminating DNases. Here we show that RP-ChIP-seq and FARP-ChIP-seq allows accurate mapping of epigenome in as few as 500 cells. We believe that with additional optimization and in conjunction with microfluidic techniques (Aguilar and Craighead, 2013), it should be possible to further reduce read depth and cell number needed in a high throughput format.

The FARP-ChIP-seq allowed us to reveal the high quality maps of H3K4me3 and H3K27me3 using low number of LT-HSCs, SH-HSCs, and MPPs compared to previously published datasets. By using pure cell populations, we found fewer H3K4me3/H3K27me3 bivalent genes in HSCs than previously reported. More importantly, the bivalent genes found in both our study and the reported studies are not involved in hematopoietic lineage specification. This shows that H3K4me3/H3K27me3 bivalency is unlikely to be the mechanism used for poising lineage-specific gene expression in HSCs. However, it is possible that other mechanisms are used to poise genes for expression. For example, in hematopoietic cells such as the established EML cell line, the hematopoietic specific genes may be poised by H3K4me2 positive and H3K4me3 negative marks (Orford et al., 2008). RNA polymerase II pausing on promoters may also poise genes for expression (Puri et al., 2015). The FARP-ChIP-seq strategy reported here should aid in the further study of how HSCs poise genes for lineage differentiation.

The methods reported here should allow large-scale epigenome association studies using pure cell populations from patients or animal models. Reduced cell heterogeneity should increase the success rate of discovering epigenetic changes that are relevant to either developmental or disease processes. The feasibility of mapping the epigenome of dissected tissues or sorted cells will allow improved understanding of epigenetic changes during each stage of organ and tissue building. Coupling such information with gene expression studies should greatly enhance our understanding of the developmental processes. The disease-associated epigenetic changes mapped with

dissected tissues, in conjunction with GWAS, should greatly improve the accuracy and power of biomarker discovery and disease diagnosis.

Materials and methods

Standard ChIP-seq

Standard ChIPs were performed according to conditions suggested by manufacturers of ChIP-grade antibodies to H3K27me3 (Millipore, 07-449) and H3K4me3 (Cell Signaling, 9751). Briefly, formaldehyde was added to mESCs to crosslink proteins to DNA and the cells were lysed in 200 µl lysis buffer (50 mM HEPES, pH 7.5, 140 mM NaCl; 1 mM EDTA; 1% Triton X-100; 0.1% sodium deoxycholate; 0.1% sodium dodecyl sulfate). Cell lysates were sonicated using a Bioruptor ultrasonic cell disruptor (Diagenode) to shear genomic DNA to an average fragment size of 150 to 250 bp and ChIP was performed following protocol provided by Millipore ChIP Assay kit (Millipore, 17-295). After washing and de-crosslinking, the precipitated DNA was purified using a QIAquick PCR purification kit (QIAGEN).

RP-ChIP-seq

500 or 2000 mESCs were mixed with ~$5x10^7$ *S. cerevisiae* and fixed in 1% formaldehyde for 10 minutes at room temperature. After fixation and washes, the mixtures were sonicated with a 1/8 inch probe for a total of 15 min at 9 watts using a tip sonicator (Misonix sonicator 3000) to obtain genomic DNA fragments with an average size of 150-250 bp. Buffers and buffer volumes were according to standard ChIP procedures. After ChIP, libraries were prepared following Illumina True-Seq protocol with 10 PCR amplification cycles. The libraries were sequenced using an Illumina HiSeq2000 with

single-end and 50 bp read length.

FARP-ChIP-seq

mESCs (500 or 1000) or sorted HSC subtypes were mixed with ~5x10^8 DH5a *E.coli* and fixed in 1% formaldehyde for 10 min at room temperature. After fixation and washes, the mixtures were sonicated with a 1/16-inch probe for 15 min at 3 watts using a tip sonicator (Misonix sonicator 3000) to obtain genomic DNA fragments with an average size of 150-250bp. Buffers and buffer volumes were according to standard ChIP procedures. The lysates were incubated with 2 µl H3K27me3 antibody (Millipore, 07-449) or 1 µl H3K4me3 antibody (Cell Signaling, 9751S) overnight at 4°C. At the meanwhile, 60 µl protein G magnetic beads (Life Technologies, 10004D) and 10 µl M-280 streptavidin beads (Life Technologies, 11206D) for each ChIP were prepared for the next step. To block any non-specific chromatin absorption, protein G beads and M-280 streptavidin beads were pre-incubated with ~5x10^8 fixed and sonicated *E.coli* lysate overnight at 4°C, respectively. After blocking step, 5 ng carrier biotin-DNA was then coupled to 10 µl M-280 streptavidin beads according to manufacturer's instruction (Life Technologies, 11206D). These treated protein G and streptavidin beads were combined and used to ChIP H3K27me3 or H3K4me3 in the sonicated *E.coli*+mESC or *E.coli*+HSC lysates for 4 h at 4°C. The beads were then recovered using a magnetic stand. All washing, de-crosslinking were performed following standard ChIP procedures. After decrosslinking, the precipitated genomic DNA and biotin-DNA were purified using Agencourt AMPure XP beads (Beckman Coulter). Library building steps were performed following True-Seq protocol with 12 PCR amplification cycles. 0.25 mM blocker oligo was added at the final

library amplification step.

The carrier biotin-DNA sequence:

Biotin5'atattaacgcttacaatttaggtggcacttttcggggaaatgtgcgcggaacccctatttgtttatttttctaaatacattca aatatgtatccgctcatgagacaataaccctgataaatgcttcaataatattgaaaaaggaagagtatgagtattcaacatttccgtg tcgcccttattccctttttgcggcattttgccttcctgttttt 3'

The amplification blocker sequence

5'A*C*A*AATAGGGGTTCCGCGCACATTTCCCCGAAAAGTGCCACCTAA -3 carbon spacer 3'

*indicate the first three phosphorothioated DNA bases.

Isolation of HSC subtypes for FARP-ChIP-seq

Femora and tibiae were dissected from one C57BL/6J male mouse (8 weeks old) and bone marrow cells were flushed with FACS buffer (PBS with 0.3% BSA and 2 mM EDTA). The cells were enriched with CD117/c-Kit MicroBeads following the guidelines (Miltenyi Biotec, #130-091-224). c-Kit enriched cells were stained with lineage cell detection cocktail-biotin (Miltenyi Biotec, #130-092-613) for 20 min at 4_oC. Cells were stained with DAPI, anti-Biotin, c-Kit, Sca1, CD34, and Flk2 antibodies (Biolegend) for 20 min followed by sorting with FACSAria™ III cell sorter (BD Bioscience). The cell populations collected were: LT-HSC: Lin$^-$, c-Kit$^+$, Sca-1$^+$, CD34$^-$, Flk2$^-$; ST-HSC: Lin$^-$, c-Kit$^+$, Sca-1$^+$, CD34$^+$, Flk2$^-$; MPP: Lin$^-$, c-Kit$^+$, Sca-1$^+$, CD34$^+$, Flk2$^+$.

Determining the number of HSC subtypes used in FARP-ChIP-seq

Different numbers of BM cells, 300, 1000, 3000, 10,000 and 100,000, were mixed with

$5x10^8$ bacteria and fixed in 1% formaldehyde for 10 min at room temperature. After fixation and washes, the mixtures were sonicated using the same conditions for HSC subtypes. The sample was then used to build library for low-depth genomic sequencing. A cell number standard was determined using the number of reads from mouse and bacteria by linear regression. To prevent the loss of sorted LT-HSCs, ST-HSCs, and MPPs during fixation and wash steps, each subtype was mixed with $5x10^8$ bacteria and fixed followed by washes to remove the fixative. After sonication, 5% of each sample was used for the same low-depth genomic sequencing as above. The mouse and bacteria reads obtained in each sample were used to determine the number of HSC subtypes based on the cell standard.

Quality-filtering, mapping, and analyses of all ChIP-seq datasets in this study

For RP-ChIP-seq and FARP-ChIP-seq libraries, reads were filtered using the quality of multiplexing indices before mapping to prevent contamination by erroneous de-multiplexing. Reads with an average index quality below 30 were discarded (Kircher et al., 2012).The reads were then mapped to mouse genome (mm9) by Bowtie, allowing 2 mismatches per read. Only uniquely mapped reads were retained. The mapped reads were further mapped to carrier genome or biotin-DNA sequences by Bowtie allowing 3 mismatches, and reads mapped to the carrier genome or biotin-DNA was discarded.

References:

Adli, M., and Bernstein, B.E. (2011). Whole-genome chromatin profiling from limited numbers of cells using nano-ChIP-seq. Nature protocols *6*, 1656-1668.

Adli, M., Zhu, J., and Bernstein, B.E. (2010). Genome-wide chromatin maps derived from limited numbers of hematopoietic progenitors. Nature methods *7*, 615-618.

Aguilar, C.A., and Craighead, H.G. (2013). Micro- and nanoscale devices for the investigation of epigenetics and chromatin dynamics. Nature nanotechnology *8*, 709-718.

Benayoun, B.A., Pollina, E.A., Ucar, D., Mahmoudi, S., Karra, K., Wong, E.D., Devarajan, K., Daugherty, A.C., Kundaje, A.B., Mancini, E.*, et al.* (2014). H3K4me3 breadth is linked to cell identity and transcriptional consistency. Cell *158*, 673-688.

Bernstein, B.E., Mikkelsen, T.S., Xie, X., Kamal, M., Huebert, D.J., Cuff, J., Fry, B., Meissner, A., Wernig, M., Plath, K.*, et al.* (2006). A bivalent chromatin structure marks key developmental genes in embryonic stem cells. Cell *125*, 315-326.

Brind'Amour, J., Liu, S., Hudson, M., Chen, C., Karimi, M.M., and Lorincz, M.C. (2015). An ultra-low-input native ChIP-seq protocol for genome-wide profiling of rare cell populations. Nature communications *6*, 6033.

Cabezas-Wallscheid, N., Klimmeck, D., Hansson, J., Lipka, D.B., Reyes, A., Wang, Q., Weichenhan, D., Lier, A., von Paleske, L., Renders, S.*, et al.* (2014). Identification of regulatory networks in HSCs and their immediate progeny via integrated proteome, transcriptome, and DNA Methylome analysis. Cell stem cell *15*, 507-522.

Daley, T., and Smith, A.D. (2013). Predicting the molecular complexity of sequencing libraries. Nature methods *10*, 325-327.

Hawse, J.R., Hejtmancik, J.F., Huang, Q., Sheets, N.L., Hosack, D.A., Lempicki, R.A., Horwitz, J., and Kantorow, M. (2003). Identification and functional clustering of global gene expression differences between human age-related cataract and clear lenses. Molecular vision *9*, 515-537.

Jia, J., Lin, M., Zhang, L., York, J.P., and Zhang, P. (2007). The Notch signaling pathway controls the size of the ocular lens by directly suppressing p57Kip2 expression. Molecular and cellular biology *27*, 7236-7247.

Jia, J., Zheng, X., Hu, G., Cui, K., Zhang, J., Zhang, A., Jiang, H., Lu, B., Yates, J., 3rd, Liu, C.*, et al.* (2012). Regulation of pluripotency and self- renewal of ESCs through epigenetic-threshold modulation and mRNA pruning. Cell *151*, 576-589.

Jiang, H., Shukla, A., Wang, X., Chen, W.Y., Bernstein, B.E., and Roeder, R.G. (2011). Role for Dpy-30 in ES cell-fate specification by regulation of H3K4 methylation within bivalent domains. Cell *144*, 513-525.

Kim, J., Cantor, A.B., Orkin, S.H., and Wang, J. (2009). Use of in vivo biotinylation to study protein-protein and protein-DNA interactions in mouse embryonic stem cells. Nat Protoc *4*, 506-517.

Kircher, M., Sawyer, S., and Meyer, M. (2012). Double indexing overcomes inaccuracies in multiplex sequencing on the Illumina platform. Nucleic acids research *40*, e3.

Landt, S.G., Marinov, G.K., Kundaje, A., Kheradpour, P., Pauli, F., Batzoglou, S., Bernstein, B.E., Bickel, P., Brown, J.B., Cayting, P.*, et al.* (2012). ChIP-seq guidelines and practices of the ENCODE and modENCODE consortia. Genome research *22*, 1813-1831.

Langmead, B., Trapnell, C., Pop, M., and Salzberg, S.L. (2009). Ultrafast and memory-efficient alignment of short DNA sequences to the human genome. Genome biology *10*, R25.

Lara-Astiaso, D., Weiner, A., Lorenzo-Vivas, E., Zaretsky, I., Jaitin, D.A., David, E., Keren-Shaul, H., Mildner, A., Winter, D., Jung, S.*, et al.* (2014). Immunogenetics. Chromatin state dynamics during blood formation. Science *345*, 943-949.

Li, W.C., Kuszak, J.R., Dunn, K., Wang, R.R., Ma, W., Wang, G.M., Spector, A., Leib, M., Cotliar, A.M., Weiss, M.*, et al.* (1995). Lens epithelial cell apoptosis appears to be a common cellular basis for non-congenital cataract development in humans and animals. The Journal of cell biology *130*, 169-181.

Liao, J., Su, X., Chen, P., Wang, X., Xu, L., Li, X., Thean, L., Tan, C., Tan, A.G., Tay, W.T.*, et al.* (2014). Meta-analysis of genome-wide association studies in multiethnic Asians identifies two loci for age-related nuclear cataract. Human molecular genetics *23*, 6119-6128.

McCaffrey, R., Harrison, T.A., Parkman, R., and Baltimore, D. (1975). Terminal deoxynucleotidyl transferase activity in human leukemic cells and in normal human thymocytes. The New England journal of medicine *292*, 775-780.

Mikkelsen, T.S., Ku, M., Jaffe, D.B., Issac, B., Lieberman, E., Giannoukos, G., Alvarez, P., Brockman, W., Kim, T.K., Koche, R.P.*, et al.* (2007). Genome-wide maps of chromatin state in pluripotent and lineage-committed cells. Nature *448*, 553-560.

Ng, J.H., Kumar, V., Muratani, M., Kraus, P., Yeo, J.C., Yaw, L.P., Xue, K., Lufkin, T., Prabhakar, S., and Ng, H.H. (2013). In vivo epigenomic profiling of germ cells reveals germ cell molecular signatures. Dev Cell *24*, 324-333.

Nishino, J., Kim, I., Chada, K., and Morrison, S.J. (2008). Hmga2 promotes neural stem cell self-renewal in young but not old mice by reducing p16Ink4a and p19Arf Expression. Cell *135*, 227-239.

Orford, K., Kharchenko, P., Lai, W., Dao, M.C., Worhunsky, D.J., Ferro, A., Janzen, V., Park, P.J., and Scadden, D.T. (2008). Differential H3K4 methylation identifies developmentally poised hematopoietic genes. Developmental cell *14*, 798-809.

Park, P.J. (2009). ChIP-seq: advantages and challenges of a maturing technology. Nat Rev Genet *10*, 669-680.

Porcher, C., Swat, W., Rockwell, K., Fujiwara, Y., Alt, F.W., and Orkin, S.H. (1996). The T cell leukemia oncoprotein SCL/tal-1 is essential for development of all hematopoietic lineages. Cell *86*, 47-57.

Puri, D., Gala, H., Mishra, R., and Dhawan, J. (2015). High-wire act: the poised genome and cellular memory. The FEBS journal *282*, 1675-1691.

Reynaud, D., Demarco, I.A., Reddy, K.L., Schjerven, H., Bertolino, E., Chen, Z., Smale, S.T., Winandy, S., and Singh, H. (2008). Regulation of B cell fate commitment and immunoglobulin heavy-chain gene rearrangements by Ikaros. Nature immunology *9*, 927-936.

Ruotolo, R., Grassi, F., Percudani, R., Rivetti, C., Martorana, D., Maraini, G., and Ottonello, S. (2003). Gene expression profiling in human age-related nuclear cataract. Molecular vision *9*, 538-548.

Rybak, J.N., Ettorre, A., Kaissling, B., Giavazzi, R., Neri, D., and Elia, G. (2005). In vivo protein biotinylation for identification of organ-specific antigens accessible from the vasculature. Nat Methods *2*, 291-298.

Segev, F., Mor, O., Segev, A., Belkin, M., and Assia, E.I. (2005). Downregulation of gene expression in the ageing lens: a possible contributory factor in senile cataract. Eye *19*, 80-85.

Shankaranarayanan, P., Mendoza-Parra, M.A., van Gool, W., Trindade, L.M., and Gronemeyer, H. (2012). Single-tube linear DNA amplification for genome-wide studies using a few thousand cells. Nature protocols *7*, 328-338.

Shankaranarayanan, P., Mendoza-Parra, M.A., Walia, M., Wang, L., Li, N., Trindade, L.M., and Gronemeyer, H. (2011). Single-tube linear DNA amplification (LinDA) for robust ChIP-seq. Nature methods *8*, 565-567.

Sun, D., Luo, M., Jeong, M., Rodriguez, B., Xia, Z., Hannah, R., Wang, H., Le, T., Faull, K.F., Chen, R.*, et al.* (2014). Epigenomic profiling of young and aged HSCs reveals concerted changes during aging that reinforce self-renewal. Cell stem cell *14*, 673-688.

Tsai, F.Y., and Orkin, S.H. (1997). Transcription factor GATA-2 is required for proliferation/survival of early hematopoietic cells and mast cell formation, but not for erythroid and myeloid terminal differentiation. Blood *89*, 3636-3643.

Voigt, P., LeRoy, G., Drury, W.J., 3rd, Zee, B.M., Son, J., Beck, D.B., Young, N.L., Garcia, B.A., and Reinberg, D. (2012). Asymmetrically modified nucleosomes. Cell *151*, 181-193.

Weishaupt, H., Sigvardsson, M., and Attema, J.L. (2010). Epigenetic chromatin states uniquely define the developmental plasticity of murine hematopoietic stem cells. Blood *115*, 247-256.

Yang, L., Bryder, D., Adolfsson, J., Nygren, J., Mansson, R., Sigvardsson, M., and Jacobsen, S.E. (2005). Identification of Lin(-)Sca1(+)kit(+)CD34(+)Flt3- short-term hematopoietic stem cells capable of rapidly reconstituting and rescuing myeloablated transplant recipients. Blood *105*, 2717-2723.

Zhang, P., Liegeois, N.J., Wong, C., Finegold, M., Hou, H., Thompson, J.C., Silverman, A., Harper, J.W., DePinho, R.A., and Elledge, S.J. (1997). Altered cell differentiation and proliferation in mice lacking p57KIP2 indicates a role in Beckwith-Wiedemann syndrome. Nature *387*, 151-158.

Zhang, Y., Liu, T., Meyer, C.A., Eeckhoute, J., Johnson, D.S., Bernstein, B.E., Nusbaum, C., Myers, R.M., Brown, M., Li, W.*, et al.* (2008). Model-based analysis of ChIP-Seq (MACS). Genome biology *9*, R137.

Zwart, W., Koornstra, R., Wesseling, J., Rutgers, E., Linn, S., and Carroll, J.S. (2013). A carrier-assisted ChIP-seq method for estrogen receptor-chromatin interactions from breast cancer core needle biopsy samples. BMC genomics *14*, 232.

Zwart, W., Theodorou, V., Kok, M., Canisius, S., Linn, S., and Carroll, J.S. (2011). Oestrogen receptor-co-factor-chromatin specificity in the transcriptional regulation of breast cancer. The EMBO journal *30*, 4764-4776.

CURRICULUM VITAE

SIBIAO YUE

Department of Biology, Johns Hopkins University

Department of Embryology, Carnegie Institution for Science

Phone: 650-387-5276; Email: syue3@jhu.com

EDUCATION

Johns Hopkins University, Baltimore, United States

- Ph.D., Cell, Molecular, Developmental biology, and Biophysics graduate program, 2018

Second Military Medical University, Shanghai, China

- M.A., Medical Immunology, 2006

Sichuan University, Chengdu, China

- B.M., Medicine, 2004

RESEARCH EXPERIENCE

Johns Hopkins University and **Carnegie Institution for Science**, MD, USA, 2012-2018

- PhD student with Dr. Yixian Zheng

  Thesis project: The role of Lamin-B1 in thymus aging

Stanford University, Stanford, USA, 2006 –2012

Research Associate with Dr. Changzheng Chen

Publications

First / Corresponding Author

Zheng X*, Yue Sibiao*, Chen H, Weber B, Jia J, Zheng Y: Low-Cell-Number Epigenome Profiling Aids the Study of Lens Aging and Hematopoiesis. Cell Rep, 201513(7):1505-1518

Si-biao Yue, Robin Trujillo, Yujie Tang, Bill O' Gorman, Chang-Zheng Chen: Loop nucleotides control primary and mature miRNA function in target recognition and repression. RNA Biology 2011;8(6)

Robin Deis Trujillo*, Si-Biao Yue*, Yujie Tang, William E O'Gorman, Chang-Zheng Chen: The potential functions of primary microRNAs in target recognition and repression. EMBO J. 2010; 29(19): 3272-85

Xiaoxing Xiong, Xianhui Kang, Yueying Zheng, Sibiao Yue*, Shengmei Zhu*: Identification of Loop Nucleotide Polymorphisms Affecting MicroRNA Processing and Function. Mol. Cells 2013

Xiaoxing Xiong, Lijuan Gu, Jian Shen, Xianhui Kang, Yueying Zheng, Sibiao Yue*, Shengmei Zhu*: Probenecid protects against transient focal cerebral ischemic injury by inhibiting HMGB1 release and attenuating AQP4 expression in mice. Neurochemical Research 2013

Co-Author

Gigante CM, Dibattista M, Dong FN, Zheng X, Yue S, Young SG, Reisert J, Zheng Y, Zhao H. Lamin B1 is required for mature neuron-specific gene expression during olfactory sensory

neuron differentiation. Nat Commun. 2017 Apr 20;8:15098

Yibing Ouyang, Lijun Xu, Sibiao Yue, Siwei Liu, Rona Giffard: Neuroprotection by astrocytes in brain ischemia: Importance of microRNAs Neurosci Lett. 2014;565:53-8

Yibing Ouyang, Lijun Xun, Yu Lu, Xiaoyun Sun, Sibiao Yue, Xiaoxing Xiong, Rona Giffard: Astrocyte-enriched miR-29a targets PUMA and reduces neuronal vulnerability to forebrain ischemia Glia. 2013; 61(11):1784-94

Rita Fragoso, Tin Mao, Song Wang, Steven Schaffert, Xue Gong, Sibiao Yue, Richard Luong, Hyeyoung Min, Yumi Yashiro-Ohtani, Mark Davis, Warren Pear, Chang-Zheng Chen: Modulating the Strength and Threshold of NOTCH Oncogenic Signals by mir-181a-1/b-1

Yibing Ouyang, Yu Lu, Sibiao Yue, Lijun Xun, Xiaoxing Xiong, Robin E White, Xiaoyun Sun, Rona Giffard: miR-181 regulates GRP78 and influences outcome from cerebral ischemia in vitro and in vivo. Neurobiology of Disease 2011

Yibing Ouyang, Yu Lu, Sibiao Yue, Rona Giffard: miR-181 targets multiple Bcl-2 family members and influences apoptosis and mitochondrial function in astrocytes. Mitochondrion 2011

Arnold CP, Tan R, Zhou B, Yue SB, Schaffert S, Biggs JR, Doyonnas R, Lo MC, Perry JM,

Renault VM, Sacco A, Somervaille T, Viatour P, Brunet A, Cleary ML, Li L, Sage J, Zhang DE, Blau HM, Chen C, Chen CZ: MicroRNA programs in normal and aberrant stem and progenitor cells. Genome Res. 2011; 21 (5): 798-810

Liu G, Min H, Yue S, Chen CZ: Pre-miRNA loop nucleotides control the distinct activities of mir-181a-1 and mir-181c in early T cell development. PLoS ONE. 2008; 3(10):e3592

Wan Xiaoxiao, Yue Sibiao, Xiong Xiaopeng, Zheng Ping, Chen Gang: Neutrophils induce the maturation of immature dendritic cells: a regulatory role of neutrophils in adaptive immune responses. Immunol Invest 2007;36 (3)337-350

REFERENCES

Yixian Zheng, PhD	Jonathan D. Powell, PhD	Chen-ming Fan, PhD
Staff member	Professor	Staff member
Department of Embryology	Department of Oncology	Department of Embryology
Carnegie Institution	Johns Hopkins University	Carnegie Institution
3520 San Martin Drive	1650 Orleans Street	3520 San Martin Drive
Baltimore, MD, 21218	Baltimore, MD, 21231	Baltimore, MD, 21218
zheng@carnegiescience.edu	poweljo@jhmi.edu	fan@carnegiescience.edu
410-246-3032	410-502-7887	410-246-3022